

MASTER'S DISSERTATION

**RHEOLOGY OF FERROFLUIDS IN SHEAR
FLOWS**

Igor Dal Osto Pereira

Brasília, November of 2019.

UNIVERSIDADE DE BRASÍLIA

FACULDADE DE TECNOLOGIA

DEPARTAMENTO DE ENGENHARIA MECÂNICA

UNIVERSIDADE DE BRASÍLIA
Faculdade de Tecnologia
Departamento de Engenharia Mecânica

MASTER'S DISSERTATION

**RHEOLOGY OF FERROFLUIDS IN SHEAR
FLOWS**

Igor Dal Osto Pereira

Dissertation submitted to the Department of Mechanical Engineering in partial fulfillment of the requirements for the degree of Master of Mechanical Sciences

Examining Committee

Prof. Francisco Ricardo da Cunha, PhD
Advisor (ENM-UnB)

Prof. Rafael Gabler Gontijo, PhD
Internal Member (ENM-UnB)

Prof. Mônica Feijó Naccache, PhD
External Member (PUC-RJ)

Brasília, November of 2019.

Dedico este trabalho aos meus pais, irmão e avós.

"I seem to have been only like a boy playing on the seashore, and diverting myself in now and then finding a smoother pebble or a prettier shell than ordinary, whilst the great ocean of truth lay all undiscovered before me".

(Isaac Newton)

"Measure what is measurable, and make measurable what is not so".

(Galileo Galilei)

Acknowledgements

Agradeço ao meu orientador e amigo, Prof. Francisco Ricardo da Cunha, por sua paciência, generosidade e confiança durante estes cinco anos de trabalho conjunto. Agradeço por todos os ensinamentos, pelas críticas construtivas e por ser um orientador presente que sempre busca inspirar em seus alunos o amor pela ciência. Agradeço também aos professores Taygoara Felamingo e Adriano Possebon por todo o conhecimento compartilhado, que fizeram grande diferença em minha formação.

Aos meus pais, Carlos e Marilei, agradeço por todo o esforço que sempre fizeram para dar uma formação moral sólida e a melhor educação que podiam a mim e ao meu irmão. Agradeço-lhes por nunca desanimarem em face às inúmeras dificuldades que a vida lhes apresentava e pelo carinho e dedicação que sempre me dedicaram. Ao meu pai, agradeço pela fortaleza que sempre representou para nossa família, sendo continuamente a voz da razão e da temperança mesmo nos momentos mais difíceis. À minha mãe, agradeço por todo cuidado e amor que generosamente me dedica. Ao meu irmão, Fábio, agradeço pelos concelhos e por sempre ter estado ao meu lado nos bons e maus momentos.

Agradeço a todos os amigos do Grupo de Mecânica dos Fluidos de Escoamentos Complexos (VORTEX), em especial aos meus colegas de sala: Filipe, Gesse e Yuri Zeniti. Muito obrigado por terem tornado nossas longas horas de trabalho suportáveis e, quase sempre, muito divertidas. Agradeço ao Filipe por ser um amigo sempre disposto a ajudar, seja em assuntos acadêmicos ou pessoais. Agradeço também por todas as trocas de conhecimento durante esses anos, muitas delas iniciadas em virtude de sua paixão pelas ciências naturais. Ao Gesse, agradeço por seu louvável companheirismo e por todos os ensinamentos compartilhados. Você é um exemplo de dedicação e um pesquisador excepcional. Ao Yuri Zeniti, agradeço por seu companheirismo, amizade e, em especial, pelas sempre frutíferas discussões sobre assuntos relacionados a realização de experimentos e à análise dos resultados obtidos. Agradeço também aos meus colegas Marcos Fabrício e Victor Shumyatsky, que também foram parte importante dessa jornada do mestrado. Agradeço-lhes pelo companheirismo, pela troca de conhecimentos e pelas boas risadas que compartilhamos.

Agradeço a Mariana por seu apoio tanto em momentos de calma quanto de tempestade e, também, por todo o carinho e compreensão que constantemente me dedica.

Agradeço ao CNPq pelo apoio financeiro durante a realização deste mestrado.

Resumo

Nesta dissertação de mestrado, o comportamento reológico de dois ferrofluidos comerciais, EFH1 e EFH3, produzidos pela Ferrotec, é caracterizado experimentalmente através do uso de um reômetro de discos paralelos equipado com uma célula magnética. Os ferrofluidos utilizados variam somente na fração volumétrica de partículas magnéticas (magnetita) que contém. As amostras dos dois ferrofluidos são testadas de acordo com três metodologias. A primeira refere-se aos ensaios em regime de cisalhamento permanente na presença de campo magnético, através do qual examina-se o comportamento da viscosidade aparente e da tensão de cisalhamento dos ferrofluidos em função da intensidade do campo magnético, da taxa de cisalhamento e da fração volumétrica de partículas do fluido complexo. Isto permite a verificação da aderência do comportamento reológico de tais fluidos aos modelos de fluido newtoniano generalizado. A segunda metodologia diz respeito aos ensaios experimentais com escoamentos do tipo transiente, em regime de impulso de deformação na presença de campo magnético. A partir desta análise experimental obtiveram-se, para os diferentes ferrofluidos, suas funções relaxação de tensão dependentes tanto da intensidade campo magnético como da intensidade do impulso aplicado, com base nelas, efetuaram-se o cálculo de seus tempos de relaxação. Verificou-se também que a tensão de cisalhamento não relaxa para zero em ferrofluidos quando na presença de um campo magnético, mas sim para uma tensão residual a qual foi avaliada tanto em função da intensidade do campo, quanto da intensidade do escoamento. A terceira metodologia refere-se a testes com cisalhamento oscilatório na presença de campo magnético, em regime de viscoelasticidade linear, no qual obtiveram-se os módulos viscoelásticos dos ferrofluidos em função da frequência e da intensidade do campo magnético para uma condição de pequenas deformações. É mostrada, para ambos ferrofluidos, a dependência da frequência característica de transição de um comportamento predominantemente dissipativo para um majoritariamente elástico em relação à intensidade do campo magnético aplicado. Verificações de compatibilidade entre o módulo viscoso e a viscosidade aparente para valores iguais de frequência e taxa de cisalhamento são realizadas e, com base nisso, a primeira diferença de tensões normais é calculada usando a regra de Laun.

Palavras-chaves: Ferrofluidos, Efeito magnetoviscoso, Pseudoplasticidade, Relaxação de tensão, Tensão residual, viscoelasticidade linear, Primeira diferença de tensões normais.

Abstract

In this master's dissertation, the rheological behavior of two commercial ferrofluids, EFH1 and EFH3, produced by Ferrotec, is experimentally characterized through the use of a parallel disc rheometer equipped with a magnetic cell. The ferrofluids used vary only in the volume fraction of magnetic particles (magnetite) it contains. Samples of both ferrofluids are tested according to three methodologies. The first one refers to tests in permanent shear regime in the presence of magnetic field, through which the behavior of the apparent viscosity and of the shear stress of the ferrofluids is analyzed as a function of magnetic field intensity, shear rate and of the volumetric fraction of particles of the complex fluid. This permits the verification of the adherence of the rheological behavior of such fluids to the generalized Newtonian fluid models. The second methodology concerns the experimental tests with transient flow under step-strain regime in the presence of magnetic field. From this experimental analysis it has been obtained, for the different ferrofluids, their stress relaxation functions dependent on both the magnetic field intensity and the applied impulse intensity. Based on them, their relaxation times were calculated. It was also found that the shear stress does not relax to zero in ferrofluids when subjected to an external magnetic field, but rather it relaxes to a residual stress which was evaluated as a function of both field strength and yield strength. The third methodology refers to tests with oscillatory shear, in the presence of magnetic field, and under a linear viscoelastic regime. From this tests, it has been obtained the viscoelastic modules of the ferrofluids as functions of frequency and intensity of the magnetic field, for a condition of small deformations. It is shown, for both ferrofluids, the dependence of the characteristic transition frequency as a function of the intensity of the magnetic field. This frequency marks the change from a predominantly dissipative to a mostly elastic behavior of the complex fluids. Compatibility checks between the viscous modulus and apparent viscosity for equal frequency and shear rate values are performed, and based on this, the first difference of normal stresses is calculated using Laun's rule.

Key-words: Ferrofluids, Magnetoviscous Effect, Pseudoplasticity, Stress Relaxation, Residual Stress, Linear Viscoelasticity, First Difference of Normal Stress.

List of Figures

| | |
|---|----|
| Figure 1 – Surface coated magnetic particles. The diameter of the particle is 10 nm and its hydrodynamic diameter is 14 nm. Figure adapted from (ODENBACH, 2003). | 2 |
| Figure 2 – The magnetic force exerted by the electromagnet to a ferrofluid is strong enough to keep it attached against the earth’s gravitational field and yet to form the characteristic spike pattern. Adapted from (ODENBACH, 2009). | 3 |
| Figure 3 – Prostate cancerous cell uptaked by magnetic large particles - " <i>ProstCA</i> " (high pigmentation) compared to a healthy cell - " <i>F</i> " (no pigmentation). Adapted from (JORDAN et al., 2001). | 5 |
| Figure 4 – On the origin of the magnetoviscous effect in a suspension of magnetic nano particles. Explanation is given in the text. | 8 |
| Figure 5 – Continuous body (\mathcal{B}), in which is presented a fluid particle (\mathcal{P}) and its typical scales, respectively, the integral (macroscopic) scale (L) and the local continuum scale (l). | 17 |
| Figure 6 – Schematics of the movement of a continuous body \mathcal{B} , with representation of the different configurations \mathcal{C} obtained throughout the process: \mathcal{C}_0 at the initial time $t = 0$, \mathcal{C}_τ at an intermediate time instant $t = \tau$ and \mathcal{C}_t at the actual instant of time t | 27 |
| Figure 7 – Schematic representation of the three possible rheological behaviors of a power-law fluid. | 30 |
| Figure 8 – Schematic representation of the three possible rheological behaviors of a power-law fluid. | 37 |
| Figure 9 – Schematics of a Maxwell’s element. | 41 |
| Figure 10 – Schematics of a complex fluid composed by N Maxwell’s elements. | 44 |
| Figure 11 – Typical result for the viscosity behavior $\eta(\dot{\gamma})$ of a shear-thinning liquid, showing the three regions of interest: the plateau characterized by the effective viscosity η_0 , the power-law and the infinite-shear viscosity plateau η_∞ | 51 |
| Figure 12 – Schematics representation of a small amplitude oscillatory shear. | 52 |

| | |
|---|----|
| Figure 13 – (a) Step-strain, (b) Applied shear-rate (impulse function). | 55 |
| Figure 14 – Rheometer Anton Paar - model Physica MCR 301. | 59 |
| Figure 15 – Pressurized air: production and treatment devices. | 60 |
| Figure 16 – Ecoline Staredition RE104 thermal bath (Lauda GmbH, Germany) . . . | 61 |
| Figure 17 – Schematic. | 61 |
| Figure 18 – Interface of the program Rheoplus during data acquisition of the complexes modulus and viscosity of a ferrofluid in a small amplitude oscillatory shear flow under a strong magnetic field. | 62 |
| Figure 19 – Viscosity of distilled water as a function of time, measured on the rheometer of parallel plates Physica MCR-301. The shear rate is fixed at 100 s^{-1} and the temperature, at 25°C . The gap between the parallel plates is 0.8 mm. | 63 |
| Figure 20 – (a) Physica MCR 301 rheometer: standard Assembly. (b) Detail of the measuring system PP50. | 64 |
| Figure 21 – (a) Physica MCR 301 rheometer: Magneto-rheology assembly. (b) Detail of the measuring system PP20. | 65 |
| Figure 22 – MRF assembly: schematic of the measuring cell. | 66 |
| Figure 23 – PS-MRD DC power supply (Anton Paar GmbH, Germany). | 66 |
| Figure 24 – Schematic representation of a parallel disk rheometer, where R is the maximum radius of the disks and H their spacing. | 68 |
| Figure 25 – Parallel plates with cylindrical coordinate system. | 68 |
| Figure 26 – Relative viscosity increment $\Delta\eta/\eta_0$ as a function of the non-dimensional magnetic field strength α subjected to a weak flow, $\text{Pe} = 4.64 \times 10^{-4}$ (■). In the insert, it is shown a comparison of the behavior of $\Delta\eta/\eta_0$ as a function of α for two magnetic fluids: (■) represents, as previously, the data obtained for the ferrofluid EFH1, which is a colloidal suspension of magnetite particles with mean diameter of 10 nm and $\phi = 7.9\%$ subjected to $\text{Pe} = 4.64 \times 10^{-4}$, (○) speaks for the data presented on the work of Odenbach (2009) for a colloidal suspension of magnetite particles with mean diameter of 10 nm and $\phi = 7.2\%$ subjected to a similar weak flow, $\text{Pe} = 1.85 \times 10^{-2}$. The curve is theoretically predicted behavior by equation ((6.11)), considering $\phi = 7.9\%$. The viscosity in the absence of magnetic field η_0 is constant and, at 25°C , equals to $0.94 \times 10^{-2} \text{ Pa.s}$ | 79 |
| Figure 27 – EFH1: Relative viscosity increment $\Delta\eta/\eta_0$ as a function of the non-dimensional magnetic field strength α for different flow intensities: $\text{Pe} = 4.64 \times 10^{-4}$ (□), $\text{Pe} = 1.18 \times 10^{-2}$ (○), $\text{Pe} = 2.32 \times 10^{-2}$ (△). The viscosity in the absence of magnetic field η_0 is constant and, at 25°C , equals to $0.94 \times 10^{-2} \text{ Pa.s}$ | 80 |

| | |
|--|----|
| Figure 28 – EFH3: Relative viscosity increment $\Delta\eta/\eta_0$ as a function of the non-dimensional magnetic field strength α for different flow intensities: $Pe = 1.01 \times 10^{-3}$ (\square), $Pe = 2.57 \times 10^{-2}$ (\circ), $Pe = 5.02 \times 10^{-2}$ (\triangle). The viscosity in the absence of magnetic field η_{nf} is constant and, at $25^\circ C$, equals to 1.80×10^{-2} Pa.s. | 81 |
| Figure 29 – Ferrofluid EFH1: (a) Relative viscosity $\tilde{\eta}$ as a function Pe for three values of the magnetic parameter: $\alpha = 0$ (\triangle), $\alpha = 4.85 \times 10^0$ (\square) and $\alpha = 1.14 \times 10^1$ (\circ). The curves are fits of the experimental data by the generalized fluid model denoted by equation ((6.12)). (b) Nondimensional shear-stress as a function of Pe for the same values of α . The curves are fits of the experimental data by the generalized fluid model denoted by equation ((6.14)). (The viscosity in the absence of magnetic field η_{nf} , at $25^\circ C$, which is equals to 0.94×10^{-2} Pa.s.) The fitting parameters obtained for the referred models are displayed on table ((5)). | 85 |
| Figure 30 – Ferrofluid EFH3: (a) Relative viscosity $\tilde{\eta}$ as a function Pe for three values of the magnetic parameter: $\alpha = 0$ (\triangle), $\alpha = 4.84 \times 10^0$ (\circ), $\alpha = 1.14 \times 10^1$ (\square). The curves are fits of the experimental data by the generalized fluid model denoted by equation ((6.12)). (b) Nondimensional shear-stress as a function of Pe for the same values of α . The curves are fits of the experimental data by the generalized fluid model denoted by equation ((6.14)). (The viscosity in the absence of magnetic field η_{nf} , at $25^\circ C$, which is equals to 1.80×10^{-2} Pa.s.). The fitting parameters obtained for the referred models are displayed on table ((5)). | 86 |
| Figure 31 – Ferrofluid EFH1: Dimensionless stress relaxation function $\tilde{\Phi}$ in terms of the nondimensional time shift \tilde{s} for different values of α . The curves are fits of the experimental data by an adaptation of the generalized Maxwell’s model, given by equation ((6.23)). The parameters for each curve are shown in table ((7)). The viscosity in the absence of magnetic field η_0 , at $25^\circ C$, is 0.94×10^{-2} Pa.s and the main time of relaxation for the lowest magnetic field applied τ_m is 1.24×10^{-1} s. In the inserts, it is shown a plot of the amplitude of the stress A_j as a function of the characteristic times $\tilde{\tau}_j$ involved in the process of stress relaxation at each condition of magnetic field strength α | 95 |

| | |
|---|-----|
| Figure 32 – Ferrofluid EFH3: Dimensionless stress relaxation function $\tilde{\Phi}$ in terms of the nondimensional time shift \tilde{s} for different values of α . The curves are fits of the experimental data by an adaptation of the generalized Maxwell’s model, given by equation ((6.23)). The parameters for each curve are shown in table. The viscosity in the absence of magnetic field η_0 , at 25°C, is 0.18×10^{-1} Pa.s and the main time of relaxation for the lowest magnetic field applied τ_m is 6.73×10^{-1} s. In the inserts, it is shown a plot of the amplitude of the stress A_j as a function of the characteristic times $\tilde{\tau}_j$ involved in the process of stress relaxation at each condition of magnetic field strength α | 97 |
| Figure 33 – Nondimensional time of relaxation $\tilde{\tau}$ as a function of the magnetic field intensity parameter α . The curves are fits of the experimental data to equation ((6.24)). The fitting parameters are displayed on table ((9)). | 100 |
| Figure 34 – Dimensionless residual stress $\tilde{\sigma}_R$ as a function of the non-dimensional magnetic field α . The curves are fits of the experimental data to equation ((6.26)). The fitting parameters are displayed on table ((9)). | 102 |
| Figure 35 – EFH1: Nondimensional stress relaxation $\tilde{\Phi}$ as a function of \tilde{s} for different values of γ_0 : (\times) - $\text{Pe} = 1.69 \times 10^{-5}$ ($\gamma_0 = 0.02$), (\bullet) - $\text{Pe} = 1.69 \times 10^{-4}$ ($\gamma_0 = 0.2$), (\blacksquare) - $\text{Pe} = 6.74 \times 10^{-4}$ ($\gamma_0 = 0.8$). | 105 |
| Figure 36 – EFH3: Nondimensional stress relaxation $\tilde{\Phi}$ as a function of \tilde{s} for different values of γ_0 : (\circ) - $\text{Pe} = 4.03 \times 10^{-6}$ ($\gamma_0 = 0.02$), (\bullet) - $\text{Pe} = 4.03 \times 10^{-5}$ ($\gamma_0 = 0.2$), (\square) - $\text{Pe} = 1.61 \times 10^{-4}$ ($\gamma_0 = 0.8$). | 106 |
| Figure 37 – EFH1: nondimensional residual stress $\tilde{\sigma}_R$ as a function of Pe for two intensities of the external magnetic field: (a) $\alpha = 8.37 \times 10^0$ and (b) $\alpha = 1.14 \times 10^1$. In the inserts is shown a detailed view of the experimental data in the range of small Pe . The lines are fits of experimental data concerning the range of small Pe to $\tilde{\sigma}_r = c_1 \text{Pe}$ The constant is, for (a), $c_1 = 5.74 \times 10^3$ and, for (b), $c_1 = 2.49 \times 10^4$ | 108 |
| Figure 38 – EFH3: nondimensional residual stress $\tilde{\sigma}_R$ as a function of Pe for two intensities of the external magnetic field: (a) $\alpha = 8.37 \times 10^0$ and (b) $\alpha = 1.14 \times 10^1$. In the inserts is shown a detailed view of the experimental data in the range of small Pe . The lines is are fit of experimental data concerning the range of small Pe to $\tilde{\sigma}_r = c_1 \text{Pe}$. The constant is, for (a), $c_1 = 5.32 \times 10^5$ and, for (b), $c_1 = 9.06 \times 10^5$ | 109 |
| Figure 39 – EFH1: Nondimensional storage modulus \tilde{G}' (\circ) and nondimensional loss modulus \tilde{G}'' (\bullet) as a function of De , for (a) $\alpha = 4.89$ and (b) $\alpha = 13.5$ | 114 |
| Figure 40 – EFH3: Nondimensional storage modulus \tilde{G}' (\circ) and nondimensional loss modulus \tilde{G}'' (\bullet) as a function of De , for (a) $\alpha = 4.89$ and (b) $\alpha = 13.5$ | 115 |

- Figure 41 – Non-dimensional storage modulus \tilde{G}' evaluated at $De = 1$ for different values of α for the ferrofluids EFH1 (\bullet) and EFH3 (\circ). The curves are fits to the experimental data to $\tilde{G}'(De = 1, \alpha) = c_1 \exp(c_2 \alpha)$. The constants for the dashed curve are $c_1 = 2.97$ and $c_2 = 0.21$. For the continuous curve, they are $c_1 = 1.39$ and $c_2 = 0.15$ 117
- Figure 42 – Nondimensional viscosity modulus $\tilde{\eta}$ evaluated at $De = 10$ for different values of α for the ferrofluids EFH1 (\bullet) and EFH3 (\circ). The curves are fits to the experimental data to $\tilde{\eta}'(De = 1, \alpha) = c_1 \exp(c_2 \alpha)$. The constants for the dashed curve are $c_1 = 7.76$ and $c_2 = 0.15$. For the continuous curve, they are $c_1 = 1.85 \pm$ and $c_2 = 0.15$ 118
- Figure 43 – EFH1: Nondimensional apparent viscosity $\tilde{\eta}$ (\bullet) and nondimensional absolute value of the complex viscosity $|\tilde{\eta}_c|$ (\circ) as functions of Pe (calculated considering $\omega = \dot{\gamma}$) at $\alpha = 4.85$. In the insert is shown a detailed view of the zone of agreement between the $\tilde{\eta}$ and $|\tilde{\eta}_c|$ 119
- Figure 44 – Nondimensional first normal stress difference \tilde{N}_1 as a function of Pe obtained by applying Laun's rule to the measured values of $G'(\omega)$ and $G''(\omega)$. The dashed curve, in the insert, is a fit of the experimental data for the range of small Pe to $\tilde{N}_1 = c_1 + c_2 \text{Pe}$, with $c_1 = 1.33 \times 10^{-1}$ and $c_2 = 1.11 \times 10^4$. The continuous curve is a fit of the experimental data for the complete range of Pe to $\tilde{N}_1 = c_1 \text{Pe}^2 + c_2 \text{Pe} + c_3$, with c_1 and c_2 equals to the one determined for the dashed line and $c_3 = 2.30 \times 10^7$ 120

List of Tables

| | |
|---|-----|
| Table 1 – Optimal gaps for carrying out rheological experiments, on fluids, as a function of the order of magnitude of their kinematic viscosity | 64 |
| Table 2 – Properties of the ferrofluids EFH1 and EFH3. | 67 |
| Table 3 – Optimal gaps used in the experimental evaluations of the magnetoviscous effect of the ferrofluids EFH1 and EFH3, for different flow intensities. | 76 |
| Table 4 – Viscosity increment of saturation $\Delta\eta(\infty)/\eta_0$ obtained, for each ferrofluid, as a function of Pe. | 82 |
| Table 5 – Parameters obtained from nonlinear regressions of the data, collected on experiments performed on permanent simple shear flow regime, for the ferrofluids EFH1 and EFH3 by the proposed generalized fluid model, which is described by equations ((6.12)) and ((6.14)). | 87 |
| Table 6 – Gaps chosen for each ferrofluid considering four different conditions of magnetic field intensity, which are here denoted by its originating electric current. | 91 |
| Table 7 – Material parameters obtained for the ferrofluid EFH1 via non-linear regression of the experimental data to the model represented by equation ((6.23)). Four intensities of the external magnetic field are considered. | 95 |
| Table 8 – Material parameters obtained for the ferrofluid EFH3 via non-linear regression of the experimental data to the model represented by equation ((6.23)). Four intensities of the external magnetic field are considered. | 98 |
| Table 9 – Fitting parameters obtained for the non-linear regression of the data concerning the magnetic field-dependent time of relaxation and the magnetic field-dependent residual stress, respectively, to the models represented by equations ((6.24)) and ((6.26)). | 102 |

List of abbreviations and acronyms

SAOS Small amplitude oscillatory shear

GNF Generalized Newtonian fluid

Symbols

Latine symbols

| | |
|----------------|--|
| A_j | Amplitude of tension Generalized Maxwell's model |
| \mathcal{B} | Continuous Body |
| \mathbf{B} | Magnetic induction vector |
| D | Stokes-Einstein's diffusion coefficient |
| \mathbf{D} | Strain rate tensor |
| \mathbf{D}_S | Hydrodynamic dipole of particle |
| E | Magnetic energy |
| $E()$ | Experimental error |
| $E_i()$ | Instrumental error |
| $E_r()$ | Random error |
| \mathbf{f} | force over a particle |
| L | Macroscopic characteristic scale |
| l | Continuum characteristic scale |
| \mathcal{F} | Functional |
| \mathbf{J} | Density of electric current |
| k_B | Boltzmann's constant |
| \mathbf{L} | Antisymmetric part of the hydrodynamic dipole |
| \mathbf{m} | Magnetic moment of dipole |
| \mathbf{M} | Magnetization |
| $G''(\omega)$ | Loss modulus |
| $G'(\omega)$ | Storage modulus |
| \mathbf{H} | Magnetic field |
| \mathcal{P} | Material particle |
| N_1 | First normal stresses difference |
| \mathbf{X} | Particle label (initial Lagrangean position) |
| N_2 | Second normal stresses difference |
| p | Mechanic pressure |
| p_0 | Thermodynamic pressure |
| \mathbf{P} | Linear momentum |

| | |
|-----------------|---|
| \mathbf{S} | Symmetric part of the hydrodynamic dipole |
| \mathbf{t} | Torque over a particle |
| $\mathbf{Q}(t)$ | Orthogonal tensor |
| $\mathbf{F}(t)$ | Gradient of deformation tensor |
| \mathbf{x} | Position vector |
| \mathcal{V} | Measured variable |
| V | Volume of a continuous body |
| v_p | Particle volume |
| W | Work |

Greek symbols

| | |
|-------------------------------------|---|
| a | particle diameter |
| α | Nondimensional magnetic field |
| γ | Angular deformation |
| δ | Virtual variation |
| $\delta(\mathbf{x} - \mathbf{x}_i)$ | Dirac's delta function |
| $\Delta\eta$ | Viscosity increment |
| λ | Molecular scale |
| h | Gap between the disks of the rheometer |
| ω | Angular frequency |
| ϕ | Volume fraction |
| ϕ_h | Hydrodynamic volume fraction |
| $\Phi(s)$ | Stress relaxation function |
| Φ_R | Residual stress relaxation parameter |
| ρ | Density |
| ρ_s | Density of free charges |
| $\eta''(\omega)$ | Complex viscosity |
| $\eta'(\omega)$ | Viscosity modulus |
| η_ϕ | Einstein's viscosity |
| η_ϕ | rotational viscosity |
| $\dot{\gamma}$ | Shear rate |
| Ω | Angular velocity |
| τ_f | Characteristic time of the flow |
| τ | Time of relaxation |
| τ_B | Brownian time of relaxation |
| τ_m | Time of relaxation for the weaker magnetic field condition |
| τ_N | Néel's time of relaxation |
| τ_j | time of relaxation associated with the j-th Maxwell's element |
| τ_p | Main relaxation time |

| | |
|-----------------------|--|
| I | Electric current |
| \mathbf{I} | Identity tensor |
| Σ | Stress tensor |
| $\boldsymbol{\sigma}$ | Deviatoric part of the stress tensor |
| σ_R | Residual stress |
| ξ | initial position |
| μ | Vacuum magnetic permeability |
| η_0 | Viscosity in the absence of magnetic field |
| \mathbf{u} | Velocity vector |
| δV | Volume of a continuum particle |
| $\delta v'$ | Volume of the smallest continuum particle |

Mathematical operators

| | |
|--------------------------|------------------------------|
| \log | Logarithm (base 10) |
| dS | Area differential element |
| dV | Volume differential element |
| ∇ | Nabla differential operator |
| $D(*)/Dt$ | Material derivative operator |
| $d(*)/dt$ | Ordinary derivative Operator |
| $L(*)$ | Langevin function |
| $\partial(*)/\partial t$ | Partial derivative operator |
| \int_V | Volume integral |
| \int_s | Surface integral |

Nondimensional parameters

| | |
|------|----------------|
| De | Deborah number |
| Kn | Knudsen number |
| Pe | Peclet number |

Summary

| | | |
|------------|--|-----------|
| | 1 INTRODUCTION | 1 |
| 1.1 | Motivation | 1 |
| 1.2 | Bibliografic review | 5 |
| 1.3 | Objectives | 14 |
| | 2 THEORETICAL BACKGROUND | 16 |
| 2.1 | Continuum hypothesis | 16 |
| 2.2 | Governing equations of fluid motion | 18 |
| 2.2.1 | Balance of Mass | 18 |
| 2.2.2 | Balance of linear momentum | 19 |
| 2.3 | Principles of electromagnetism | 20 |
| 2.3.1 | Maxwell's equations | 20 |
| 2.3.2 | Force and torque over a magnetic particle | 23 |
| | 3 CONSTITUTIVE MODELS | 25 |
| 3.1 | Constitutive formalism | 25 |
| 3.2 | Constitutive modeling for diluted magnetic suspensions | 30 |
| 3.2.1 | Concept of magnetization | 30 |
| 3.2.2 | Stress tensor for a dilute magnetic fluid | 31 |
| 3.3 | The generalized Newtonian fluids | 36 |
| 3.3.1 | Power-law model | 37 |
| 3.3.2 | Sisko's model | 38 |
| 3.3.3 | Herschel-Bulckley's model | 38 |
| 3.3.4 | Bingham's model | 39 |
| 3.4 | The general linear viscoelastic fluids | 39 |
| 3.4.1 | Linear viscoelasticity | 40 |
| 3.4.2 | Maxwell's viscoelastic model | 41 |
| 3.4.3 | Generalized Maxwell's viscoelastic model | 43 |
| 3.4.4 | Determination of the viscoelastic modules | 45 |
| 3.4.5 | Relationship between the stress relaxation function and viscoelastic modules | 47 |

| | | |
|---------|--|------------|
| 3.4.6 | Determination of the relaxation time from the stress relaxation function . . . | 47 |
| | 4 RHEOLOGICAL FLOWS AND MATERIAL FUNCTIONS . . . | 49 |
| 4.1 | The stress tensor: an overview | 49 |
| 4.2 | Permanent simple shear | 50 |
| 4.3 | Small amplitude oscillatory shear | 52 |
| 4.4 | Step-strain | 55 |
| 4.5 | Empirical correlations for material functions | 56 |
| 4.5.1 | Cox-Merz's rule | 57 |
| 4.5.2 | Laun's rule | 57 |
| | 5 MATERIALS AND METHODS | 58 |
| 5.1 | Experimental apparatus | 58 |
| 5.1.1 | Rheometer | 58 |
| 5.1.1.1 | Standard assembly | 64 |
| 5.1.1.2 | Magneto-rheology assembly | 65 |
| 5.2 | Fluids under analysis | 66 |
| 5.3 | Rheometry | 67 |
| 5.3.1 | Measurement of the apparent viscosity on a parallel plate rheometer | 67 |
| | 6 RESULTS: RHEOLOGY OF FERROFLUIDS | 73 |
| 6.1 | Permanent shear analysis | 73 |
| 6.1.1 | Magnetoviscous effect | 75 |
| 6.1.1.1 | Experimental procedure | 75 |
| 6.1.1.2 | Discussion | 77 |
| 6.1.2 | Pseudo-plasticity | 82 |
| 6.1.2.1 | Experimental procedure | 82 |
| 6.1.2.2 | Discussion | 84 |
| 6.2 | Transient shear analysis | 89 |
| 6.2.1 | Step-strain part I: Magnetic field influence | 90 |
| 6.2.1.1 | Experimental procedure | 90 |
| 6.2.1.2 | Discussion | 91 |
| 6.2.2 | Step-strain part II: Effects of the magnitude of the applied strain | 102 |
| 6.2.2.1 | Experimental procedure | 103 |
| 6.2.2.2 | Discussion | 103 |
| 6.2.3 | Small amplitude oscillatory shear | 110 |
| 6.2.3.1 | experimental procedure | 110 |
| 6.2.3.2 | Discussion | 111 |
| | 7 FINAL CONSIDERATIONS | 121 |
| 7.1 | Conclusions | 121 |
| 7.2 | Suggestions for future works | 124 |

| | | |
|------------|---|------------|
| | BIBLIOGRAPHY | 126 |
| | APPENDIX | 132 |
| | APPENDIX A – UNCERTAINTY ANALYSIS | 133 |
| A.1 | Uncertainty associated with the viscosity measured in simple shear | 134 |

1 INTRODUCTION

1.1 Motivation

Ferrofluids are colloidal suspensions of nanosized ferro/ferrimagnetic particles dispersed in a carrier liquid (ROSENSWEIG, 2013; ODENBACH, 2003). The particles are usually composed of magnetite (Fe_3O_4) with an average diameter around 10 nm. The base fluids are usually oils, water, ester or kerosene with a Newtonian behavior. As the particles are extremely small, their sedimentation due to the gravitational field or due to the agglomeration arising from the interaction of the magnetic dipoles is avoided by thermal agitation, that is, by the Brownian effect (EINSTEIN et al., 1905).

The magnetic nanoparticles in suspension are considered to be small magnets with permanent magnetic moment of dipole. Yang et al. (2006) argues that, due to the small sizes of the magnetic particles, particle agglomeration is one of the main issues concerning the preparation of stable magnetic fluids. The particles tend to aggregate by the action of Van Der Waals and dipolar interactions. However this process can be avoided by coating the particles with surfactants. According to Rosensweig (2013), the surfactants are usually organic long molecules, such as oleic acid, perfluoropolyether acid or tetramethylammonium hydroxide. Landfester and Ramirez (2003) punctuates that an appropriate coating not only gives a better stability to the magnetic particles in a carrier fluid, but it is also able to modify the surface properties of the particles. For example, if a biocompatible surfactant is used, it may result in a biocompatible magnetic fluid. According to Odenbach (2003), the thickness of the surfactant layer is around 2-3 nm, which leads to the concept of hydrodynamic diameter, that is defined as the diameter of the particle after the addition of the surfactant layer. In the works of Odenbach and Thurm (2002), Li, Xuan and Wang (2005) are stressed that the viscosity of magnetic fluids depends on the various components of the complex fluid and on its surfactant concentration. In figure (1) is shown an schematic representation of particles with surfactant coatings. They are representatives of a magnetic colloidal suspension which volume fraction of particles is 7%, whereas, the hydrodynamic volume fraction (considering the surfactant) is 23%.

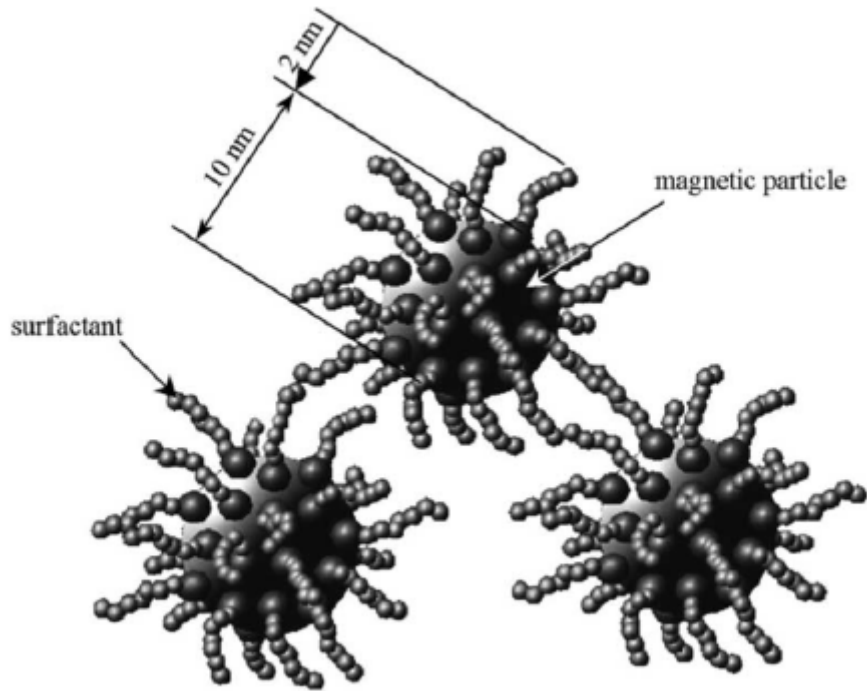


Figure 1 – Surface coated magnetic particles. The diameter of the particle is 10 nm and its hydrodynamic diameter is 14 nm. Figure adapted from (ODENBACH, 2003).

The rheological behavior of ferrofluids is for the most part determined by their magnetic properties. As it was stated above, each magnetic nanoparticle is considered as a thermally agitated permanent magnet dispersed in the carrier liquid. In the presence of an external magnetic field \mathbf{H} , the magnetic moment \mathbf{m} of the particles will try to align with the magnetic field direction, leading to a macroscopic magnetization of the liquid. According to Odenbach (2003), the magnetization \mathbf{M} can be described by a paramagnetic behavior, due to the fact that the particles are extremely small. The referred author also punctuates that the number of magnetic units, in a magnetic particle, interacting with the external magnetic field is high. As a result, a ferrofluid experiences a strong increase on its magnetization for weak magnetic fields, that is, this material presents an intense initial magnetic susceptibility. Because the force exerted by a magnetic field gradient on a magnetized system is proportional to its magnetization, ferrofluids experience strong magnetic forces, even for weak magnetic fields due to their high initial susceptibility. This magnetic force enables an efficient control of the liquids flow by moderate magnetic fields with a strength of less than 50 mT, which can be easily produced by permanent magnets or small electromagnets.



Figure 2 – The magnetic force exerted by the electromagnet to a ferrofluid is strong enough to keep it attached against the earth’s gravitational field and yet to form the characteristic spike pattern. Adapted from (ODENBACH, 2009).

Ferrofluids were firstly developed by NASA in 1965 to be used as a fuel of low viscosity in low gravity environments (STEPHEN, 1965). Nonetheless, according to Rosensweig (2013), ferrofluids are interesting to be used in technical applications for no other reason than the uniqueness of their giant magnetic response, which, as discussed previously, make them possibly remote controllable by an external magnetic field. This fact has motivated many efforts in the design of applications using the influence of a magnetic field, especially when the ferrofluid is located inside a technical device. This has led to the creation of several patents concerning this kind of applications, which are described on (BERKOVSKI; BASHTOVOY, 1996). Some interesting applications are: design of zero-leakage rotary shafts seals used in computer disk drives (BAILEY, 1983), design of pressure seals for compressor and blowers (ROSENSWEIG, 1979), design of electric rotating machines with improved efficiency, in which the ferrofluid is placed between the stator and the rotor to enhance strength and quantity of movement (NETHE; SCHOLZ; STAHLMANN, 2006). Besides those applications, ferrofluids are highly applied nowadays on the loudspeakers of Hi-Fi sound systems. In these devices, the membrane of the speaker is attached to the voice coil, which is controlled by a magnetic field generated by a permanent toroidal magnet. Placing a ferrofluid in the magnetic field around the voice coil enhances thermal conductivity in this region, resulting on an increased heat transfer to the speaker’s structure. This increases the devices cooling capacity and, thus, permits the increase of the maximum power of the sound system (ODENBACH, 2003).

Other front of ferrofluid’s applications is in the field of biomedicine, in which they have been a focus of research for more than three decades. Scherer and Neto (2005) summarize these applications on four groups:

- Magnetic drug targeting: applications on this area are based on coating the magnetic particles of a ferrofluid with chemotherapeutic drugs, which are, then, injected on a cancer tumor. Through a suitably focused magnetic field, the fluid is kept in the target area during some time, in order for the drug to reach its maximum action. Besides that, it is important to remark that the amount of drug needed is much less than the one that would be necessary if it was dispersed in the whole body. Also, when the magnetic field is turned off, the drug will disperse in the body, but, since the total amount is very small, there will be practically no side effects. [Lübbe, Alexiou and Bergemann \(2001\)](#) present various options of treatment lines using the technique described above. [Alexiou et al. \(2002\)](#) report the use of a ferrofluid coated with a powerful chemotherapeutic drug on 26 tumor-bearing rabbits, showing absolute success on healing the tumors with minimal side effects. Further bibliography on the topic can be obtained on ([MÜLLER; JACOBS; KAYSER, 2001](#)) and ([JURGONS et al., 2006](#));
- Magnetic hyperthermia: this application is based on the property of ferrofluids of absorbing electromagnetic energy at a frequency that is different from the frequency at which water absorbs energy. It allows one to heat up a localized portion of a living body, where a ferrofluid has been injected, such as example a tumor, without heating at the same time the surrounding parts of the body. In applications, the temperature reached by the contaminated tissue is in the range of 43 - 55 °C, depending on the concentration and specific heat of the material and also on the parameters of the applied magnetic field ([DIAS, 2015](#)). Reports on the use of nanoparticles to locally heat tumors can be found on ([JORDAN et al., 2001](#)), ([BRUSENTOV et al., 2002](#)), ([BRUNKE et al., 2006](#)) and ([GLÖCKL et al., 2006](#)). Figure (3), adapted from ([JORDAN et al., 2001](#)), shows a prostate cell remarkably pigmented, due to large magnetic nanoparticles uptake, ready for undertaking a process of magnetic hyperthermia;
- Contrast enhancement for magnetic resonance imaging (MRI): this image acquiring technique has been one of the most powerful diagnose techniques used in medicine nowadays. Its ability to distinguish between different tissues relies on the different relaxation times T2 of the proton's magnetic moments when they are inside different environments. Frequently, however, the differences are not strong enough to render well resolved images. If magnetic particles from a biocompatible ferrofluid are selectively absorbed by some kind of tissue, this will become very clearly visible by MRI. [Pouliquen et al. \(1989\)](#) report a new contrast composed by biocompatible magnetic nanoparticles for better visualization of liver tissues. Further successful applications of ferrofluids as contrast enhancer are discussed on ([PANKHURST et al., 2003](#));
- Magnetic separation of cells: It is often advantageous to separate out specific biological entities from their native environment, for different possible reasons: to

produce concentrated samples of these entities or to freed an infected sample from them. [Scherer and Neto \(2005\)](#) argue that the separation process is carried out on two steps: the first is to fix a biocompatible magnetic particle to the desired biological entity, and the second is to pull the magnetic particles, together with their "prey" out of the native environment by the action of a magnetic field gradient. Examples of applications and details on the technique can be found on ([ŠAFARĚIK; ŠAFARĚIKOVÁ, 1999](#)).

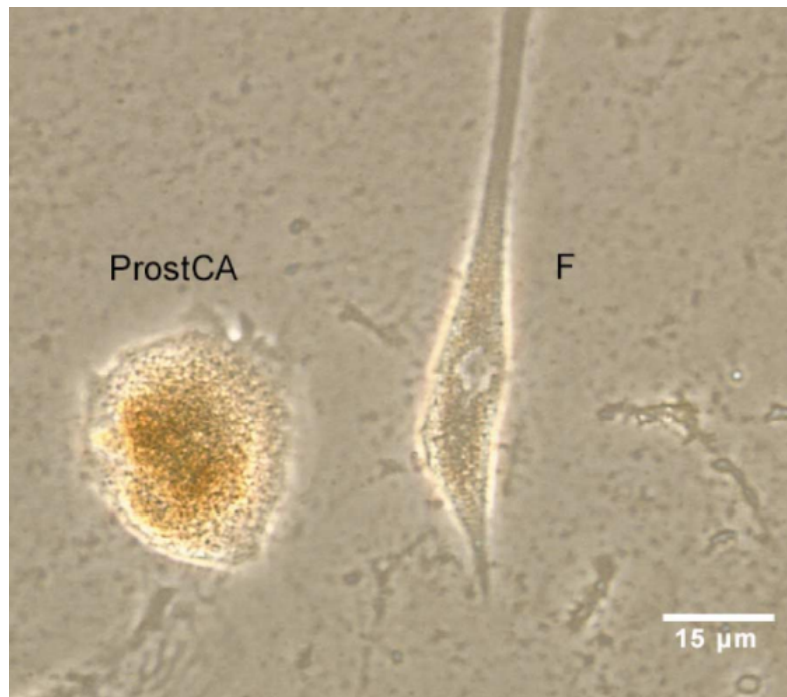


Figure 3 – Prostate cancerous cell uptaked by magnetic large particles - "*ProstCA*" (high pigmentation) compared to a healthy cell - "*F*" (no pigmentation). Adapted from ([JORDAN et al., 2001](#)).

Motivated by phenomenological interests on the complex rheology of ferrofluids when subjected to an external magnetic field and by its several and constantly evolving applications, it will be studied, in this dissertation, the field-induced rheological properties of two commercial ferrofluids.

1.2 Bibliografic review

The modeling of the hydrodynamics of magnetic fluids combines the fluid mechanics of colloidal suspensions with the fundamental equations of electromagnetism. [Cunha \(2012\)](#) and [Rosensweig \(2013\)](#) punctuate that the intersection of those areas for a non-conductor magnetic fluid, free of the action of electric fields and currents, defines the area of ferrohydrodynamics (FHD). In the absence of external magnetic fields, the Brownian motion (thermal agitation) orients the the magnetic dipoles of the particles randomly,

resulting on a state characterized by the nonexistence of a mean magnetization and, as a result, on a fluid that behaves as an ordinary suspension. On the other hand, when an external magnetic field is applied, the magnetic dipoles begin to experience the action of the magnetic forces resulting from magnetic field gradients and of the action of magnetic torques arising from the misalignment between the dipole and the magnetic field. Considering the ferrofluid as an equivalent continuous fluid (KIM; KARRILA, 2013), the actions of the magnetic field over the particles are considered to propagate to the base fluid as extra stresses. That being said, the stress tensor for the referred theoretical fluid has the following stress tensor:

$$\Sigma = \Sigma_h + \Sigma_m, \quad (1.1)$$

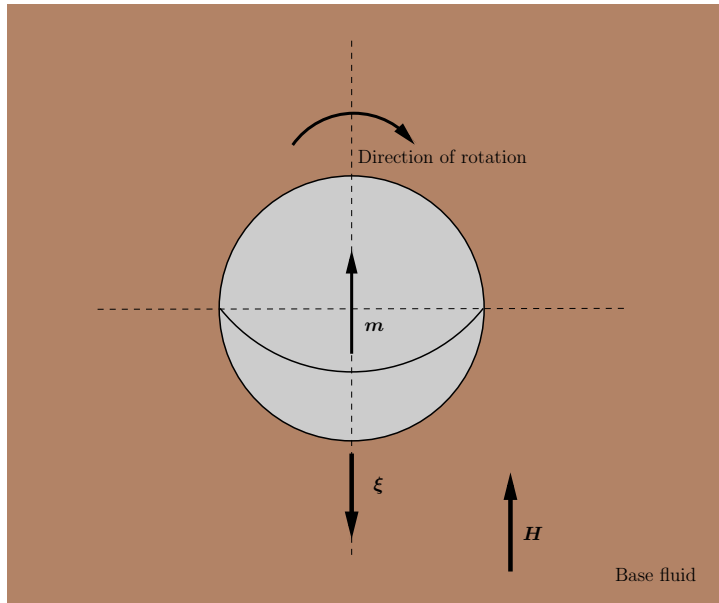
where Σ_h is the purely hydrodynamic tensor and Σ_m is the magnetic contribution. The equivalent stress tensor cannot be deduced only from the balance equations of continuum mechanics, due to the fact that it needs constitutive models that describe the material. The formulation of Σ_m is one of the open problems concerning the hydrodynamics of magnetic fluids. The problem becomes more complex when the magnetic fluid is concentrated, because, in this regime, hydrodynamic and magnetic interactions between the particles start to become relevant, even leading to the generation of fluctuations on the velocity of the particles.

The complex relation between the electromagnetic and hydrodynamic quantities leads to the necessity of performing thorough characterizations of the rheological behavior of ferrofluids from both, theoretical and experimental, points of view. In this context, rheometry plays a key role, owing to the fact that it permits the evaluation of the dependence of the complex fluid's material functions, such as the apparent viscosity and the shear stress, on both flow- and magnetic-related parameters. According to Tanner (2000), such evaluations can be done using various types of rheometric flows, like simple shear (linear), oscillatory shear, step-strain or even quadratic shear, observed in capillary. Each of these flows provide information on specific material functions, which can be used to study the adherence of a wide range of constitutive models, theoretical and *ad-hoc*, to specific experimental data, in a process aiming the description of the rheological behavior of the complex fluid.

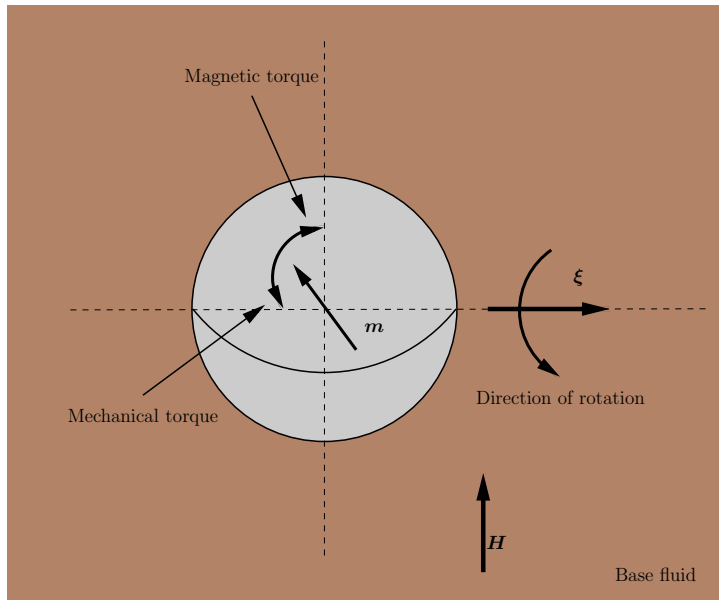
Generally, the effect of a magnetic field on a sample of ferrofluid leads to two effects: the appearance of magnetic forces over the magnetic particles and the emergence of internal magnetic torques on the particles due to the misalignment between the magnetization and the magnetic field. The first one leads to applications like the magnetic separation used, as discussed, on medical applications, but also explored by Cunha and Sobral (2004) as possible remediation technology to oil spills in natural environments. Besides that, this effect is also used in drag reduction in pipe flow (ROSA; GONTIJO; CUNHA, 2016). The second effect, the one arising from the field induced magnetic torques, is of extreme importance to understand the rheological behavior of ferrofluids, being therefore, the focus of this work. Our experiments are carried out on a rheometer of parallel disks, which is

also able to apply an uniform magnetic field orthogonal to the plates.

The first step into the comprehension of the rheological implications of applying an external magnetic field on a magnetic colloid was done by [McTague \(1969\)](#). In this work, the author used a ferrofluid composed by cobalt (Co) particles, with a core diameter of 10nm and a hydrodynamic diameter of 30nm (considering the polymeric surfactant coating), dispersed in an organic solvent with a volume concentration as low as 0.05%. He measured the viscosity of this magnetic colloid using a capillary viscometer, whose test area was immersed on a uniform magnetic field, with controllable intensity and direction. From this experiments, [McTague \(1969\)](#) discovered that the viscosity of the referred fluid increased in the presence of a magnetic field. The viscosity was found to depend not only on the intensity of the magnetic field, but also on its direction relative to the flow. In this paper and in the paper of [Hall and Busenberg \(1969\)](#), the effect was explained by a hindrance of rotation of the suspended particles due to the action of the magnetic field. In order to completely understand this concept, consider a situation in which a magnetic fluid is subjected to a shear flow. It can be assured that the particles inside the fluid will start to rotate with the axis of rotation parallel to the vorticity ξ of the flow due to the mechanic torque resultant of viscous friction in the fluid. Nonetheless, when an external magnetic field \mathbf{H} is applied to the system, the magnetic moment \mathbf{m} of the particles will align with the field direction. In a situation where the field direction and the vorticity of the flow are collinear, as shown in figure (4a), the magnetic alignment will only lead to the fact that the magnetic moment of the particles will align with the direction of the vorticity, that is, the particle will rotate around the field direction and, as a result, no influence on the flow will appear. In contrast, if the field is perpendicular to vorticity, as shown in figure (4b), the mechanic torque will tilt the particle's magnetic moment against the field direction, assuming that the moment of dipole is spatially fixed in the particle. The resulting finite angle between the magnetic moment and the field direction will give rise to a magnetic torque, which counteracts the viscous torque and try to realign the moment of dipole with the magnetic field. The counter action of the torques results in a hindrance of free rotation of the particles in the flow, an thus in an increase of the fluid's viscosity. The magnetic field-dependent viscosity was named rotational viscosity and the effect, magetoviscous effect ([ODENBACH, 2003](#)).



(a)



(b)

Figure 4 – On the origin of the magnetoviscous effect in a suspension of magnetic nano particles. Explanation is given in the text.

Four years after the discovery of the magnetoviscous effect, [Shliomis \(1971\)](#) faced the problem from a theoretical point of view. Taking into account the Brownian effect on an previous explanation by [Hall and Busenberg \(1969\)](#), he derived an expression for the change of the rotational viscosity as a function of the strength and direction of the magnetic field \mathbf{H} , which is given by

$$\eta_r = \frac{3}{2} \phi_h \eta_0 \frac{\alpha - \tanh(\alpha)}{\alpha + \tanh(\alpha)} \langle \sin^2 \beta \rangle, \quad (1.2)$$

where, η_0 denotes the viscosity of the fluid in the absence of external magnetic field¹, ϕ_h is the hydrodynamic volume fraction of particles (includes surfactant), $\langle \sin^2 \beta \rangle$ is a spatial average of the angle between the vorticity and magnetic field direction. Besides that, α is a parameter that denotes the ratio of magnetic and thermal energy of the particles, given by

$$\alpha = \frac{\mu_0 m H}{k_b T}, \quad (1.3)$$

where μ_0 is the vacuum permeability, m is the intensity of the particle's magnetic moment, k_b Boltzmann's constant and T is the absolute temperature. Shliomi's explanation of rotational viscosity has been built based on two constrains: first, the magnetic moment is fixed in the particle, and second, the particles do not interact. According to [Odenbach \(2009\)](#), the first assumption depends on the way that the magnetization relaxes. [Fannin \(2002\)](#) argues that the relaxation process can be carried out by thermal agitation effects, that is by Brownian motion ([FRENKEL, 1955](#)), through which this property relaxes by random rotations of the whole magnetic particle, implicating that \mathbf{m} is fixed on the particle. The magnetization can also relax by the rotation of the magnetic dipole vector within the particle (Néel process) ([NÉEL, 1953](#)). According to the refereed author, the magnetization will relax through the process with the small characteristic time. As reported by [Fannin \(2002\)](#) both times depend on the size of the particles but the Brownian time scales only linear with the particle's volume while the Néel time depends exponentially on it. This implies that small particles will relax by Néel's process, while particles above a certain critical diameter will follow the Brownian process. Particles that relax by the Brownian effect have the moment of dipole spatially fixed on them, being denominated magnetically hard. [Odenbach and Thurm \(2002\)](#) affirm that only hard particles contribute to changes on viscosity. For magnetite, the transition from Néel's process to Brownian relaxation occurs for diameters about 13 nm.

Regarding this context, commercial ferrofluids containing magnetite particles with a mean diameter of 10 nm would be expected to present weak magnetoviscous effect due to the fact that only a small volume fraction of large particles contained in the fluid would be able to contribute to magnetoviscosity. Nonetheless, [Rosensweig \(1979\)](#), [Odenbach, Rylewicz and Heyen \(1999\)](#), [Patel, Upadhyay and Mehta \(2003\)](#) reported observation of strong magnetoviscous effect in concentrated colloids of magnetite, which is the case of commercial ferrofluids, whose volume concentration of particles are in the range of 7-10%. This could only be explained by the formation of magnetic-induced structures build up by action of dipolar interactions between the numerous particles contained in the fluid. Other factor that speaks in favor of this assumption is the fact that those fluids exhibit a field dependent shear-thinning as was observed by [Odenbach and Störk \(1998\)](#), that is, their field-induced structures nor only exists, but are being broken by the action of the shear, which leads to a reduction of their hydrodynamic size and, as a result,

¹ The suspensions considered by [Shliomis \(1971\)](#) are highly dilute, thus η_0 is Einstein's viscosity ([EINSTEIN, 1911](#)), given by $\eta_0 = \eta_{s0}(1 + 2.5\phi_h)$. In this equation, η_{s0} is the viscosity of the base fluid (without particles) and ϕ_h is the hydrodynamic volume fraction of particles.

of their influence in the flow. [Odenbach \(2003\)](#) states that, since the magnetic dipole interaction energy of particles with diameter below 13 nm is less than their thermal energy, such particles cannot form permanent structures. This leads to the hypothesis that only a small fraction of large particles gives rise to the strong magnetoviscous effect, which was experimentally validated by [Odenbach and Raj \(2000\)](#). More recently, [Gontijo and Cunha \(2015\)](#) have carried out dynamic simulations of a magnetic suspension with particles interacting magnetically in a periodic box, in the presence of an applied magnetic field. These simulations demonstrated the gradual formation of particle structures like aggregates and their transitions to anisotropic chains of aligned particles, induced by magnetic effects.

[Cunha, Rosa and Dias \(2016\)](#) present an experimental investigation of the rheological behavior of very diluted magnetic suspensions with micro-structures of nanoparticles. The suspensions are composed by magnetite particles with a mean diameter of 8nm dispersed on mineral oil, being produced in a wide variety of particle volume fractions. The viscosity of the suspensions are measured as a function of the intensity of the applied magnetic field, shear rate and particle volume fraction. They also investigate the microstructure transitions provoked by the application of an external magnetic field to the suspensions. The authors observed that, under the action of magnetic fields, there is a strong connection between the rheological behavior of the magnetic suspensions and their microstructure, even in regimes of high dilution. The authors report the increase of the viscosity of the magnetic suspensions with the applied magnetic field, stating that this behavior is directly related to the formation of networks of particles or micro blobs-like aggregates through the suspension. In this work is also shown that, in the absence of magnetic field and in a regime of highly diluted suspensions, the effective viscosity of the suspensions presents a linear dependence on the particles volume fraction, i. e. Einstein regime. It was also reported a shear-thinning behavior of the suspensions when in the presence of an external magnetic field, which was directly linked to the stretching and breaking of the field-induced structures of different shapes and sizes by the action of shear-flow. Images of the anisotropic chains and aggregates have been acquired, what made possible to visually associated changes on the rheological behavior of the suspensions to modifications in the size and shapes of the particles chains and aggregates.

An opposite effect to magnetoviscosity has also been reported on the literature, which is called the "negative" rotational viscosity. [Bacri, Cebers and Perzynski \(1994\)](#) showed and proved by experimental evidence that when a rotating magnetic field is applied to the flow of a ferrofluid the dependence of its rotational viscosity on the frequency of rotation is given by:

$$\eta_r = \frac{3}{2}\eta_0\phi_h \frac{\Omega - \omega_p}{\Omega}, \quad (1.4)$$

where, Ω is the angular velocity resultant from the fluid's vorticity evaluated in the particle's center of mass and ω_p is the angular velocity of the particle induced by the rotating magnetic field. If the frequency ω_p is smaller than Ω , the free particle rotation will be

impeded and as a result a viscosity increase will be observed (magneto viscous effect). However, for large field frequencies, ω_p may become larger than Ω and, as a result, the particles will spin up the flow, converting magnetic energy on kinetic. This gives rise to a reduction of viscosity due to the negative dependent term in the expression for the rotational viscosity. For extremely high frequencies $\omega_p \gg \Omega$, the rotational viscosity was observed to assume negative values. It is important to remark that $\eta_r = \eta(H) - \eta_0$, thus a negative value of η_r implicates that the viscosity evaluated in the presence of the magnetic field $\eta(H)$ is smaller than the viscosity of the fluid in the absence of magnetic field.

The formation of particle's chains due to the action of an external magnetic field will not only enhance the field dependent increase of viscosity on a ferrofluid. According to [Odenbach \(2000\)](#), it will also provide the possibility to generate field dependent viscoelastic effects, which may give rise to new classes of applications of ferrofluids. The existence of viscoelastic effects in commercial ferrofluids was firstly predicted in the theoretical work of [Zubarev \(1992\)](#), in which the author foresees the appearance of field-induced normal stresses differences on magnetic colloids. This prediction led to an experimental search for the existence of the Weissenberg effect in commercial ferrofluids. This effect, the rise of a free surface of a viscoelastic fluid around a rotating axis should be dependent on the intensity of the magnetic field and on the shear flow in the case of a ferrofluid. For vanishing magnetic field, the liquid behaves Newtonian and, as a result, the free surface lowers at the rod axis due to the action of centrifugal forces. In commercial ferrofluids, this effect was found to be too small to be observed in normal terrestrial experiments, nonetheless, an amplification of the free-surface elongation effects is possible by performing the experiments under reduced gravity conditions. This has been done by [Odenbach, Rylewicz and Rath \(1999\)](#), using parabolic flights that provided 20s of microgravity environment. The Weissenberg effect was observed, which was the first experimental confirmation of the existence of normal stress differences in this kind of fluid and, thus, of viscoelasticity in commercial magnetic fluids containing magnetite particles with a mean diameter of 10nm.

Since the appearance of viscoelastic behavior on commercial ferrofluids had been confirmed, theoretical and experimental works have been carried out exploring this phenomenon. [Odenbach and Thurm \(2002\)](#) report the use of a rheometer cone-and-plate to directly evaluate the viscoelastic properties of the commercial ferrofluid APG513A through experiments of small amplitude oscillatory shear. The author affirms that this kind of flow has an important advantage, which is the fact that it does not change the "zero-shear-rate" structure of the fluid, due to small applied amplitudes of the shear applied. In the referred study, it has been measured the phase shift δ between shear and stress. It is important to remark that for an elastic body this phase shift should be zero, while for a Newtonian liquid, $\delta = \pi/2$ is expected. The samples used in the experiments had different concentration of large particles, which was achieved by means of magnetic separation. [Odenbach and Thurm \(2002\)](#) report the use of a trapezoidal container, where

a sample of 300 ml of APG513A is placed. After, this device is subjected to a vertical magnetic field gradient of 10^7 A/m². This gives rise to two kinds of derivative samples: the upper fraction (collected from the upper part of the container) presented an average diameter of 11.6 nm, while the lower fraction, a mean diameter of 12.1 nm. It is important to remark that the original mean diameter of APG513A is 12 nm. Even under the action of an external magnetic field, the upper fraction showed a linear relation between stress and shear rate, indicating Newtonian behavior. This was confirmed by the fact that the measured phase shift, $\delta = \pi/2$, was constant over the whole range of oscillating frequencies ω . In contrast, two behaviors were observed for the lower fraction, in a condition of absence of external magnetic field, no phase shift was observed, indicating that the fluid behaves Newtonian. On the other hand, when a magnetic field was applied, the lower fraction presented a phase shift δ between 0 and $\pi/2$. The last effect comes from the fact that the lower fraction has a big amount of large particles what makes it more likely for chains and aggregates to form, injecting, thus, elasticity in the system. The phase shift was found to increase as the shear rate decreased, what is related to the fact that, in this condition, the length of the particle chains enhances, indicating that progressively the elastic-like behavior is becoming predominant. The phase shift of the original fluid takes values in between the phase shifts of the upper and lower fractions. To sum up, the authors punctuate that the higher number of large particles in the lower fraction fluid enhances the appearance of viscoelasticity and a reduction of the number of bigger particles in the upper fraction sample leads to a pure Newtonian system.

In the work of [Odenbach \(2009\)](#), it is reported the experimental analysis of field-induced viscoelasticity resultant from the application of an oscillatory stress on a ferrofluid. The author investigates the behavior of the complex viscosity of a ferrofluid for different magnetic field strengths, as a function of the frequency of the stress oscillations. It is reported that for vanishing magnetic field, the imaginary part of the complex viscosity $\eta''(\omega)$ also vanishes, as it is expected for a Newtonian fluid. Nonetheless, increasing the magnetic field strength, η'' enhances, clearly indicating the rise of viscoelastic effects in the fluid. It is also stressed that the frequency at which a pronounced maximum of the complex viscosity occurs corresponds to the inverse of the relaxation time of the magnetic structures in the fluid. It is pointed out that the increase of the frequency of the maximum indicates a reduction of the relaxation time with increasing field strength, which is explained by an enhanced alignment of the growing structure with the field direction.

The thematic of stress relaxation has been the focus of more recent rheological studies, both from a theoretical and experimental point of view. [Borin et al. \(2011\)](#) perform experiments on the relaxation of shear stress in a diluted ferrofluid with clustered magnetic nanoparticles ($\phi = 0.1\%$). It was observed that the fluid under analysis showed field-induced viscoelasticity, resulting in slow relaxation phenomena. Elasto-thixotropy of the fluid and further transient behavior under shear-flow result from the deformation and destruction of agglomerates of the magnetic clusters and depend strongly on the relation

between magnetic field strength and the rate of mechanical deformation. The authors punctuate that the transient time until shear stress in the fluid become steady can reach several minutes, what should be taken into account when carrying out rheological measurements and on the design of applications that use ferrofluid with strong interacting particles. It is also observed that a polymer-like behavior of the ferrofluids appears and is enhanced as the intensity of the external magnetic field increases. According to the authors, this rheological phenomena arises from the fact that, as the intensity of the field rises, magnetic-induced linear chains of those high interacting particles dominate the microstructure. [Yang et al. \(2006\)](#) by perpetrating experimental rheological investigations on aqueous ferrofluids in a regime of oscillatory shear report a constant value of the elastic modulus $G'(\omega)$ for a wide range of frequencies of oscillation. This behavior has a parallel on polymer dynamics, being, according to [Doi and Edwards \(1988\)](#), an indication of formation of a 3D network. Similar to the theory of polymers, the authors consider that the result discussed above is a rheological evidence of formation of 3D structure by particles and particle's aggregates in ferrofluids.

In other theoretical and experimental work, [Borin et al. \(2014\)](#) consider the stress relaxation of a ferrofluid based on clustered iron nanoparticles, under the influence of a magnetic field, when a simple shear flow is suddenly interrupted. The authors remark that, in this condition, the shear stress does not relaxes to zero after a sudden cessation of the flow, but instead, it reaches a constant value, named residual stress. The residual stress was found to increase as the magnetic field intensity enhances, due to the fact that high intensities of the magnetic field lead to the formation of aggregates with large size and improved overall stability. Moreover, it was also reported that the residual stress presented a dependence on the intensity of the shear being applied before the cessation of the flow. The residual stress was found to decrease as the shear rate increased. The reason of this behavior is the breakup of the field induced structures by the intensification of shear.

In the study by [Shahnazian and Odenbach \(2008\)](#), the appearance of yield stress was evaluated for three ferrofluids with different volume fractions of magnetic particles and mean particle diameter. From the fluid characteristics, a parameter was calculated that accounts for particle-particle interactions. It was observed that the yield stress increases with the square of the intensity of the magnetic field. Comparing ferrofluids with particles of the same average size (16 nm), the fluid with the smallest volume fraction of large particles did not exhibit yield stress even at the higher field strength (80 kA/m). On the other hand, for the fluid composed of particles with an average diameter of 10 nm, it was obtained higher values of yield stress due to its bigger fraction of large particles. This shows that there is a relationship between the yield stress and the amount of larger particles, owing to the fact that they are responsible for the formation of chains and aggregates. It was also observed that the yield stress increases as the distance between the rheometer discs decreases. This can be due to the interaction between the particles as

well as the amount of large ones in the measuring gap of the instrument. In this sense, the study by [Liu and Jin \(2011\)](#) analyzed the influence of the volume of liquid used between the discs of a rheometer. They found that the shear stress increases as the volume of liquid heightens due to the larger amount of magnetized particles

1.3 Objectives

The main objective of this work is the characterization of the rheological behavior of two ferrofluids, differing on their volume fractions of magnetic particles. The analysis will be mostly experimental, using a parallel plate rheometer with a magnetic cell. This device permits the application of several regimes of shear flow in the complex fluid under analysis and, also, to produce and maintain a controlled magnetic field in the zone where the fluid sample is being tested. Regarding this context, this dissertation has the following specific objectives:

- Perform a bibliographic review on themes related to the constitutive modeling of ferrofluids and to the rheological effects that arise from the interaction of a ferrofluid with a magnetic field;
- Investigate, through experiments in permanent simple shear in the presence of a magnetic field, the rheological behavior of the apparent viscosity of the ferrofluid as a function of the magnetic field intensity and of the shear rate. That is, to perform the characterization of the magnetoviscous effect and of the pseudoplastic behavior of the ferrofluid when tested in the presence of an external magnetic field;
- Using the same flow regime, perform the characterization of the behavior of the shear stress as a function of the shear rate for different intensities of the external magnetic field. Besides that, verify the existence of yield stress and the adherence of the collected experimental data to generalized Newtonian fluid constitutive models;
- Through experiments in the regime of transient shear, specifically the step-strain, obtain the stress relaxation functions for different conditions of magnetic field and flow intensities. Analyze the likely complex relaxation and obtain the main and secondary relaxation times as functions of the magnetic field intensity. Verify the adherence of the data collected for the stress relaxation functions to Maxwell's generalized viscoelastic model. Besides that, obtain the residual stress and study its dependence on the intensity of the magnetic field and on the shear rate;
- Using small amplitude oscillatory shear, verify the viscoelastic behavior of the ferrofluid in the presence of a magnetic field. Obtain the viscoelastic modules and analyze their dependence on the intensity of the magnetic field. Investigate the effect of the magnetic field on the viscous and elastic properties of the ferrofluids;

- For each fluid and magnetic condition, compare the modulus of the complex viscosity, measured on oscillatory shear, and the apparent viscosity, obtained from simple permanent shear, for compatible values of frequency and shear-rate. In case of agreement between the behavior of the referred material function, verify the applicability of empirical relations to determine the first normal stresses difference.

2 THEORETICAL BACKGROUND

In this chapter, it will be presented the fundamental laws of the mechanics of continuous media and of the electromagnetism. This is necessary due to the fact that these equations are the basis for the physical description of the flow of a magnetic fluid. Nonetheless, they are not enough to give a complete description of the fluid flow, what will be evident on the following sections.

2.1 Continuum hypothesis

Materials have a discontinuous molecular structure, since their mass is concentrated in the nucleus of the atoms that make up their molecules. As a result, it is found that this property is not evenly distributed throughout the volume of the material, even in liquids and solids, where the distance between molecules is reduced compared to gases. According to [Batchelor \(2000\)](#), other properties of the fluid, such as composition and velocity, exhibit a strongly nonlinear distribution when the fluid is analyzed from a sufficiently small scale to allow analysis of the behavior of individual molecules.

However, fluid mechanics has a focus on the behavior of matter on a macroscopic scale, which is characterized by a much larger typical length scale (L) when compared to the molecular scale (λ), associated to the mean distance between the molecules that compose the material. Between the macroscopic and the molecular scale is the local continuum scale (l). This scale defines a volume of material sufficiently small that it can be considered "local" relative to the volume comprised by the macroscopic scale, and large enough to contain a sufficient number of molecules. Such characteristics allow the behavior of the material to be analyzed assuming, by hypothesis, a perfectly continuous distribution of its microscopic structure and therefore of its physical properties, such as its mass. The scales referred to above are shown in the figure (5), which schematically represents a fluid particle \mathcal{P} in a continuous body \mathcal{B} .

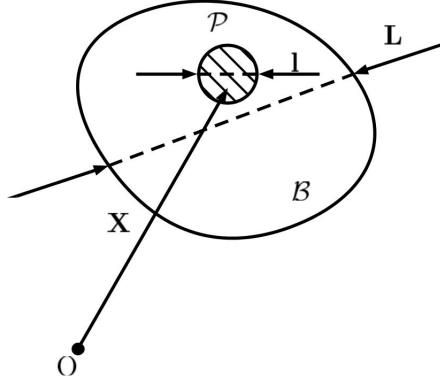


Figure 5 – Continuous body (\mathcal{B}), in which is presented a fluid particle (\mathcal{P}) and its typical scales, respectively, the integral (macroscopic) scale (L) and the local continuum scale (l).

(BATCHELOR, 2000) remarks that, on the continuum scale, the measured properties are effectively volumetric averages of the effects of molecules on the sensible volume (defined by the local continuum scale). Thus, it is observed that the fluctuations of the properties at the molecular level do not affect this average, which remains constant. However, with the increase of the scale parameter, we arrive at the integral scale, in which the spatial distribution of the property under study becomes important.

The continuum hypothesis ensures the possibility of associating a definite meaning to the notion of point (local) value of the most varied properties of a material, such as density, velocity and temperature. As a consequence, in the scale of the continuum, these properties are considered as continuous functions of the position in the local material volume and of the time. As an example, considering valid the continuum hypothesis, the density of a material can be defined as follows :

$$\rho = \lim_{\delta V \rightarrow \delta V'} \frac{1}{\delta V} \int_{\delta V} \sum_i m_i \delta(\mathbf{x} - \mathbf{x}_i) dV, \quad (2.1)$$

where $\delta V'$ is the volume of a material point, that is, the property is obtained as a volumetric average in the vicinity of that point. Based on this, it is possible to establish governing equations for the motion of the material particle that are independent of its constituent particles.

Arising out of the local scale (l) and molecular scale (λ) definitions, the Knudsen number (K_n), which is a nondimensional parameter, is specified as:

$$K_n = \frac{\lambda}{l}. \quad (2.2)$$

This dimensionless number is of great importance in determining the applicability of the continuum hypothesis. If the Knudsen number is close to or greater than one, the free mean path of a molecule is comparable to the length scale of the problem, so the consideration of continuity of the material properties is no longer a good approximation, and other fields of statistical mechanics must be used. Considering the case in which $0.01 < K_n < 0.1$, the

problem presents an interface condition, where the validity of the continuum hypothesis must be evaluated. Nonetheless, for values of $K_n < 0.01$ the hypothesis is strictly valid.

2.2 Governing equations of fluid motion

Fluids are substances that continuously deform (flow) when subjected to tangential stresses. Fluid flow is governed by a set of balance equations, namely: the continuity equation, the linear momentum balance equation, the angular momentum balance equation, and the energy equation.

2.2.1 Balance of Mass

The density of a given material is locally defined as follows:

$$\rho = \lim_{\delta V \rightarrow \delta V'} \frac{\delta m}{\delta V}, \quad (2.3)$$

where $\delta V'$ and δm are, respectively, the volume and the mass of the smallest material particle (\mathcal{P}), belonging to a material body \mathcal{B} , of volume V and mass m . Considering that \mathcal{B} meets the continuum hypothesis, the total mass of the body is given by:

$$m = \int_V \rho dV. \quad (2.4)$$

From the principle of conservation of mass, it is known that in a given control volume, the net effect of input, output and mass generation is null, which is mathematically expressed as:

$$\frac{Dm}{Dt} = 0, \quad (2.5)$$

where $\frac{D}{Dt}$ is the substantive derivative operator, which is defined based on an observer moving along with the material particle. This operator is expressed as follows:

$$\frac{D(*)}{Dt} = \frac{\partial(*)}{\partial t} + \mathbf{u} \cdot \nabla(*), \quad (2.6)$$

in which, $(*)$ is any property of the fluid and \mathbf{u} , the velocity field of the flow.

Replacing equation (2.4) into (2.5), one obtains:

$$\frac{D}{Dt} \int_V \rho dV = 0. \quad (2.7)$$

Then, applying the Reynolds transport theorem (ARIS, 2012), equation (2.7) is rewritten as:

$$\frac{D}{Dt} \int_V \rho dV = \int_V \frac{\partial \rho}{\partial t} dV + \int_S \rho \mathbf{u} \cdot \hat{\mathbf{n}} dS = 0, \quad (2.8)$$

where \mathbf{u} is the velocity field, S is the control surface and $\hat{\mathbf{n}}$ is the unit vector normal to S in the outward direction. From Gauss theorem (ARIS, 2012), it can be affirmed that:

$$\int_S \rho \mathbf{u} \cdot \hat{\mathbf{n}} = \int_V \nabla \cdot (\rho \mathbf{u}) dV. \quad (2.9)$$

Replacing this result on equation (2.8), one obtains that:

$$\frac{D}{Dt} \int_V \rho dV = \int_V \left(\frac{\partial \rho}{\partial t} + \nabla \cdot (\rho \mathbf{u}) \right) dV = 0. \quad (2.10)$$

As this equation is valid in all the volume of the material body \mathcal{B} , the theorem of localization (ARIS, 2012) can be applied to equation (2.10), which results in:

$$\frac{\partial \rho}{\partial t} + \nabla \cdot (\rho \mathbf{u}) = 0. \quad (2.11)$$

Developing equation (2.11), one obtains:

$$\frac{\partial \rho}{\partial t} + \rho \nabla \cdot \mathbf{u} + \mathbf{u} \cdot \nabla \rho = 0. \quad (2.12)$$

rearranging the terms of equation (2.12), it can be rewritten as:

$$\frac{D\rho}{Dt} + \rho \nabla \cdot \mathbf{u} = 0, \quad (2.13)$$

which is named the equation of continuity. Expression (2.13) represents mathematically the physical principle of mass conservation applied to an element of a continuous material.

2.2.2 Balance of linear momentum

The linear momentum (\mathbf{P}) of a continuous body \mathcal{B} is given by:

$$\mathbf{P} = \int_V \rho \mathbf{u} dV. \quad (2.14)$$

From Newtons' second law of motion, it is known that the variation of linear momentum is equal to the sum of all external forces that act on the continuous body. Formalizing this principle, one obtains that:

$$\frac{D\mathbf{P}}{Dt} = \mathbf{f}, \quad (2.15)$$

where \mathbf{f} is the resultant of all external forces, which can be divided in two groups: field and surface forces. As a result, \mathbf{f} can be rewritten as :

$$\mathbf{f} = \int_V \rho \mathbf{b} dV + \int_S \mathbf{t} dS, \quad (2.16)$$

in which \mathbf{b} is a force per unit of volume and \mathbf{t} is the stress vector, also called traction, which is defined from Cauchy's theorem (BATCHELOR, 2000) as:

$$\mathbf{t} = \hat{\mathbf{n}} \cdot \boldsymbol{\Sigma}, \quad (2.17)$$

where $\boldsymbol{\Sigma}$ is the stress tensor. Replacing this result in equation (2.16), one obtains:

$$\mathbf{f} = \int_V \rho \mathbf{b} dV + \int_S \hat{\mathbf{n}} \cdot \boldsymbol{\Sigma} dS. \quad (2.18)$$

This expression can be rewritten by applying the theorem of divergence (ARIS, 2012) as:

$$\mathbf{f} = \int_V (\rho \mathbf{b} + \nabla \cdot \boldsymbol{\Sigma}) dV. \quad (2.19)$$

From the theorem of localization (ARIS, 2012) and regarding equation (2.15), one can write that:

$$\frac{\rho D(\mathbf{u})}{Dt} = \rho \mathbf{b} + \nabla \cdot \boldsymbol{\Sigma}, \quad (2.20)$$

in which, \mathbf{b} is the gravity acceleration vector. The stress tensor $\boldsymbol{\Sigma}$ determines the distribution of stress in the continuous medium, the presents the following form:

$$\boldsymbol{\Sigma} = -p\mathbf{I} + \boldsymbol{\sigma}, \quad (2.21)$$

where p is the mechanic pressure and \mathbf{I} is the identity tensor, which together form the isotropic part of the stress tensor, $\boldsymbol{\sigma}$ is the deviatoric part of it, being associated with the shear stresses that develop over the material.

Equations (2.13) and (2.20) govern the flow of any homogeneous continuous medium, however, they are not able to describe the response of the material. To do that, it is necessary to know the relationship between stress and strain specifically for the material being analyzed, which is done by proposing constitutive equations for $\boldsymbol{\sigma}$, what allows the obtainment of the stress tensor $\boldsymbol{\Sigma}$. Constitutive equations are generally determined from experimental observations or theoretically by a process of proposing hypotheses. However, such expressions should fit a set of fundamental principles, which will be covered in the next chapter.

2.3 Principles of electromagnetism

In this section it will be discussed the fundamental quantities and the governing equations of the electromagnetism. The Maxwell's equations are presented and particularized for the regime of the ferrohydrodynamics. After that, it will be deduced the magnetic force and torque acting upon a magnetic dipole. Such discussions are of high importance for the deduction of a constitutive equation for the deviatoric part of the stress tensor of a magnetic fluid, which will be done in section (3.2.2).

It is important to remark that the International System of Units will be used in this work, thus the form of the governing equations may differ from those presented on other studies that use the CGS system.

2.3.1 Maxwell's equations

The electromagnetism is governed by the four Maxwell's equations, that relate the main electric and magnetic quantities. In order to derive those equations, we will start by

discussing the phenomenological laws, which are: Gauss' Law of Electricity, Gauss' Law of Magnetism, Faraday's Law and Ampère's Law.

The Gauss' law of electricity relates the net rate of an electric field vector \mathbf{E} to the charge q in the interior of an enclosed surface S of a certain volume V , that is

$$\int_S \mathbf{E} \cdot \hat{\mathbf{n}} dS = \frac{q}{\epsilon_0}, \quad (2.22)$$

to which applying the theorem of divergence, one obtains

$$\int_V \nabla \cdot \mathbf{E} dV = \frac{q}{\epsilon_0}, \quad (2.23)$$

where ϵ_0 is the vacuum permittivity, whose value in the in the international system of units is $8.854 \times 10^{-12} \text{C}^2/\text{Nm}^2$. Using on equation (2.23) the localization theorem (ARIS, 2012), one obtains that

$$\nabla \cdot \mathbf{E} = \frac{\rho_q}{\epsilon_0}, \quad (2.24)$$

where ρ_q is the charge density in the volume V . For dielectrics, this parameter is given by

$$\rho_q = \rho_l + \rho_p, \quad (2.25)$$

in which, ρ_l is the free-charge density and ρ_p is the density of polarized charges, that is defined as

$$\rho_p = \nabla \cdot \mathcal{P}, \quad (2.26)$$

where \mathcal{P} is the polarizing vector of the dielectric. Now, substituting expression (2.26) and (2.25) on equation (2.24), one obtains, after rearranging the terms, that

$$\nabla \cdot (\epsilon_0 \mathbf{E} + \mathcal{P}) = \rho_l. \quad (2.27)$$

The vector $\epsilon_0 \mathbf{E} + \mathcal{P}$ is defined as the electric displacement vector \mathcal{D} . Based on this, equation (2.27) becomes:

$$\nabla \cdot \mathcal{D} = \rho_l. \quad (2.28)$$

This expression is the Gauss Law of Electricity and also the first Maxwell's equation on its differential non-relativistic form.

The fundamental quantities regarding the magnetism are the vector of magnetic field density \mathbf{B} and the effective magnetic field vector \mathbf{H} . In general, it can be considered that \mathbf{B} is the fundamental physical quantity given its further generality granted by the fact that it can defined directly from the law of Biot-Savart (GRANT; PHILLIPS, 2013) applied to an electric circuit C traversed by a current \mathbf{I} ,

$$\mathbf{B} = \frac{\mu_0}{4\pi} \oint_C \frac{\mathbf{I} \times \mathbf{x}}{x^3} dl, \quad (2.29)$$

where, \mathbf{r} is the position vector of the line element dl . The Gauss' law of the magnetism is a direct consequence of the nonexistence of magnetic monopoles, postulating that the flux of \mathbf{B} trough an enclosed surface S is null,

$$\int_S \mathbf{B} \cdot \hat{\mathbf{n}} dS = 0, \quad (2.30)$$

in which $\hat{\mathbf{n}}$ is the unit vector normal to the surface S point outwards from it. Applying the divergence theorem to equation (2.30), one obtains

$$\int_V \nabla \cdot \mathbf{B} dV = 0. \quad (2.31)$$

Applying the theorem of localization to the last equation, it comes that

$$\nabla \cdot \mathbf{B} = 0. \quad (2.32)$$

This is the Gauss' Law of Magnetism and also the Second Maxwell's equation.

Faraday's Induction Law relates the circulation of the electric field vector on a closed circuit C to the temporal variation of the density of magnetic flux \mathbf{B} that transverses the surface S limited by C , which is represented mathematically as

$$\int_C \mathbf{E} \cdot d\mathbf{l} = -\frac{D}{Dt} \int_S \mathbf{B} \cdot \hat{\mathbf{n}} dS. \quad (2.33)$$

Applying Leibniz theorem for surface integrals, one obtains:

$$\frac{D}{Dt} \int_A \mathbf{B} \cdot \hat{\mathbf{n}} dS = \int_S \left(\frac{\partial \mathbf{B}}{\partial t} + \nabla \cdot \mathbf{u} \mathbf{B} \right) \cdot \hat{\mathbf{n}} dS - \int_S \mathbf{B} \hat{\mathbf{n}} : \nabla^T \mathbf{u} dS. \quad (2.34)$$

Considering the surface S fixed in the space, that is $\mathbf{u} = 0$, equation (2.34) assumes the following form:

$$\frac{D}{Dt} \int_A \mathbf{B} \cdot \hat{\mathbf{n}} dS = \int_S \frac{\partial \mathbf{B}}{\partial t} \cdot \hat{\mathbf{n}} dS. \quad (2.35)$$

Replacing this result on equation (2.33), it comes that:

$$\int_C \mathbf{E} \cdot d\mathbf{l} = - \int_S \frac{\partial \mathbf{B}}{\partial t} \cdot \hat{\mathbf{n}} dS. \quad (2.36)$$

Since the domain under analysis is considered to be regular, Stokes' Theorem can be applied to the integral on the left of equation (2.36), what leads to:

$$\int_S (\nabla \times \mathbf{E}) \cdot \hat{\mathbf{n}} dS = - \int_S \frac{\partial \mathbf{B}}{\partial t} \cdot \hat{\mathbf{n}} dS. \quad (2.37)$$

Rearranging the terms, one obtains:

$$\int_S \left(\nabla \times \mathbf{E} - \frac{\partial \mathbf{B}}{\partial t} \right) \cdot \hat{\mathbf{n}} dS = 0. \quad (2.38)$$

Applying to this equation the Theorem of Localization, one obtains the third Maxwell's equation:

$$\nabla \times \mathbf{E} = \frac{\partial \mathbf{B}}{\partial t}. \quad (2.39)$$

Ampère's law postulates that the circulation of the effective magnetic field vector \mathbf{H} around a closed circuit C is equals to the net rate of the intensity of current vector \mathbf{J} (i.e. the free current I_f) through the area S limited by C , which is expressed mathematically as

$$\int_C \mathbf{H} \cdot d\mathbf{l} = \int_S \mathbf{J} \cdot \hat{\mathbf{n}} dS = I_f. \quad (2.40)$$

Applying Stokes's Theorem on the left integral on this equation, one obtains

$$\int_S (\nabla \times \mathbf{H}) \cdot \hat{\mathbf{n}} dS = \int_S \mathbf{J} \cdot \hat{\mathbf{n}} dS. \quad (2.41)$$

Rearranging the terms, one gets

$$\int_S (\nabla \times \mathbf{H} - \mathbf{J}) \cdot \hat{\mathbf{n}} dS = 0. \quad (2.42)$$

Now applying the Localization Theorem to the last equation, it comes that

$$\nabla \times \mathbf{H} = \mathbf{J}, \quad (2.43)$$

which is the differential form of Ampère's Law, also named fourth Maxwell's equation in the case of steady regime of the current displacement ($\partial \mathcal{D} / \partial t = \mathbf{0}$).

As shown in this section, the Maxwell's equations of the electromagnetism are given by

$$\begin{cases} \nabla \cdot \mathcal{D}_e = \rho_l, & \text{(Gauss' law of the electricity)} \\ \nabla \cdot \mathbf{B} = 0, & \text{(Gauss' law of the magnetism)} \\ \nabla \times \mathbf{E} = \frac{\partial \mathbf{B}}{\partial t} & \text{(Faraday's law of induction).} \\ \nabla \times \mathbf{H} = \mathbf{J} + \frac{\partial \mathcal{D}_e}{\partial t}, & \text{(Ampère's law)} \end{cases} \quad (2.44)$$

Nonetheless, for applications in ferrohydrodynamics, it will be considered the magneto-static regime in which the effects of the flux of electric current and of the electric field can be disregarded, that is:

$$\mathbf{J} = \mathbf{0}, \quad (2.45)$$

and

$$\mathbf{E} = \mathbf{0}. \quad (2.46)$$

With those assumptions, the Maxwell's equations, for applications in ferrohydrodynamics, are given by:

$$\begin{cases} \nabla \cdot \mathbf{B} = 0, \\ \nabla \times \mathbf{H} = 0, \\ \frac{\partial \mathbf{B}}{\partial t} = \mathbf{0}. \end{cases} \quad (2.47)$$

2.3.2 Force and torque over a magnetic particle

Consider a punctual magnetic particle, with moment of magnetic dipole \mathbf{m} fixed on it, under the action of an external magnetic field \mathbf{H} . The moment of magnetic dipole can be defined by the product of the electric current I and the area S of a small closed plane circuit, that is

$$\mathbf{m} = IS\hat{\mathbf{n}}, \quad (2.48)$$

where $\hat{\mathbf{n}}$ is the unit vector normal to the circuit, oriented according to the right-hand convention. The magnetic force and torque over this particle resulting from the external

field \mathbf{H} will be analyzed using the principle of virtual work. According to [Grant and Phillips \(2013\)](#), the potential energy associated to this particle is given by

$$E_m = -\mu_0 \mathbf{H} \cdot \mathbf{m}. \quad (2.49)$$

Lets suppose a virtual angular displacement $\delta\boldsymbol{\theta}$ over the particle. As a result, the variation of the potential energy is

$$\delta E_m = \delta(-\mu_0 \mathbf{H} \cdot \mathbf{m}) = \mu_0 (\mathbf{H} \times \mathbf{m}) = \mu_0 (\mathbf{H} \times \mathbf{m}) \cdot \delta\boldsymbol{\theta}. \quad (2.50)$$

This energy variation is equal to minus the work exerted by the magnetic torque \mathbf{t}_m over the particle, thus

$$-\mathbf{t}_m \cdot \delta\boldsymbol{\theta} = \mu_0 (\mathbf{H} \times \mathbf{m}) \cdot \delta\boldsymbol{\theta}. \quad (2.51)$$

Then, by the principle of virtual work, the magnetic torque over the particle is:

$$\mathbf{t}_m = \mu_0 \mathbf{m} \times \mathbf{H}. \quad (2.52)$$

In order to obtain the magnetic force action on the particle, lets suppose a virtual displacement of translation $\delta\mathbf{x}$ applied to the particle. In this condition, the variation of potential energy becomes

$$\delta E_m = \delta(-\mu_0 \mathbf{H} \cdot \mathbf{m}) = -\mu_0 \nabla(\mathbf{H} \cdot \mathbf{m}) \cdot \delta\mathbf{x}. \quad (2.53)$$

In this case, the variation of energy is equals to minus the work exerted by the force \mathbf{f}_m over the particle, thus

$$-\mathbf{f}_m \cdot \delta\mathbf{x} = -\mu_0 \nabla(\mathbf{H} \cdot \mathbf{m}) \cdot \delta\mathbf{x}. \quad (2.54)$$

Applying the principle of virtual work, one obtains

$$\mathbf{f}_m = \nabla(\mu_0 \mathbf{H} \cdot \mathbf{m}). \quad (2.55)$$

The last expression leads to the definition of the magnetic scalar potential

$$\Psi_m = \mu_0 \mathbf{m} \cdot \mathbf{H}. \quad (2.56)$$

Since the dipole is constant for a given translation, the expression for the magnetic force can be rewritten as:

$$\mathbf{f}_m = \nabla(\Psi_m) = \mu_0 \mathbf{m} \cdot \nabla \mathbf{H}. \quad (2.57)$$

3 CONSTITUTIVE MODELS

This chapter begins by presenting a set of principles that any constitutive equation must fit in order to truly describe the rheological properties of a given material. After that, a constitutive model for the stress tensor of a highly diluted ferrofluid is obtained using concepts of continuum mechanics, electromagnetism and microhydrodynamics. In the rest of the chapter, other constitutive models for non-Newtonian fluids, case of ferrofluids in the presence of a magnetic field, are presented, due to the fact that most of them will be used in the analysis of the experimental results.

First, it is discussed the generalized Newtonian fluids, also called viscous non-Newtonian fluids, which are models based on the fact that viscosity, for non-Newtonian fluids, are not constant as a function of shear rate, are addressed. Based on this, very useful models for modeling this relationship are proposed in the literature, which are developed from empirical observations of the behavior of the most diverse fluids, usually performed in simple permanent shear experiments. However, a defining feature of these models is that they do not clearly capture the characteristics arising from the elastic properties of many non-Newtonian fluid classes, such as memory effects.

Then, the viscoelastic-linear models will be treated, aiming at the proposition of constitutive equations capable of modeling the behavior of viscoelastic fluids, that is, of materials that present, at the same time, elastic characteristics, associated with the typical behavior of solids. and dissipative, typical of fluids. These models will be demonstrated from the approach of small deformations, which, in turn, will allow the linearization of the problem. In addition, analogies with other physical systems such as mass spring-damper systems will be discussed to obtain the constitutive equations in order to capture the elastic and dissipative modules, besides the stress relaxation function, from which it is possible to determine The relaxation time spectrum for the most complex fluids is shown. It will also be presented the general model, proposed by [Oldroyd \(1956\)](#), for the constitutive equations in linear-viscoelasticity regime.

3.1 Constitutive formalism

In the later chapter, it has been verified the necessity of establishing a constitutive equation for the deviatoric part of the stress tensor ($\boldsymbol{\sigma}$) in order to complete the set of the

equations of motion, which associated with the equation of continuity, lead to a complete characterization of the problem. The purpose of the constitutive equations is to model the relationship between stress and strain as a function of material constitution, that is, from an informal point of view, it can be said that they inform the balance equation of momentum about the characteristics of material.

According to [Yamaguchi \(2008\)](#), the construction of constitutive equations for complex materials basically follows three different approaches: The first seeks to develop the constitutive equation from the generalization of a simple one-dimensional rheological equation, taking into account the principles of continuum mechanics in association with experimental analyzes. The second approach is derived solely from the general concepts of continuum mechanics, with a more phenomenological bias. The third is based on molecular dynamics in combination with the concept of the continuum, taking into account the molecular structure of the fluid. In this work, it will be presented a constitutive modeling for the stress tensor of magnetic fluids using the second approach.

However, regardless of the approach used in constructing a given constitutive equation, according to [Truesdell and Noll \(2004\)](#), there is a set of fundamental principles to which they must fit in order to truly describe the rheological properties of a given material, which are:

- Principle of causality;
- Principle of local action;
- Principle of coordinate invariance;
- Principle of fading memory;
- Principle of absence of a reference state; and
- Principle of the material frame indifference (objectivity).

Materials whose description fits these conditions are called simple materials. These principles are described in detail below.

Principle of causality

The principle of causality, also called the principle of determinism, or of cause and effect, postulates that the stress tensor $\boldsymbol{\sigma}$ depends on the recent history of the motion, i.e. the velocity field or deformation. From a more general point of view, a constitutive equation is said to relate the stress of the material in time t to the present and to previous experiences of deformation suffered by it, thus:

$$\boldsymbol{\sigma}(t) = \mathfrak{F}(\text{Deformation history of the material}), \quad (3.1)$$

where, $\boldsymbol{\sigma}$ is the stress tensor and \mathfrak{F} is a functional that involves derivatives and integrals of the velocity field with respect to time and space, and contains coefficients that can be associated with physical properties of the material (SALAS, 2006).

Principle of local action

The principle of local action postulates that only the material particles in a small neighborhood must be involved on the determination of the stress at a given point, i.e., this principle is consistent with the idea of short range forces between the particles of the material.

Consider a Lagrangian description of movement, in which the material body \mathcal{B} , at an initial position $\boldsymbol{\xi}$ in $t = 0$ moves to the position $\mathbf{X}(\boldsymbol{\xi}, \tau)$ in time τ and, after that, to the position $\boldsymbol{x}(\boldsymbol{\xi}, t)$ at instant t . A schematic interpretation of the referred movement (map) is presented on figure (6).

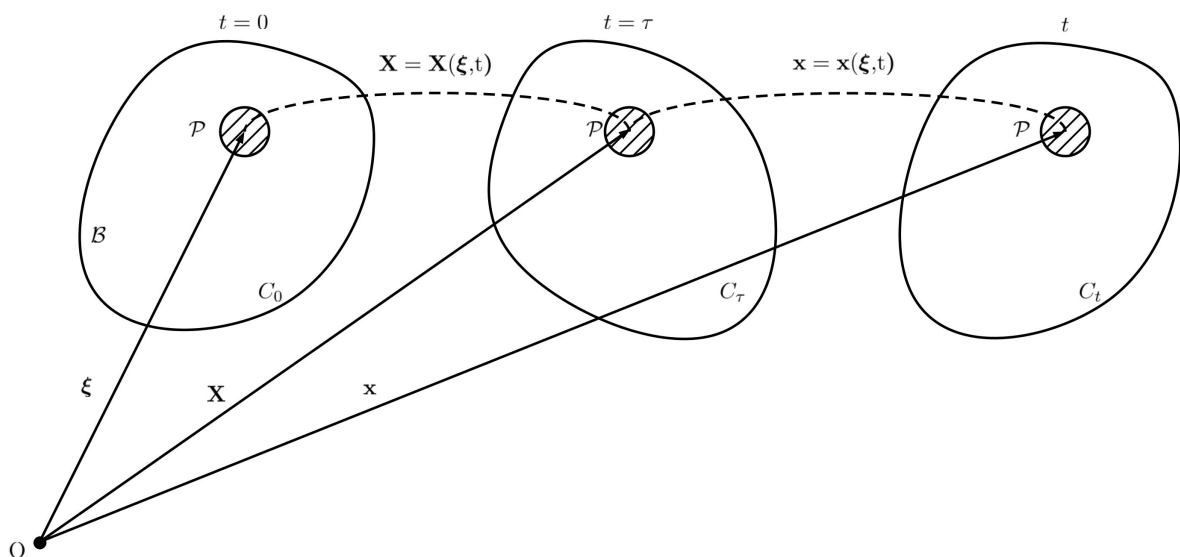


Figure 6 – Schematics of the movement of a continuous body \mathcal{B} , with representation of the different configurations \mathcal{C} obtained throughout the process: \mathcal{C}_0 at the initial time $t = 0$, \mathcal{C}_τ at an intermediate time instant $t = \tau$ and \mathcal{C}_t at the actual instant of time t .

Performing an analysis in the vicinity of a point, at the moment τ , we have, by a Taylor series expansion that:

$$\mathbf{X}(\boldsymbol{\xi} + d\boldsymbol{\xi}) = \mathbf{X}(\boldsymbol{\xi}) + \frac{\partial \mathbf{X}}{\partial \boldsymbol{\xi}} d\boldsymbol{\xi} + O(|d\boldsymbol{\xi}|^2), \quad (3.2)$$

thus,

$$d\mathbf{X} = \mathbf{X}(\boldsymbol{\xi} + d\boldsymbol{\xi}) - \mathbf{X}(\boldsymbol{\xi}) = \frac{\partial \mathbf{X}}{\partial \boldsymbol{\xi}} d\boldsymbol{\xi} + O(|d\boldsymbol{\xi}|^2). \quad (3.3)$$

Similarly, we have that:

$$d\mathbf{x} = \mathbf{x}(\boldsymbol{\xi} + d\boldsymbol{\xi}) - \mathbf{x}(\boldsymbol{\xi}) = \frac{\partial \mathbf{x}}{\partial \boldsymbol{\xi}} d\boldsymbol{\xi} + O(|d\boldsymbol{\xi}|^2). \quad (3.4)$$

This analysis is based on the continuum hypothesis, what implicates that the scale $|d\mathbf{X}|$ must be much bigger than the molecular scale λ and much smaller than the microscopic scale L . Regarding this context, the second-order terms can be neglected due to the fact that they are second-order infinitesimals. Based on this, it comes that

$$d\mathbf{X} = \frac{\partial \mathbf{X}}{\partial \boldsymbol{\xi}} d\boldsymbol{\xi} \quad \text{em} \quad t = \tau, \quad (3.5)$$

and

$$d\mathbf{x} = \frac{\partial \mathbf{x}}{\partial \boldsymbol{\xi}} d\boldsymbol{\xi} \quad \text{em} \quad t. \quad (3.6)$$

The tensor gradient of strain ([ARIS, 2012](#)) is define in terms of the variables used to in this movement as

$$\mathbf{F}(t) = \frac{\partial \mathbf{X}}{\partial \boldsymbol{\xi}}. \quad (3.7)$$

As a result, the stress tensor of the material can be written in terms of the functional \mathfrak{F} as follows:

$$\boldsymbol{\sigma}(t) = \mathfrak{F}\{\mathbf{F}(\tau)\}_{0 \leq \tau \leq t}. \quad (3.8)$$

Equation (3.8) shows that the stress tensor is a functional of the tensor gradient of strain, which, as it was demonstrated, is influenced only by the nearby vicinities of the material particle \mathcal{P} .

Principle of coordinate invariance

A constitutive equation must be always valid, independently of the coordinate systems in which the position and velocity vectors or the stress tensor is described, i.e., the functional \mathfrak{F} must be held valid,

A constitutive equation must always be valid, regardless of the coordinate system in which the position and velocity vectors or the stress tensor is described, i.e., the functional \mathfrak{F} must be maintained, independently of whether $\boldsymbol{\sigma}$ and $\nabla \mathbf{u}$ are described in Cartesian, spherical, cylindrical coordinates, or even curvilinear coordinate systems. Physically, this principle implies that new constitutive equations should not emerge as a consequence of a change in coordinates.

Principle of Fading Memory

The Fading memory principle postulates, according to [Truesdell and Noll \(2004\)](#), that deformations which occurred in the distant past should have less influence on the

determination of present stress than those that occurred in the recent past, i.e. the instantaneous structure of the stress field is more closely related to more recent events (strains).

Generally, in the literature, one instant of time t' is defined in the past of material deformation history and one in the present t , so, based on this principle, it is said that the effect of Strain tensions $\boldsymbol{\sigma}$) is greater for $t \sim t'$ than for $t' \ll t$.

Principle of absence of a reference state

This principle postulates that there is no natural equilibrium (or preferential) state of the material, in contrast to the behavior of solid materials.

Principle of the material frame indifference (objectivity)

The principle of material indifference, according to [Truesdell and Noll \(2004\)](#), postulates that if a constitutive equation is satisfied by a given process, characterized by a movement (successive configuration changes) and a symmetric tensor, respectively denoted by:

$$\boldsymbol{x} = \boldsymbol{x}(X, t), \quad \boldsymbol{\sigma} = \boldsymbol{\sigma}(X, t), \quad (3.9)$$

in which X is the label of a given material particle and t is the time, then it also should be satisfied by an equivalent process $\{\boldsymbol{x}^*, \boldsymbol{\sigma}^*\}$, in which the movement and the stress tensor are given by:

$$\boldsymbol{x}^* = \boldsymbol{x}^*(X, t^*) = \boldsymbol{c}(t) + \boldsymbol{Q}(t)\boldsymbol{x}(X, t), \quad (3.10)$$

$$\boldsymbol{\sigma}^* = \boldsymbol{\sigma}^*(X, t^*) = \boldsymbol{\sigma}(t) + \boldsymbol{Q}(t)\boldsymbol{\sigma}(X, t)\boldsymbol{Q}(t)^T, \quad (3.11)$$

$$t' = t - a, \quad (3.12)$$

where, $\boldsymbol{c}(t)$ is an arbitrary function of point associated with a rigid body translation, $\boldsymbol{Q}(t)$ is an orthogonal time-dependent tensor linked to a rigid body rotation and a an arbitrary constant.

The physical foundation of this principle lies in the fact that the material must be independent of the referential. That is, the instantaneous field of stresses (material response) must be independent of the observer or the referential motion. In other words, the mechanical response of a material must be invariant with respect to arbitrary rigid body motion. This principle is mathematically expressed by the equation (3.11), called, in the literature, the homogeneous transformation of [Truesdell and Noll \(2004\)](#).

The quantities that transform according to the linear homogeneous transformations shown in (3.11) and (3.12) are said to be objectives. As a result a direct consequence of principle of the material frame indifference is that constitutive equations must contain

only objective quantities, because of that, this principle is also called principle of objectivity.

3.2 Constitutive modeling for diluted magnetic suspensions

3.2.1 Concept of magnetization

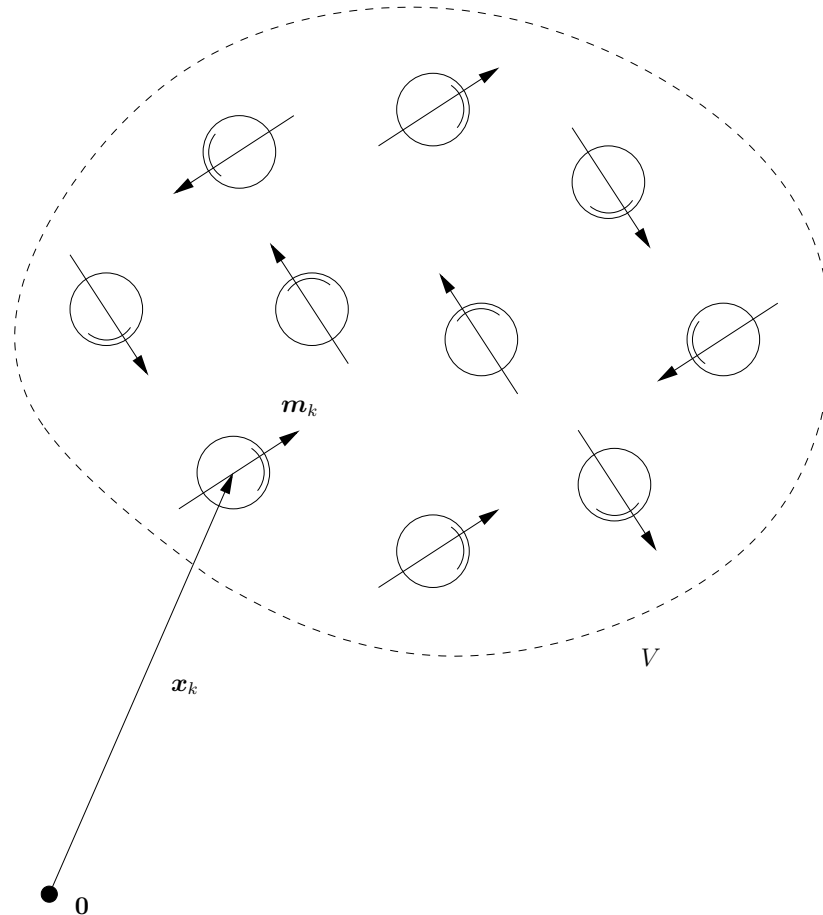


Figure 7 – Schematic representation of the three possible rheological behaviors of a power-law fluid.

As stated by Cunha (2012), the magnetization is a macroscopic property that measures the degree of polarization of a given continuum magnetizable material. Ferromagnetic materials, such as cobalt, iron and nickel can intensify the applied field in the order of a few hundred times. From a microscopic point of view, the magnetization is an average of the moment of dipoles presented in the material per unit of volume. In the case of a magnetic fluid, each magnetic particle contains a moment of magnetic dipole \mathbf{m}_k , immersed on a non-magnetizable fluid, as shown in figure (7). The magnetic moment of dipole is given by

$$\mathbf{m}_k = M_d v \hat{\mathbf{d}}_k, \quad (3.13)$$

where, M_d is the saturation magnetization of the ferromagnetic solid, v is the volume of the particle and $\hat{\mathbf{d}}_k$ is the orientation of the magnetic moment. It is supposed a monodisperse distribution of particles with the same intensity of magnetic dipole m . However the orientation of each magnetic dipole can vary from particle to particle, it is possible to define a mean moment of dipole $\overline{\mathbf{m}}$, considering a volume V containing N particles, as

$$\overline{\mathbf{m}} = \frac{1}{N} \sum_{k=1}^N \mathbf{m}_k. \quad (3.14)$$

It is defined, then, a microscopic continuum quantity \mathbf{M} , named local magnetization, that is given by a probability average of the dipole moments of the medium per unit of volume. If the distribution of moments is statistically homogeneous and independent of the volume V , that contain a sufficient high number of particles, the standard probability average can be replaced by a volumetric average. Then, the magnetization can be written as

$$\mathbf{M} = \frac{1}{V} \int_V d\mathbf{m}, \quad (3.15)$$

in which $d\mathbf{m}$ is the moment of dipole associated to a differential element dV . The volume V corresponds to the volume of the base fluid V_f added of the volume of each particle v_p , being the moment of dipole of the fluid null. Thus,

$$\mathbf{M} = \frac{1}{V} \int_{V_f} d\mathbf{m} + \frac{1}{V} \sum_{k=1}^N \int_{v_k} d\mathbf{m} = \frac{1}{V} \sum_{k=1}^N \mathbf{m}_k = \frac{N}{V} \overline{\mathbf{m}}. \quad (3.16)$$

The ratio N/V corresponds to the density number n of the suspension, being equal to the ratio of the volumetric fraction of particles ϕ and the volume of a particle v . Then,

$$\mathbf{M} = n\overline{\mathbf{m}} = \frac{\phi}{v} \overline{\mathbf{m}}. \quad (3.17)$$

3.2.2 Stress tensor for a dilute magnetic fluid

As any other fluid, complex or Newtonian, the description of the hydrodynamics of magnetic fluids is given by the balance equations of the continuum mechanics. As stated previously, the way that stresses and strains are related on a given fluid is informed to the equation of Cauchy by the stress tensor $\boldsymbol{\Sigma}$, whose deviatoric part $\boldsymbol{\sigma}$ need to be described through a constitutive equation. Cunha (2019) suggests a deduction of the stress tensor based on microhydrodynamics. In his demonstration, the referred author considers a diluted suspension composed by rigid magnetic particles randomly dispersed on a Newtonian base fluid. Also, by hypotheses, the suspension is considered to be statistically homogeneous, what allows, by the principle of ergodicity (LANDAU; LIFSHITZ, 1987; BATCHELOR, 2000), the formal probability averages to be replaced by volumetric averages. Regarding these constraints, the suspension can be treated as an equivalent continuous medium, being its average stress tensor given by

$$\overline{\boldsymbol{\sigma}} = \frac{1}{V} \int_V \boldsymbol{\sigma} dV. \quad (3.18)$$

Following a process similar to the one presented on [Graham \(2018\)](#), the volume V corresponds to the sum of the volume of the base fluid and of the particles, that is

$$V = V_f + \sum_{k=1}^N v_k, \quad (3.19)$$

where, V_f is the volume of the base fluid and v_k the volume of the particle k . Replacing equation (3.19) into (3.18), one obtains

$$\bar{\boldsymbol{\sigma}} = \frac{1}{V} \int_{V_f} \boldsymbol{\sigma} dV + \frac{1}{V} \sum_{k=1}^N \int_{v_k} \boldsymbol{\sigma} dV, \quad (3.20)$$

The stress tensor for a Newtonian fluid $\boldsymbol{\sigma}^N$ is

$$\boldsymbol{\sigma}^N = -p\mathbf{I} + 2\eta_0\mathbf{D}, \quad (3.21)$$

where, p is the mechanic pressure, η_0 is the dynamic viscosity of the fluid and \mathbf{D} is the rate of strain tensor, which is defined as the symmetric part of the tensor gradient of velocity $\nabla\mathbf{u}$. Replacing equation (3.21) on (3.20), it comes that

$$\bar{\boldsymbol{\sigma}} = \frac{1}{V} \int_{V_f} (-p\mathbf{I} + 2\eta_0\mathbf{D}) dV + \frac{1}{V} \sum_{k=1}^N \int_{v_k} \boldsymbol{\sigma} dV. \quad (3.22)$$

The integrals on equation (3.22) will be evaluated indirectly by calculating averages of other properties. Firstly, consider the average pressure of the fluid, which is defined as

$$\bar{p}_f = \frac{1}{V} \int_{V_f} p dV. \quad (3.23)$$

Now, consider the definition of the average rate of strain tensor

$$\bar{\mathbf{D}} = \frac{1}{V} \int_{V_f} \mathbf{D} dV + \frac{1}{V} \sum_{k=1}^N \int_{v_k} \mathbf{D} dV. \quad (3.24)$$

Due to the fact that the particles are rigid, its rate of strain is null. This implicates that the volume integral over the particle's volume, on equation (3.24), is also null. Thus, the average strain rate tensor is given by

$$\bar{\mathbf{D}} = \frac{1}{V} \int_{V_f} \mathbf{D} dV. \quad (3.25)$$

Replacing the results obtained in the equations (3.23) and (3.25) on the expression for the average stress tensor, equation (3.22), one obtains

$$\bar{\boldsymbol{\sigma}} = -\bar{p}_f\mathbf{I} + 2\eta_0\bar{\mathbf{D}} + \frac{1}{V} \sum_{k=1}^N \int_{v_k} \boldsymbol{\sigma} dV. \quad (3.26)$$

Aiming to evaluated the integral of the stress tensor over the volume of the rigid particles, one starts by using the following identity,

$$\boldsymbol{\sigma} = \nabla \cdot (\boldsymbol{\sigma}\mathbf{x}) - \mathbf{x}(\nabla \cdot \boldsymbol{\sigma}), \quad (3.27)$$

where \mathbf{x} is the position vector. Replacing this identity on the volume integral in equation (3.26), it comes that

$$\int_{v_k} \boldsymbol{\sigma} dV = \int_{v_k} \nabla \cdot (\boldsymbol{\sigma} \mathbf{x}) dV - \int_{v_k} \mathbf{x} (\nabla \cdot \boldsymbol{\sigma}) dV. \quad (3.28)$$

Now, applying the divergence theorem on the first volume integral after the equality on this expression, one obtains

$$\int_{v_k} \boldsymbol{\sigma} dV = \int_{v_k} \mathbf{x} (\hat{\mathbf{n}} \cdot \boldsymbol{\sigma}) dV - \int_{v_k} \mathbf{x} (\nabla \cdot \boldsymbol{\sigma}) dV. \quad (3.29)$$

In order to evaluate these integrals, it is necessary to study the flow of a spheric rigid magnetic particle under the action of an external field. Lets consider that the Reynolds' number in the scale of the particle to be much smaller than 1, that is

$$Re_p = \frac{a^2 \dot{\gamma}_c \rho}{\eta_0} \ll 1, \quad (3.30)$$

where a is the radius of the particle, $\dot{\gamma}_c$ is the flows characteristic shear-rate, ρ and η_0 are, respectively, the density and the dynamic viscosity of the fluid. In this condition, the flow around a given particle centered at \mathbf{x}_0 is described by a multipole expansion of the Stokes' flow (KIM; KARRILA, 2013), which is represented by

$$-\nabla p + \eta_0 \nabla^2 \mathbf{u} = \mathbf{f} \delta(\mathbf{x}_0) + \mathbf{D}_s \nabla \delta(\mathbf{x}_0) + \dots, \quad (3.31)$$

in which \mathbf{f} is the force over the particle and \mathbf{D}_s is the hydrodynamic dipole in the particle. The particle dipole generated by the k -th particle in suspension is given by the surface integral in (3.29).

$$\mathbf{D}_s^k = \int_{s_k} \mathbf{x} (\hat{\mathbf{n}} \cdot \boldsymbol{\sigma}) dS. \quad (3.32)$$

The dipole can be split into

$$\mathbf{D}_s^k = \mathbf{S}^k + \mathbf{L}^k, \quad (3.33)$$

in which \mathbf{S}^k is the symmetric part, called Stresslet or particle tension, and \mathbf{L}^k is the anti-symmetric part, named torque tensor. By Faxèns' third law (BATCHELOR; GREEN, 1972), the stresslet for the k -th particle in the suspension is given by

$$\mathbf{S}^k = 5\eta_0 v_k \mathbf{D}^k. \quad (3.34)$$

The torque tensor is related to the magnetic torque \mathbf{t}_m acting upon the k -th particle by the dual relation (ARIS, 2012), that is

$$\mathbf{L}^k = -\frac{1}{2} \boldsymbol{\epsilon} \cdot \mathbf{t}_m^k, \quad (3.35)$$

where $\boldsymbol{\epsilon}$ is the tensor of Levi-Civita. For a magnetic particle with dipole moment \mathbf{m}_k , free of inertia, its magnetic torque \mathbf{t}_m^k , is given by

$$\mathbf{t}_m^k = \mu_0 \mathbf{m}_k \times \mathbf{H}. \quad (3.36)$$

Replacing this expression in equation (3.35), one obtains

$$\mathbf{L}^k = -\frac{1}{2}\boldsymbol{\epsilon} \cdot (\mu_0 \mathbf{m}_k \times \mathbf{H}), \quad (3.37)$$

which can be rewritten as

$$\mathbf{L}^k = \frac{\mu_0}{2}(\mathbf{H}\mathbf{m}_k - \mathbf{m}_k\mathbf{H}). \quad (3.38)$$

Now, applying the results (3.38) and (3.34) on equation (3.29), one obtains

$$\int_{v_k} \boldsymbol{\sigma} dV = 5\eta_0 v_k \mathbf{D}^k + \frac{\mu_0}{2}(\mathbf{H}\mathbf{m}_k - \mathbf{m}_k\mathbf{H}) - \int_{v_k} \mathbf{x}(\nabla \cdot \boldsymbol{\sigma}) dV. \quad (3.39)$$

In pursuance of solving the last volume integral in (3.39), it must be noted that the term $\nabla \cdot \boldsymbol{\sigma} = -\mathbf{f}^k$ is the force per unit of volume acting upon the particle, which corresponds to the magnetic force \mathbf{f}_m^k which is defined by

$$\mathbf{f}^k = \frac{\nabla \psi_m}{v_k}, \quad (3.40)$$

where Ψ_m is the scalar magnetic potential, given by

$$\Psi_m = \mu_0 \mathbf{m} \cdot \mathbf{H}. \quad (3.41)$$

Thus,

$$\mathbf{f}^k = \frac{\mu_0 \mathbf{m}_k \cdot \mathbf{H}}{v_k}, \quad (3.42)$$

Regarding this result, the referred integral becomes

$$\int_{v_k} \mathbf{x}(\nabla \cdot \boldsymbol{\sigma}) dV = - \int_{v_k} \mathbf{x} \nabla \left(\frac{\mu_0 \mathbf{m}_k \cdot \mathbf{H}}{v_k} \right) dV, \quad (3.43)$$

which, after some vectorial manipulations and the application of Gauss theorem, can be reduced to

$$\int_{v_k} \mathbf{x}(\nabla \cdot \boldsymbol{\sigma}) dV = - \int_{s_k} \left(\mathbf{x} \frac{\mu_0 \mathbf{m}_k \cdot \mathbf{H}}{v_k} \right) \hat{\mathbf{n}} dS. \quad (3.44)$$

In the surface of the sphere, $\mathbf{x} = \mathbf{x}_0 + a\hat{\mathbf{n}}$, where a is the radius of the sphere, thus

$$\int_{v_k} \mathbf{x}(\nabla \cdot \boldsymbol{\sigma}) dV = - \int_{s_k} \left(\mathbf{x}_0 \frac{\mu_0 \mathbf{m}_k \cdot \mathbf{H}}{v_k} \right) \hat{\mathbf{n}} dS - \int_{s_k} \left(a \frac{\mu_0 \mathbf{m}_k \cdot \mathbf{H}}{v_k} \right) \hat{\mathbf{n}} \hat{\mathbf{n}} dS. \quad (3.45)$$

Since the magnetic moment dipole and the magnetic field are constants in the scale of the sphere,

$$\int_{v_k} \mathbf{x}(\nabla \cdot \boldsymbol{\sigma}) dV = - \left(\mathbf{x}_0 \frac{\mu_0 \mathbf{m}_k \cdot \mathbf{H}}{v_k} \right) \int_{s_k} (\mathbf{I} \cdot \hat{\mathbf{n}}) dS - \left(a \frac{\mu_0 \mathbf{m}_k \cdot \mathbf{H}}{v_k} \right) \int_{s_k} \hat{\mathbf{n}} \hat{\mathbf{n}} dS. \quad (3.46)$$

Applying the theorem of divergence to the first integral after the equality sign, one obtains:

$$\left(\mathbf{x}_0 \frac{\mu_0 \mathbf{m}_k \cdot \mathbf{H}}{v_k} \right) \int_{s_k} (\mathbf{I} \cdot \hat{\mathbf{n}}) dS = \int_{v_k} \nabla \cdot \mathbf{I} dV = \mathbf{O}. \quad (3.47)$$

The second one is isotropic, being calculated as follows

$$\int_{s_k} \hat{\mathbf{n}} \hat{\mathbf{n}} dS = \frac{4}{3} \pi a^2 \mathbf{I} = \frac{v_k}{a} \mathbf{I}, \quad (3.48)$$

what leads to

$$\int_{v_k} \mathbf{x}(\nabla \cdot \boldsymbol{\sigma}) dV = -(\mu_0 \mathbf{m}_k \cdot \mathbf{H}) \mathbf{I}. \quad (3.49)$$

Replacing this result into equation (3.39), one obtains

$$\int_{v_k} \boldsymbol{\sigma} dV = 5\eta_0 v_k \mathbf{D}^k + \frac{\mu_0}{2} (\mathbf{H} \mathbf{m}_k - \mathbf{m}_k \mathbf{H}) + (\mu_0 \mathbf{m}_k \cdot \mathbf{H}) \mathbf{I}, \quad (3.50)$$

which replaced on equation (3.26), leads to the following expression for the average stress tensor of the suspension,

$$\bar{\boldsymbol{\sigma}} = -\bar{p}_f \mathbf{I} + 2\eta_0 \bar{\mathbf{D}} + \frac{1}{V} \sum_{k=1}^N \left[5\eta_0 v_k \mathbf{D}^k + \frac{\mu_0}{2} (\mathbf{H} \mathbf{m}_k - \mathbf{m}_k \mathbf{H}) + (\mu_0 \mathbf{m}_k \cdot \mathbf{H}) \mathbf{I} \right]. \quad (3.51)$$

Due to the fact that the suspension is monodispersed on the diameters of the particles and on the moment of dipoles, equation (3.51) can be rewritten as

$$\bar{\boldsymbol{\sigma}} = -\bar{p}_f \mathbf{I} + 2\eta_0 \bar{\mathbf{D}} + 5nv_p \eta_0 \bar{\mathbf{D}} + \frac{\mu_0}{2} (\mathbf{H} n \bar{\mathbf{m}} - n \bar{\mathbf{m}} \mathbf{H}) + \frac{n}{N} \sum_{k=1}^N (\mu_0 \mathbf{m}_k \cdot \mathbf{H}) \mathbf{I}. \quad (3.52)$$

Observing that $nv_p = \phi$ and $\mathbf{M} = n \bar{\mathbf{m}}$, this expression becomes

$$\bar{\boldsymbol{\sigma}} = -\bar{p}_f \mathbf{I} + 2\eta_\phi \bar{\mathbf{D}} + \frac{\mu_0}{2} (\mathbf{H} \mathbf{M} - \mathbf{M} \mathbf{H}) + \frac{n}{N} \sum_{k=1}^N (\mu_0 \mathbf{m}_k \cdot \mathbf{H}) \mathbf{I}, \quad (3.53)$$

where, $\eta_\phi = (1 + 5\phi/2)\eta_0$ is Einstein's viscosity for a diluted suspension of rigid spheres. This expression is the constitutive equation of the stress tensor for a diluted magnetic fluid firstly presented on (MALVAR; GONTIJO; CUNHA, 2018). It can be rewritten as

$$\bar{\boldsymbol{\sigma}} = -\bar{p} \mathbf{I} + 2\eta_\phi \bar{\mathbf{D}} + \frac{\mu_0}{2} (\mathbf{H} \mathbf{M} - \mathbf{M} \mathbf{H}), \quad (3.54)$$

in which,

$$\bar{p} = \bar{p}_f - \frac{n}{N} \sum_{k=1}^N (\mu_0 \mathbf{m}_k \cdot \mathbf{H}), \quad (3.55)$$

is the mixture pressure, composed by contributions arising from the fluid and from the magnetic particles. It is also important to remark that this pressure is also the mechanical pressure of the equivalent fluid, what can be easily proven by calculating the trace of equation (3.54).

This constitutive model presents a asymmetric stress tensor, what is originated by the fact that the magnetic particles, when under the action of a magnetic field, experiment a resultant magnetic torque. As, in this condition, the resultant of external torques over the equivalent fluid particles are different from zero, the principles of angular momentum conservation, on its differential formulation (BATCHELOR, 2000), requires the stress tensor of the referred to be asymmetric.

Replacing the expression for the stress tensor (3.52) on the equation of balance of linear momentum (2.20), which results on the modified Navier-Stokes equation for a diluted magnetic fluid:

$$\frac{\rho D \mathbf{u}}{Dt} = -\nabla p + \eta_\phi \nabla^2 \mathbf{u} + \frac{\mu_0}{2} \nabla \times (\mathbf{M} \times \mathbf{H}) + \mu_0 \mathbf{M} \cdot \nabla \mathbf{H}. \quad (3.56)$$

It is important to note that the first magnetic term $\mu_0 \nabla \times (\mathbf{M} \times \mathbf{H})/2$ is related to the magnetic torques over the particles, arising when there is a misalignment between the magnetic field and the magnetization. The second magnetic term $\mu_0 \mathbf{M} \cdot \nabla \mathbf{H}$ is related to the magnetic forces acting upon the particles and arises when there is a gradient of magnetic field. In this work, only the first term is important, due to the fact that we are interested only in the effect of an uniform magnetic field when the magnetization is misaligned in reference to it by the action of the vorticity.

3.3 The generalized Newtonian fluids

The constitutive equation for generalized Newtonian fluids (GNF), according to [Morrison \(2001\)](#), was developed based on the constitutive of incompressible Newtonian fluids, which is given by :

$$\boldsymbol{\sigma} = \mu \dot{\boldsymbol{\gamma}}, \quad (3.57)$$

where,

$$\dot{\boldsymbol{\gamma}} = \sqrt{2\mathbf{D} : \mathbf{D}}. \quad (3.58)$$

In those equations, $\boldsymbol{\sigma}$ is the stress tensor, $\dot{\boldsymbol{\gamma}}$ is the shear-rate tensor and \mathbf{D} is the tensor rate of strain, defined as the symmetric part of the tensor gradient of velocity $\nabla \mathbf{u}$. However, equation (3.57) predicts a constant viscosity, independent from the shear-rate $\dot{\boldsymbol{\gamma}}$. This feature must be changed in order to cope with the dynamical description of materials whose viscosity is not constant, what leads to the adequacy of equation (3.57) to the following form:

$$\boldsymbol{\sigma} = \eta(\dot{\boldsymbol{\gamma}}) \dot{\boldsymbol{\gamma}}, \quad (3.59)$$

where, $\eta(\dot{\boldsymbol{\gamma}})$ is a scalar function and $\dot{\boldsymbol{\gamma}} = |\dot{\boldsymbol{\gamma}}|$. The material function $\eta(\dot{\boldsymbol{\gamma}})$ is called apparent viscosity, due to the fact that it varies as a function of the shear-rate. Nonetheless, it is related to the effective viscosity of the fluid μ as follows:

$$\lim_{\dot{\boldsymbol{\gamma}} \rightarrow 0} \eta(\dot{\boldsymbol{\gamma}}) = \mu. \quad (3.60)$$

It is important to note that, even though the form of the stress tensor for the generalized Newtonian fluids are given by equation (3.59), for it to truly represent the rheological characteristics of a given material, it is necessary to propose constitutive models for the apparent viscosity function $\eta(\dot{\boldsymbol{\gamma}})$. [Bird, Armstrong and Hassager \(1987\)](#) argues that the majority of models for this material function come from experimental observations, being referred as ad-hoc expressions. The models used in the analysis carried out in this dissertation are describe in the next subsections.

3.3.1 Power-law model

One of the best known viscous non-Newtonian fluid models in the literature is the power-law model, also called the Ostwald-De-Waele model (BIRD; ARMSTRONG; HASSAGER, 1987). This model describes viscosity as a function proportional to some power of the shear-rate ($\dot{\gamma}$), being mathematically expressed by:

$$\eta(\dot{\gamma}) = K\dot{\gamma}^{n-1}, \quad (3.61)$$

which presents two parameters that must be adjusted to experimental data. The first one is the power ($n - 1$) of $\dot{\gamma}$, which represents the slope of the line obtained by representing equation (3.61) on a *log-log* graph. The second parameter is the consistency index, K , whose logarithm indicates the intersection with the ordinates axis in the graph of $\log(\eta)$ vs $\log(\dot{\gamma})$. Besides that, K directly related to the magnitude of the fluid's viscosity.

The power law model can be used to describe a Newtonian fluid, in this case $K = \mu$ and $n = 1$. For $n > 1$, the graph of $\log(\eta)$ vs $\log(\dot{\gamma})$ is a rising line and the material is said Shear-thickening, since it has the property of its apparent viscosity increasing with the intensification of the applied shear-rate. For $n < 1$, the $\log(\eta)$ vs $\log(\dot{\gamma})$ graph is a descending line and the fluid behavior is said to be shear-thinning, showing a decrease in apparent viscosity as a function of increased shear-rate. These behaviors are shown in the figure (8).

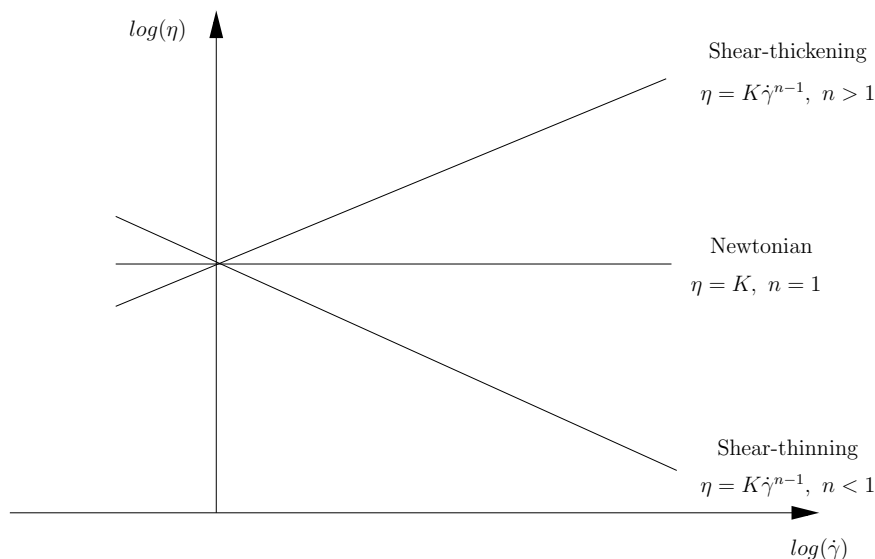


Figure 8 – Schematic representation of the three possible rheological behaviors of a power-law fluid.

According to Morrison (2001), this model is well suited for modeling non-Newtonian fluids subjected to medium to high shear-rate regimes, such as polymer extrusion processes. In addition, this model allows simplified calculations and good modeling in predicting flow measurements as a function of pressure drop in various industrial applications. However, this has some limitations, such as not capturing the Newtonian plateau at small

shear-rates η_0 . Another disadvantage is that this model is purely experimental and, therefore, its description of a particular material is specific, that is, it is not possible to predict the behavior of a material knowing the parameters of the power-law model of a similar material. It may be added, furthermore, that this model has no temporal constant between its parameters, what makes it unable to capture any material relaxation time, i.e. this model is not able to predict how quickly the fluid will relax after the flow is finished.

3.3.2 Sisko's model

This model was proposed by Sisko (1958) as an excellent alternative for modeling the rheological behavior of shear-thinning fluids, such as greases, emulsions and many other complex fluids when subjected to medium-high shear-rates. The constitutive equation for the relation between the apparent viscosity and the shear-rate suggested by this model is

$$\eta(\dot{\gamma}) = \eta_\infty + K_s \dot{\gamma}^{(n-1)}. \quad (3.62)$$

As it can be immediately seen, this model comes from the addition of another parameter to the power-law model. This parameter is the infinite shear viscosity η_∞ , that represents the constant value to which the viscosity tends when the shear-rate increases. The other parameters K_s and $(n - 1)$ have the same interpretation that was for the parameters of the power-law model.

3.3.3 Herschel-Bulckley's model

This model describes complex fluids that present yield stress, that is, a minimum level of shear stress is needed for this kind of fluid to start flowing. Generally, these fluids present a well consolidated microstructure at equilibrium, having a solid-like behavior. Nevertheless, when the shear-stress reaches the yielding point, the microstructure of the complex fluid begins to break, what is reflected in a severe reduction of the apparent viscosity. The constitutive equation proposed by this model is:

$$\eta(\dot{\gamma}) = \begin{cases} \frac{\sigma_0}{\dot{\gamma}} + K_H \dot{\gamma}^{n-1}, & se \ |\sigma| > |\sigma_0| \\ \infty, & se \ |\sigma| \leq |\sigma_0|, \end{cases} \quad (3.63)$$

where σ_0 is the yield stress, K_H is the consistency parameter and n is the power-law index. It is important to note that the constitutive equation of this model predicts an infinite viscosity for the case in which the intensity of the shear-stress is lower than the yield stress. This implicates that in this condition the complex fluid will not flow, presenting then a solid-like behavior.

Applying this constitutive equation to equation (3.59), one obtains the following relation for the shear-stress:

$$\sigma(\dot{\gamma}) = \begin{cases} \sigma_0 + K_H \dot{\gamma}^n, & \text{if } |\sigma| > |\sigma_0| \\ \dot{\gamma} = 0, & \text{if } |\sigma| \leq |\sigma_0|, \end{cases} \quad (3.64)$$

From this equation, it is immediate that this model predicts a non-linear relation between the shear stress and the shear rate.

3.3.4 Bingham's model

This model is similar to Hershel-Bulckley's, from which it can be obtained by making $n = 0$ on equation (3.63). As a result, it also describes complex fluids that need a critical stress σ_0 to start flowing. These material are generally called Bingham plastics. The equation proposed for the relationship between apparent viscosity and shear rate by this model is:

$$\eta(\dot{\gamma}) = \begin{cases} \frac{\sigma_0}{\dot{\gamma}} + \eta_p, & \text{if } |\sigma| > |\sigma_0|, \\ \infty, & \text{if } |\sigma| \leq |\sigma_0|, \end{cases} \quad (3.65)$$

where σ_0 is the yield stress and η_p is the plastic viscosity, which indicates the viscosity to which the fluid's apparent viscosity tends at flow conditions of high shear-rates.

Using equation equation (3.59), one can easily show that the relation between the shear-stress and the shear-rate predicted by this model is:

$$\sigma(\dot{\gamma}) = \begin{cases} \sigma_0 + \eta_p \dot{\gamma}, & \text{if } |\sigma| > |\sigma_0|, \\ \dot{\gamma} = 0, & \text{if } |\sigma| \leq |\sigma_0|. \end{cases} \quad (3.66)$$

It is important to note that this model predicts a linear relation for the functional dependence of the shear-stress on the shear-rate after the yield point being reached. In this regime, the complex fluid is said to present a Newtonian behavior.

3.4 The general linear viscoelastic fluids

The word viscoelasticity refers to the simultaneous existence of viscous and elastic characteristics in a material. According to [Barnes, Hutton and Walters \(1989\)](#), it is reasonable to assume that all materials are viscoelastic, *i.e.* in all of them, both viscous and elastic properties coexist. This is because the response of a given material sample in a given experiment depends on the relationship between the observer's time scale and the characteristic time scale of the material (the time it takes the material to respond to a given external stimulus.). For example, if an experiment is relatively slow, the sample will be more viscous than elastic, however, if the experiment is relatively fast, the effect will be opposite and therefore the sample will behave more elastic than viscous. However,

if the experiment scale has an order of magnitude compatible with the material's natural time scale, a viscoelastic response is observed.

The above description leads to the definition of a very important dimensionless number, the Deborah number (De), defined as the ratio of a material's timescale τ , whose origin is closely related to its microstructure, and a characteristic time scale of the flow τ_f , of macroscopic origin, that is:

$$De = \frac{\tau}{\tau_f}. \quad (3.67)$$

In this context, it is clear that a Hookean solid has $De = \infty$, since its characteristic relaxation time is theoretically infinite, on the other hand, Newtonian fluids have $De = 0$, since its characteristic time is very small compared to common experiment scales. It also appears that viscoelastic materials have $De \approx 1$, as both time scales have the same order of magnitude.

3.4.1 Linear viscoelasticity

According to (CUNHA, 2016), linear viscoelasticity is a description of the viscoelastic response ($De \approx 1$) of non-Newtonian fluids, whose main feature is to be a small deformation regime. It was, according to Barnes, Hutton and Walters (1989), the first study for transient description of non-Newtonian fluids, where the elastic response of the fluid becomes important. In this type of approach, the fluid response, i.e., the stress at any time is directly proportional to the strain or strain rate.

Due to linearity, the differential equations that govern the phenomenon are linear and the coefficients of the temporal derivatives are constant, i.e. they are independent of strain and stress. Nevertheless, according to Barnes, Hutton and Walters (1989), the main consequence of linearity is that the principle of effects superposition can be applied to the system, a fact explored in the proposition made by Oldroyd (1956) of an general equation for the linear viscoelasticity regime, which is:

$$\left(1 + \tau_1 \frac{\partial}{\partial t} + \tau_2 \frac{\partial^2}{\partial t^2} + \dots + \tau_n \frac{\partial^n}{\partial t^n}\right) \boldsymbol{\sigma}(t) = \left(\beta_0 + \beta_1 \frac{\partial}{\partial t} + \beta_2 \frac{\partial^2}{\partial t^2} + \dots + \beta_m \frac{\partial^m}{\partial t^m}\right) \boldsymbol{\gamma}(t) \quad (3.68)$$

where τ_n and β_m are material parameters, which can be measured experimentally, $\boldsymbol{\sigma}(t)$ and $\boldsymbol{\gamma}(t)$ are, respectively, the stress tensor and the strain tensor.

Bird, Armstrong and Hassager (1987) state that there are many reasons to determine the viscoelastic-linear response of fluids, firstly, it allows the understanding of the effects of the microstructure of the material on its behavior when flowing. In addition, the experimentally measured parameters and material functions in small deformation flow have been very useful in the quality control of industrial processes. Another important reason is the fact that a good basis in linear viscoelasticity is of paramount importance for understanding nonlinear viscoelastic models.

3.4.2 Maxwell's viscoelastic model

Maxwell was a pioneer on the proposition of a constitutive model to describe the characteristics of viscoelastic materials. According to [Bird, Armstrong and Hassager \(1987\)](#), Maxwell developed the theory of elasticity, in the belief that gases could exhibit viscoelastic behavior.

In order to obtain the constitutive equation of Maxwell's model in a two-dimensional approach, [Barnes, Hutton and Walters \(1989\)](#) propose a system composed by a spring whose elastic constant is G , and a damper with damping constant μ , connected in series and subjected to periodic small amplitude excitations, in which the spring continuously shifts γ and the damper observes a damping rate $\dot{\gamma}$. This system is known as the Maxwell element and is represented in the figure (9).

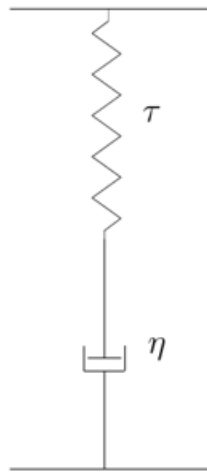


Figure 9 – Schematics of a Maxwell's element.

Considering a Hookean spring, it comes that

$$\sigma_E = G\gamma_E. \quad (3.69)$$

Then, differentiating equation (3.69), one obtains:

$$\dot{\sigma}_E = G\dot{\gamma}_E, \quad (3.70)$$

on the other hand, for the damper:

$$\sigma_V = \eta\dot{\gamma}_V. \quad (3.71)$$

Since the system is composed of elements in a series arrangement, the spring and the damper will suffer the same stress and the total damping rate will be the sum of the damping rate of both components, i.e.:

$$\sigma_E = \sigma_v = \sigma \quad e \quad \dot{\gamma} = \dot{\gamma}_E + \dot{\gamma}_V, \quad (3.72)$$

Therefore, substituting the results obtained from the equations (3.70) and (3.71) in the equation (3.72), we obtain that:

$$\dot{\gamma} = \frac{\dot{\sigma}_E}{G} + \frac{\sigma_V}{\eta} = \frac{\dot{\sigma}}{G} + \frac{\sigma}{\eta}. \quad (3.73)$$

By reorganizing the terms of the equation (3.73), we arrive at the differential one-dimensional formulation of Maxwell's model, given by the following ordinary differential equation:

$$\sigma + \frac{\eta}{G} \frac{\partial \sigma}{\partial t} = \eta \dot{\gamma}. \quad (3.74)$$

In this analogy, the viscous effects and hence the dissipative characteristics, related to the liquid behavior of the viscoelastic material, are represented by the damper and the elastic characteristics, linked to the solid behavior, are represented by the spring.

A general formulation of Maxwell's model, in tensor notation, is obtained by observing that this constitutive model is based on the precepts of linear viscoelasticity, and therefore its constitutive equation must meet Oldroyd's general form, equation (3.68), discussed in the previous section. Keeping nonzero only the terms τ_1 and β_1 in the equation (3.68) and equating β_1 with the viscosity η , one obtains the following differential equation:

$$\boldsymbol{\sigma} + \tau_1 \frac{\partial \boldsymbol{\sigma}}{\partial t} = \eta \frac{\partial \boldsymbol{\gamma}}{\partial t}, \quad (3.75)$$

where

$$\dot{\boldsymbol{\gamma}} = \partial \boldsymbol{\gamma} / \partial t = 2\mathbf{D}. \quad (3.76)$$

In these expressions, \mathbf{D} is the rate of strain tensor and $\tau_1 = \eta/G$ is a material time constant, more specifically named time of relaxation, and G is the elastic modulus. With this alteration, equation (3.75) becomes:

$$\boldsymbol{\sigma} + \tau_1 \frac{\partial \boldsymbol{\sigma}}{\partial t} = 2\eta \mathbf{D}. \quad (3.77)$$

The solution of the ordinary differential equation (3.77) is obtained by the method of the integrating factor (*F.I.*). Defining $F.I. = e^{(t/\tau_1)}$ and multiplying both sides of equation (3.77) by this factor, one obtains:

$$e^{(t/\tau_1)} \frac{d\boldsymbol{\sigma}}{dt} + \frac{1}{\tau_1} e^{(t/\tau_1)} \boldsymbol{\sigma} = \frac{2\eta}{\tau_1} \mathbf{D}(t) e^{(t/\tau_1)}, \quad (3.78)$$

and, thus:

$$\frac{d}{dt} \left(\boldsymbol{\sigma} e^{(t/\tau_1)} \right) = \frac{2\eta}{\tau_1} \mathbf{D}(t) e^{(t/\tau_1)}. \quad (3.79)$$

Integrating equation (3.79), it is obtained the constitutive equation for the stress tensor for a Maxwell's fluid, which is expressed by:

$$\boldsymbol{\sigma}(t) = \frac{2\eta}{\tau_1} \int_{-\infty}^t e^{-(t-t')/\tau_1} \mathbf{D}(t') dt'. \quad (3.80)$$

From this equation, it is defined the stress relaxation function as:

$$\Phi(t - t') = \frac{2\eta}{\tau_1} e^{-(t-t')/\tau_1} \quad (3.81)$$

where, $\Phi(t - t')$ is a positive function that depends on the nature of the fluid. Besides that, it decreases monotonically for zero as $t - t' \rightarrow 0$. Based on this, the stress tensor of a Maxwell's fluid can be rewritten as:

$$\boldsymbol{\sigma}(t) = \int_{-\infty}^t \Phi(t - t') \mathbf{D}(t') dt'. \quad (3.82)$$

That is, according to Salas (2006), for a viscoelastic incompressible fluid subject to small displacement gradients or arbitrary strain rates, the expression for the total stress tensor $\boldsymbol{\Sigma}$ is given by:

$$\boldsymbol{\Sigma}(t) = -p\mathbf{I} + \boldsymbol{\sigma}(t), \quad (3.83)$$

where $-p\mathbf{I}$ is the isotropic part of the stress tensor and $\boldsymbol{\sigma}(t)$ is its deviatoric part, that in this case is given by equation (3.82).

The equation (3.82) is interpreted from the perspective of the causality principle, which states that stress depends on the history of loading, i.e., the stress in the present-time (t) depends on the strain-rate or history of deformation in earlier times (t'). In this context, the exponential shown in the equation (3.81), which mathematically represents the stress relaxation function, can be understood as a multiplicative factor of that equation, which assumes higher values for times closer to the present time and smaller for later times, thus indicating that stress is more susceptible to the more recent history of deformation. As a result, Maxwell fluids are said to have memory, as their current state depends on past states and, moreover, their memory decreases rapidly for events that occurred at a time away from the present, showing that this model fits the principle of fading memory.

3.4.3 Generalized Maxwell's viscoelastic model

It was previously stated that Maxwell's fluid has memory and that a good measure of this parameter is the relaxation time τ_1 . Now consider a complex material composed of N Maxwell's elements, as shown in the figure (10).

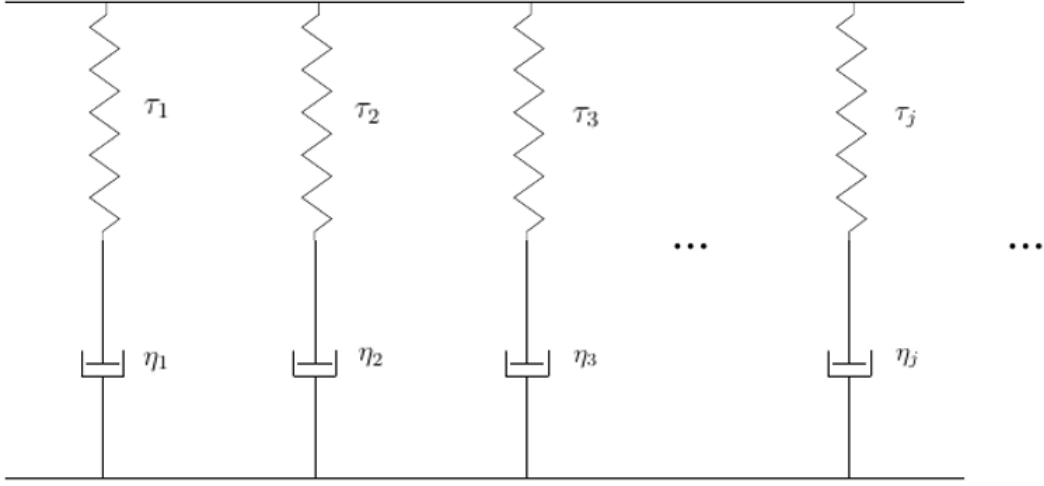


Figure 10 – Schematics of a complex fluid composed by N Maxwell's elements.

The two-dimensional form of Maxwell's model is obtained by integrating equation (3.75) through the integrating factor technique, whose procedure is analogous to that approached for the general solution addressed in the section (3.74). Solving the said ordinary differential equation, one obtains that:

$$\sigma(t) = \frac{\eta}{\tau_1} \int_{-\infty}^t e^{-(t-t')/\tau_1} \dot{\gamma}(t') dt'. \quad (3.84)$$

Regarding the principle of superposing effects, which is one of the foundations of linear viscoelasticity theory, it can be stated that the total stress felt by the material formed by N Maxwell's elements is given by the sum of the stress for each element, that is:

$$\sigma(t) = \sum_{j=1}^N \frac{\eta_j}{\tau_j} \int_{-\infty}^t e^{-(t-t')/\tau_j} \dot{\gamma}(t') dt', \quad (3.85)$$

which, in terms of the stress relaxation function can be rewritten as follows:

$$\sigma(t) = \int_{-\infty}^t \sum_{j=1}^N \Phi_j(t-t') \dot{\gamma}(t') dt'. \quad (3.86)$$

This equation shows us that in a linear viscoelastic regime the relaxation of a given stress applied to a complex material develops as a combined relaxing effect of the N elements that compose it, i.e. there are N relaxation times which characterize the typical time scale of a complex fluid in this flow regime. One can, therefore, write the stress relaxation function by considering Maxwell's N elements as follows:

$$\Phi(s) = \sum_{j=1}^N \Phi_j(s) = \sum_{j=1}^N \frac{\eta_j}{\tau_j} e^{-s/\tau_j}, \quad (3.87)$$

where $s = t - t'$.

3.4.4 Determination of the viscoelastic modules

Consider a Maxwell's fluid subjected to a small amplitude oscillatory shear. In this conditions, from equation (3.84), one obtains:

$$\sigma(t) = \frac{\eta_1}{\tau_1} \int_{-\infty}^t e^{-(t-t')/\tau_1} \dot{\gamma}(t') dt', \quad (3.88)$$

where, η_1 is the viscosity of the fluid for a condition of null frequency (equilibrium) and τ_1 its characteristic time of relaxation. Given the characteristics of the small amplitude oscillatory shear, it is defined that:

$$\sigma(t) = \dot{\gamma}(t) \eta^*(\omega), \quad (3.89)$$

in which, $\eta^*(\omega)$ is the complex viscosity modulus of the fluid.

Besides that, the angular strain is given by:

$$\gamma(t') = \gamma_0 e^{i\omega t'}. \quad (3.90)$$

Now, the shear-rate is defined by differentiating equation (3.90), which results in:

$$\dot{\gamma}(t') = i\omega \gamma_0 e^{i\omega t'}. \quad (3.91)$$

Replacing this expression into equation (3.88), one obtains:

$$\sigma(t) = \frac{\eta_1}{\tau_1} \int_{-\infty}^t e^{-(t-t')/\tau_1} i\omega \gamma_0 e^{i\omega t'} dt'. \quad (3.92)$$

Applying a substitution of variables $s = t - t'$ in equation (3.92), that results in $ds = -dt'$, and inverting the limits of integration, one obtains:

$$\sigma(t) = \frac{\eta_1}{\tau_1} \int_0^{\infty} e^{-s/\tau_1} i\omega \gamma_0 e^{i\omega(t-s)} ds. \quad (3.93)$$

Removing constant terms from the integral,

$$\sigma(t) = \frac{\eta_1}{\tau_1} i\omega \gamma_0 e^{i\omega t} \int_0^{\infty} e^{-s/\tau_1} e^{-i\omega s} ds, \quad (3.94)$$

and using equation (3.91), (3.94) can be rewritten in the following form:

$$\sigma(t) = \frac{\eta_1}{\tau_1} \dot{\gamma}(t) \int_0^{\infty} e^{-s/\tau_1} e^{-i\omega s} ds. \quad (3.95)$$

Now, adding the powers of the exponentials in the integrand of (3.95), factorizing s and rearranging the terms, one obtains:

$$\sigma(t) = \frac{\eta_1}{\tau_1} \dot{\gamma}(t) \int_0^{\infty} e^{[-s(1+i\omega\tau_1)/\tau_1]} ds. \quad (3.96)$$

Integrating (3.96),

$$\sigma(t) = \frac{\eta_1}{\tau_1} \dot{\gamma}(t) \left[\frac{-\tau_1}{(1+i\omega\tau_1)} e^{[-s(1+i\omega\tau_1)/\tau_1]} \right] \Bigg|_{s=0}^{s \rightarrow \infty}, \quad (3.97)$$

and taking equation (3.97) into account, one obtains:

$$\sigma(t) = \frac{\eta_1}{(1 + i\omega\tau_1)} \dot{\gamma}(t). \quad (3.98)$$

Besides that, using the definition stated on equation (3.89), it comes that:

$$\eta^* = \frac{\eta_1}{(1 + i\omega\tau_1)}. \quad (3.99)$$

Multiplying and dividing equation (3.99) by the conjugate of the denominator:

$$\eta^* = \frac{\eta_1 - i\omega\tau_1\eta_1}{(1 + \omega^2\tau_1^2)}, \quad (3.100)$$

and observing that:

$$\eta^*(\omega) = \eta'(\omega) - i\eta''(\omega), \quad (3.101)$$

it is easily shown that:

$$\eta'(\omega) = \frac{\eta_1}{(1 + \omega^2\tau_1^2)} \quad (3.102)$$

and

$$\eta''(\omega) = \frac{\eta_1\tau_1\omega}{(1 + \omega^2\tau_1^2)}. \quad (3.103)$$

Finally, using the definition $G^* = i\omega\eta^*$, one obtains that:

$$G^*(\omega) = \frac{i\omega\eta_1}{(1 + i\omega\tau_1)}, \quad (3.104)$$

from which, through a process analogous to the one carried out on equation (3.100), it is obtained that:

$$G'(\omega) = \omega\eta''(\omega) = \frac{\eta_1\tau_1\omega^2}{(1 + \omega^2\tau_1^2)}, \quad (3.105)$$

and

$$G''(\omega) = \omega\eta'(\omega) = \frac{\eta_1\omega}{(1 + \omega^2\tau_1^2)}. \quad (3.106)$$

Now admitting a fluid composed of N elements of Maxwell, as discussed in the section (3.4.3), it is shown by the superposition principle that:

$$\eta'(\omega) = \sum_j^N \frac{\eta_j}{(1 + \omega^2\tau_j^2)}, \quad (3.107)$$

$$\eta''(\omega) = \sum_j^N \frac{\eta_j\tau_j\omega}{(1 + \omega^2\tau_j^2)}, \quad (3.108)$$

$$G'(\omega) = \sum_j^N \frac{\eta_j\tau_j\omega^2}{(1 + \omega^2\tau_j^2)}, \quad (3.109)$$

e

$$G''(\omega) = \sum_j^N \frac{\eta_j\omega}{(1 + \omega^2\tau_j^2)}. \quad (3.110)$$

3.4.5 Relationship between the stress relaxation function and viscoelastic modules

Consider again a Maxwell fluid subjected to a small amplitude oscillatory shear. In this case, the system excitation given in terms of the shear-rate is expressed as:

$$\dot{\gamma}(t') = \dot{\gamma}_0 \cos(\omega t'). \quad (3.111)$$

Replacing the expression (3.111) into the bidimensional constitutive equation for the stress tensor of a Maxwell's fluid, equation (3.84), one obtains:

$$\sigma(t) = \int_{-\infty}^t \Phi(t-t') \dot{\gamma}_0 \cos(\omega t') dt'. \quad (3.112)$$

Defining $s = t - t'$ on equation (3.112), it comes that:

$$\sigma(s) = \int_{-\infty}^t \Phi(s) \dot{\gamma}_0 \cos(\omega(t-s)) ds. \quad (3.113)$$

Developing the term $\cos(\omega(t-s))$, it can be easily shown that:

$$\sigma(s) = \int_{-\infty}^t [\Phi(s) \cos(\omega s) ds] \dot{\gamma}_0 \cos(\omega t) ds + \int_{-\infty}^t [\Phi(s) \sin(\omega s) ds] \dot{\gamma}_0 \sin(\omega t) ds. \quad (3.114)$$

Comparing this result with equation (4.11), it is obtained that:

$$\eta'(\omega) = \int_{-\infty}^t \Phi(s) \cos(\omega s) ds, \quad (3.115)$$

$$\eta''(\omega) = \int_{-\infty}^t \Phi(s) \sin(\omega s) ds. \quad (3.116)$$

Alternatively, using complex variables, one obtains:

$$\eta^*(\omega) = \eta'(\omega) - i\eta''(\omega) = \int_{-\infty}^t \Phi(s) e^{-i\omega s} ds. \quad (3.117)$$

Using the inverse Fourier transform, it is immediate that:

$$\Phi(s) = \frac{2}{\pi} \int_{-\infty}^t \eta'(\omega) \cos(\omega s) d\omega \quad (3.118)$$

$$\Phi(s) = \frac{2}{\pi} \int_{-\infty}^t \eta''(\omega) \sin(\omega s) d\omega \quad (3.119)$$

3.4.6 Determination of the relaxation time from the stress relaxation function

The relaxation time (τ) for a simple Maxwell's fluid (composed of one Maxwell element) or the main relaxation time for a complex memory fluid can be calculated from the stress relaxation function. For that, let's calculate the following relation:

$$\lim_{\omega \rightarrow 0} \frac{\eta''(\omega)/\omega}{\eta'(\omega)}, \quad (3.120)$$

where $\eta'(\omega)$ and $\eta''(\omega)$ are given by (3.115), thus:

$$\lim_{\omega \rightarrow 0} \frac{\eta''(\omega)/\omega}{\eta'(\omega)} = \lim_{\omega \rightarrow 0} \left[\frac{\int_{-\infty}^t \frac{\Phi(s) \sin(\omega s)}{\omega} ds}{\int_{-\infty}^t \Phi(s) \cos(\omega s) ds} \right]. \quad (3.121)$$

Evaluating the limit of the denominator of the fraction located on the left side of equity on equation (3.121), one obtains:

$$\lim_{\omega \rightarrow 0} \eta'(\omega) = \lim_{\omega \rightarrow 0} \int_{-\infty}^t \Phi(s) \cos(\omega s) ds = \int_{-\infty}^t \Phi(s) ds = \eta(0) = \eta_0, \quad (3.122)$$

where η_0 is the viscosity of the fluid in the limit of flow absence (equilibrium). The limit of the numerator is calculated as follows:

$$\lim_{\omega \rightarrow 0} \frac{\eta''(\omega)}{\omega} = \lim_{\omega \rightarrow 0} \int_{-\infty}^t \frac{\Phi(s) \sin(\omega s)}{\omega} ds \quad (3.123)$$

to which, applying the rule of L'Hôpital, it is obtained that:

$$\lim_{\omega \rightarrow 0} \frac{\eta''(\omega)}{\omega} = \lim_{\omega \rightarrow 0} \int_{-\infty}^t s \Phi(s) \cos(\omega s) ds = \int_{-\infty}^t s \Phi(s) \cos(\omega s) ds. \quad (3.124)$$

Now, substituting the results obtained in (3.123) and (3.124) into (3.121), one obtains that:

$$\lim_{\omega \rightarrow 0} \frac{\eta''(\omega)/\omega}{\eta'(\omega)} = \frac{\int_{-\infty}^t s \Phi(s) \cos(\omega s) ds}{\int_{-\infty}^t \Phi(s) ds} = \frac{\beta}{\mu}, \quad (3.125)$$

By dimensional analysis, knowing that s has unit of time and $\Phi(s)$ unit of tension, it is obtained, as a result, that $[\beta] = Pa.s^2$ and $[\mu] = Pa.s$, then the quotient shown on equation (3.125) has unit of time, being defined as the relaxation time τ of the material.

Based on that:

$$\tau = \frac{\int_{-\infty}^t s \Phi(s) \cos(\omega s) ds}{\int_{-\infty}^t \Phi(s) ds}. \quad (3.126)$$

4 RHEOLOGICAL FLOWS AND MATERIAL FUNCTIONS

The description of the flow behavior of complex fluids, such as magnetic fluids, differs strongly from that predicted by the Newton viscosity law. An incompressible, constant temperature Newtonian fluid is completely characterized by only two material constants: its specific mass ρ and the viscosity η . Therefore, having measured these quantities, the governing equations for the stress and velocity distribution in the fluid are fixed for any type of flow (BIRD; ARMSTRONG; HASSAGER, 1987).

The situation becomes considerably more complicated when it comes to the experimental description of incompressible non-Newtonian fluids, as such materials do not necessarily have a constant viscosity and, in addition, exhibit normal stresses and elastic effects such as stress relaxation.

While different types of experiments applied to Newtonian fluids lead to the measurement of a single material constant (viscosity), the same ones applied to a magnetic fluid may lead to a set of material functions, which depend on the intensity of the applied external magnetic field, the shear rate, the frequency, the time and of other parameters. According to Bird, Armstrong and Hassager (1987), these functions are intended to promote the classification of various types of non-Newtonian fluids, and are essential for determining constants of specific constitutive equations for these fluid classes.

4.1 The stress tensor: an overview

Newtonian fluids subjected to a simple shear present only σ_{xy} different from zero. Nonetheless, for non-Newtonian fluids, in the absence of any applicable constitutive equation, it must be considered that the six components of the stress tensor are different from zero. According to Bird, Armstrong and Hassager (1987), for viscometric flows of incompressible liquids, it can be shown that a maximum of three combinations of components of the stress tensor can be measured. Based on that, the most general form that this tensor

can assume is given by:

$$\Sigma = -pI + \sigma = \begin{pmatrix} -p + \sigma_{xx} & \sigma_{xy} & 0 \\ \sigma_{xy} & -p + \sigma_{yy} & 0 \\ 0 & 0 & -p + \sigma_{zz} \end{pmatrix} \quad (4.1)$$

Since for incompressible fluids it is not possible to separate the contribution of pressure and normal stresses in the measurement of normal forces on surfaces, the only amounts of experimental interest are shear stress and two normal stress differences, defined as:

- Shear stress: σ_{yx} ;
- First normal stress difference: $N_1 = \sigma_{xx} - \sigma_{yy}$;
- Second normal stress difference: $N_2 = \sigma_{yy} - \sigma_{zz}$.

In this chapter it will be discussed the material functions that come from three types of viscometric flow of non-Newtonian fluids: permanent simple shear, small amplitude oscillatory shear, and impulse of strain (step-strain).

4.2 Permanent simple shear

Permanent simple shear is a viscometric flow used to evaluate the dependence of viscometric functions on the shear-rate $\dot{\gamma}$. This type of flow is widely used to characterize rheological behavior from constitutive models that consider complex fluid as a system without memory, which are generically called generalized Newtonian fluids. Furthermore, it is important to note that the viscometric functions obtained experimentally by measuring instruments based on this flow are of fundamental importance for engineering applications. This type of flow can be also carried out in the presence of an external magnetic field \mathbf{H} , what makes it possible to evaluate the material functions not only in terms of the shear-rate, but also as a function of the intensity of the applied magnetic field.

Considering a situation where the external magnetic field is constant and homogeneous, the stress tensor depends only of the flow field, thus, it can be said that the stresses, in permanent regime when the fluid is subjected to a simple shear, are functions only of the shear-rate $\dot{\gamma}$ (BIRD; ARMSTRONG; HASSAGER, 1987). The Viscosity η , also called shear-rate dependent viscosity, is defined analogously to Newtonian fluids:

$$\sigma_{xy} = \eta(\dot{\gamma})\dot{\gamma}_{yx}. \quad (4.2)$$

Following the same logic we define the normal stress coefficients Ψ_1 and Ψ_2 as follows:

$$N_1 = \sigma_{xx} - \sigma_{yy} = \Psi_1(\dot{\gamma})\dot{\gamma}_{yx}^2, \quad (4.3)$$

$$N_2 = \sigma_{yy} - \sigma_{zz} = \Psi_2(\dot{\gamma})\dot{\gamma}_{yx}^2. \quad (4.4)$$

The Ψ_1 and Ψ_2 functions are known as the first and second normal stress coefficients, respectively. The set of material functions η , Ψ_1 and Ψ_2 is called viscometric functions of the simple shear flow.

Morrison (2001) states that the viscosity η is the best known experimental viscometric function, being also the most important in terms of engineering applications. According to such authors, a usual way to study it is by plotting the $\eta(\dot{\gamma})$ function keeping all external variables fixed (temperature, magnetic field intensity and others). In this type of curve, three regions of rheological behavior are defined. At low shear rates, stress is proportional to $\dot{\gamma}$ and viscosity approaches a constant value η_0 , called effective viscosity (zero-shear viscosity). For high shear-rate values, the viscosity of most non-Newtonian fluids decreases with the increase of $\dot{\gamma}$, usually according to a power law. This effect is called shear-thinning. On the other hand, there are some liquids whose apparent viscosity η increases as a function of $\dot{\gamma}$, which are called shear-thickening. Under very high shear-rates, the viscosity may again be independent of the shear-rate, becoming constant and approaching η_∞ , called infinite-shear viscosity. Such viscometric functions are arranged in the figure (11).

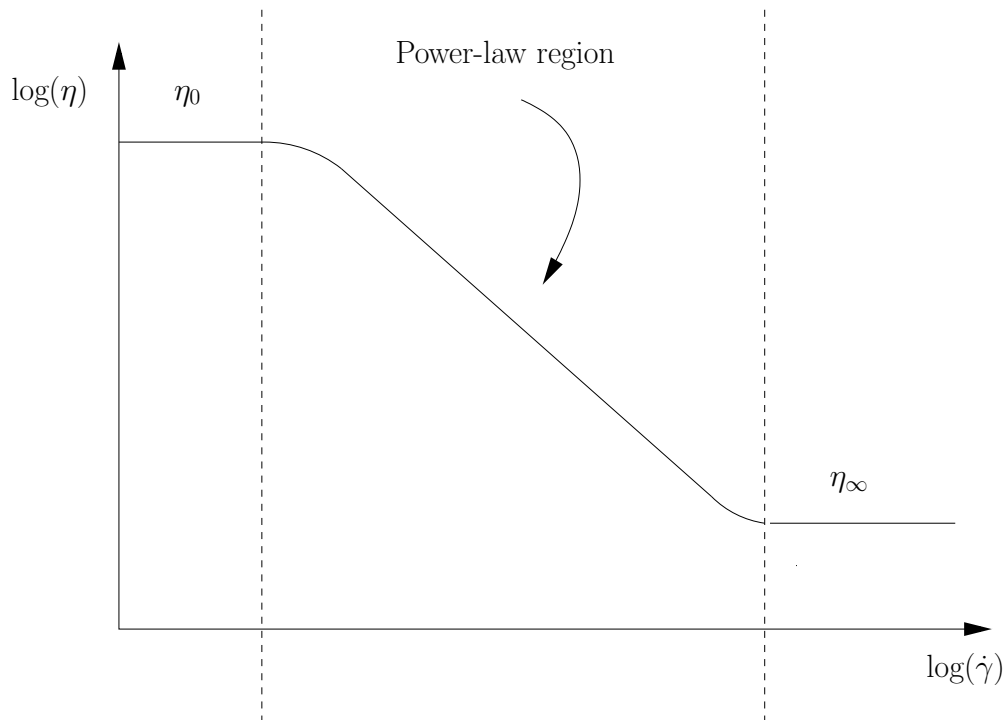


Figure 11 – Typical result for the viscosity behavior $\eta(\dot{\gamma})$ of a shear-thinning liquid, showing the three regions of interest: the plateau characterized by the effective viscosity η_0 , the power-law and the infinite-shear viscosity plateau η_∞ .

Morrison (2001) states, based on several experimental studies, that Ψ_1 is a generally positive amount. In addition, this material function has a large power-law type region of decrease, in which this function can be reduced by a factor of up to 10^6 . The rate of decrease of Ψ_1 from $\dot{\gamma}$ is often higher than that observed for η due to $\dot{\gamma}$. At low shear-rates, the first normal stress difference N_1 is proportional to $\dot{\gamma}^2$, so by looking at the equation

(4.3), it is observed that Ψ_1 tends to a constant $\Psi_{1,0}$, the first normal stress coefficient in the absence of shear, when $\dot{\gamma}$ tends to zero (SALAS; OLIVEIRA; CUNHA, 2006). The second normal stress coefficient Ψ_2 is much less experimentally explored than Ψ_1 , since its measurement implies specific and highly complex instruments (BARNES; HUTTON; WALTERS, 1989). For the vast majority of non-Newtonian fluids, their value is negative and, moreover, their absolute value is generally 10% lower than Ψ_1 .

4.3 Small amplitude oscillatory shear

The viscoelastic properties of non-Newtonian fluids with memory, as the magnetic fluids when subjected to a non-zero external magnetic field, can be determined by experiments in small amplitude oscillatory shear regime, by evaluating the viscoelastic response of the given fluid to a known external excitation.

The system is assumed to oscillate at a given frequency ω . Considering a small and therefore linear deformation regime, it is assumed that the shear stress oscillates at the same frequency as the system, but not necessarily at the same phase. To illustrate this flow type, let's consider a complex fluid located between two parallel plates, one movable and the other fixed, as shown in the figure (12). The movable one is considered to oscillate with an small amplitude and frequency, which is traduced to the fluid as a simple oscillatory shear, whose velocity field is given by

$$\mathbf{u} = \dot{\gamma}(t)y\hat{\mathbf{e}}_x, \quad (4.5)$$

where $\dot{\gamma}$ is the oscillatory shear-rate, y is the vertical position measured from the fixed plate and $\hat{\mathbf{e}}_x$ is the unit vector of the x-direction.

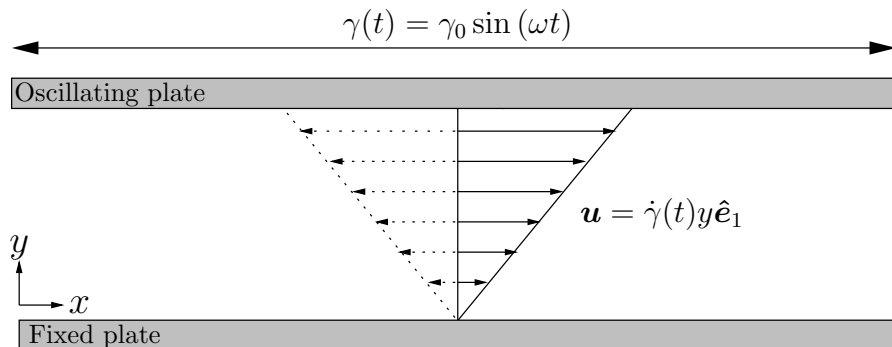


Figure 12 – Schematics representation of a small amplitude oscillatory shear.

The excitation applied to the system by the movable plate is in the form of an oscillating small deformation, that is:

$$\gamma(t) = \gamma_0 \text{sen}(\omega t), \quad (4.6)$$

where, γ_0 is the deformation amplitude ($\gamma_0 \ll 1$). Differentiating equation (4.6) with respect to time, one obtains the shear-rate excitation:

$$\dot{\gamma} = \frac{d\gamma}{dt} = \omega\gamma_0\cos(\omega t) = \dot{\gamma}_0\cos(\omega t), \quad (4.7)$$

in which the amplitude of the shear-rate is defined as $\dot{\gamma}_0 = \omega\gamma_0$.

The response to the excitation imposed to the system will be represented by a shear stress σ , which will be written in terms of the strain amplitude γ_0 and the strain itself $\gamma(t)$, or in terms of the shear rate $\dot{\gamma}(t)$. In addition, we also consider the phase of the response, which is not necessarily equal to the phase of the excitation, so in terms of the strain amplitude γ_0 , it is obtained that:

$$\sigma(t) = A(\omega)\gamma_0\text{sen}(\omega t + \alpha), \quad (4.8)$$

and, in terms of the shear-rate, $\dot{\gamma}(t)$:

$$\sigma(t) = B(\omega)\dot{\gamma}_0\cos(\omega t - \beta), \quad (4.9)$$

in which, $0 \leq \alpha \leq \pi/2$, $0 \leq \beta \leq \pi/2$ e $\beta = \frac{\pi}{2} - \alpha$.

It is convenient to rewrite (4.8) and (4.9) in terms of sine and cosine sums to make explicit the components of the shear stress in phase and out of phase with excitation. Based on this, it comes that:

$$\sigma(t) = G'(\omega)\gamma_0\text{sen}(\omega t) + G''(\omega)\gamma_0\cos(\omega t), \quad (4.10)$$

or,

$$\sigma(t) = \eta'(\omega)\dot{\gamma}_0\cos(\omega t) + \eta''(\omega)\dot{\gamma}_0\text{sen}(\omega t), \quad (4.11)$$

where, G', G'', η' and η'' are viscoelastic functions of the material (complex fluid).

It is important to remark that for a perfect elastic solid, $G''(\omega) = 0$ and, as a result, $\sigma = G'\gamma(t)$, where $G'(\omega) = G_0$ is known as the shear elastic modulus of the material. Additionally, for a Newtonian fluid, $\eta''(\omega) = 0$, which leads to $\sigma(t) = \eta'(\omega)\dot{\gamma}(t)$, where $\eta'(\omega) = \eta_0$ is called the dynamic shear viscosity of the fluid.

Expanding equations (4.8) e (4.9), one obtains:

$$\begin{aligned} \sigma(t) = & A(\omega)\gamma_0\cos(\alpha)\text{sen}(\omega t) + \\ & A(\omega)\gamma_0\text{sen}(\alpha)\cos(\omega t), \end{aligned} \quad (4.12)$$

and,

$$\begin{aligned} \sigma(t) = & B(\omega)\dot{\gamma}_0\cos(\beta)\cos(\omega t) + \\ & B(\omega)\dot{\gamma}_0\text{sen}(\beta)\text{sen}(\omega t). \end{aligned} \quad (4.13)$$

Comparing equations (4.12) and (4.13), respectively with (4.8) and (4.9), it can be easily noted that the components in phase with $\gamma(t)$ and $\dot{\gamma}(t)$ are, in this order, $G'(\omega) =$

$A(\omega)\cos(\alpha)$ and $\eta'(\omega) = B(\omega)\cos(\beta)$. Besides that, the components out of phase are $G''(\omega) = A(\omega)\sin(\alpha)$ and $\eta''(\omega) = B(\omega)\sin(\beta)$. As a result, it comes that:

$$A(\omega) = \sqrt{G'(\omega)^2 + G''(\omega)^2}, \quad (4.14)$$

$$\tan(\alpha) = \left(\frac{G''(\omega)}{G'(\omega)} \right), \quad (4.15)$$

and,

$$B(\omega) = \sqrt{\eta'(\omega)^2 + \eta''(\omega)^2}, \quad (4.16)$$

$$\tan(\beta) = \left(\frac{\eta''(\omega)}{\eta'(\omega)} \right). \quad (4.17)$$

The viscoelastic parameters have the following physical interpretations: G' is called storage modulus, as it is associated with the elastic character of the fluid, i.e. to the energy stored during deformation; G'' is called loss modulus and is associated with the viscous character of the fluid and, thus, to the energy dissipation during flow, η' is called dynamic viscosity, which also relate to dissipative effects, and η'' which represents the imaginary part of the complex viscosity, is associated with elastic effects. Another important system parameter is $\tan(\alpha)$, as it is a measure of system damping capacity.

Another way to approach this problem is using complex variables, where the oscillating excitation imposed to the system with a frequency ω , is described as follows:

$$\gamma(t) = \gamma_0 e^{i\omega t}. \quad (4.18)$$

The shear-rate is then obtained by deriving the equation (4.18) with respect to time, what results in:

$$\dot{\gamma}(t) = i\omega\gamma_0 e^{i\omega t}, \quad (4.19)$$

from which the shear-rate amplitude is defined as $\dot{\gamma}_0 = i\omega\gamma_0$. The stress, obtained as a response to the excitation stated in equation (4.19) is given as follows:

$$\sigma(t) = \tilde{\sigma} e^{i(\omega t + \phi)}, \quad (4.20)$$

which is analogous to

$$\sigma(t) = \sigma' e^{i\omega t}, \quad (4.21)$$

where $\sigma' = \tilde{\sigma} e^{i\phi}$ is a complex amplitude. As it was done previously on this section, the shear stress is defined as a function of the deformation $\gamma_0(t)$ or from the shear-rate $\dot{\gamma}(t)$, as follows:

$$\sigma^*(t) = G^*(\omega)\gamma(t) = \gamma_0 G^*(\omega) e^{i\omega t}, \quad (4.22)$$

or

$$\sigma^*(t) = \eta^*(\omega)\dot{\gamma}(t) = \eta^*(\omega)\dot{\gamma}_0 e^{i\omega t} = \eta^*(\omega)i\omega\gamma_0 e^{i\omega t}. \quad (4.23)$$

Comparing equations (4.22) and (4.23), one obtains that:

$$G^*(\omega) = i\omega\eta^*(\omega), \quad (4.24)$$

but, since:

$$G^*(\omega) = G'(\omega) + iG''(\omega), \quad (4.25)$$

and

$$\eta^*(\omega) = \eta'(\omega) - i\eta''(\omega). \quad (4.26)$$

Replacing equations (4.25) and (4.26) into (4.24), it comes that:

$$G'(\omega) - iG''(\omega) = \omega\eta''(\omega) - i\omega\eta'(\omega), \quad (4.27)$$

that is, the viscoelastic modules are related as follows:

$$G'(\omega) = \omega\eta''(\omega), \quad (4.28)$$

and

$$G''(\omega) = i\omega\eta'(\omega). \quad (4.29)$$

4.4 Step-strain

The step-strain is a viscometric flow used to characterize the memory effects of a given complex fluid, since it allows its stress relaxation function Φ to be obtained and, from this, its main relaxation time τ .

Consider that an elastic fluid, and therefore with memory, is at rest in a region between two parallel plates for all instants $t < t_0$ where t_0 is a given reference instant. At $t = t_0$, the top plate is instantly moved in the x direction, i.e. the fluid senses a deformation γ_0 as shown in the figure (13a). The system excitation, given by the applied shear rate $\dot{\gamma}$ over a short period of time $t_0 - (t_0 - \epsilon)$, can be understood as an impulse-like function, being mathematically expressed by:

$$\dot{\gamma}(t) = \frac{\gamma_0}{t_0 - (t_0 - \epsilon)} = \frac{\gamma_0}{\epsilon}, \quad (4.30)$$

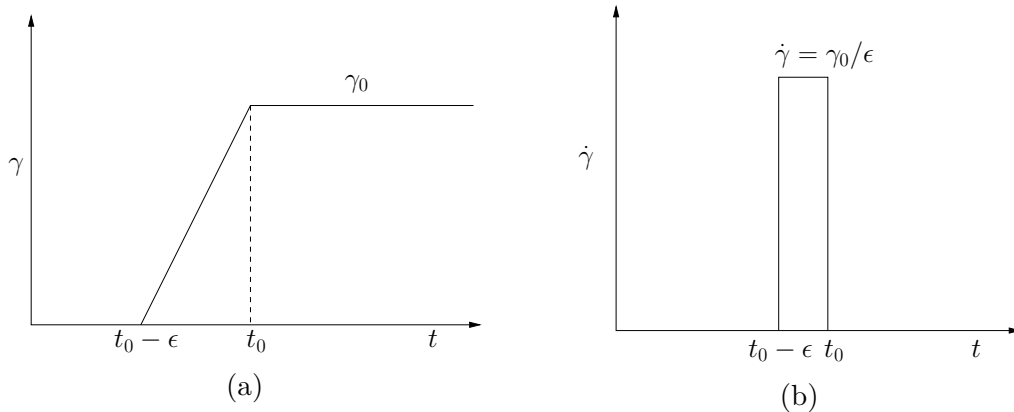


Figure 13 – (a) Step-strain, (b) Applied shear-rate (impulse function).

Let us get the expression for the stress tensor $\sigma(t)$, under linear viscoelasticity, for the case of the strain impulse:

$$\sigma(t) = \int_{-\infty}^{t_0-\epsilon} \Phi(t-t')\dot{\gamma}(t')dt' + \int_{t_0-\epsilon}^{t_0} \Phi(t-t')\dot{\gamma}(t')dt' + \int_{t_0-t}^{t_0-\epsilon} \Phi(t-t')\dot{\gamma}(t')dt'. \quad (4.31)$$

However:

$$t' \in [t < t_0 - \epsilon] \quad \longrightarrow \quad \dot{\gamma}(t') = 0 \quad \longrightarrow \quad \int_{-\infty}^{t_0-\epsilon} \Phi(t-t')\dot{\gamma}(t')dt' = 0, \quad (4.32)$$

and

$$t' \in [t > t_0] \quad \longrightarrow \quad \dot{\gamma}(t') = 0 \quad \longrightarrow \quad \int_{-\infty}^{t_0-\epsilon} \Phi(t-t')\dot{\gamma}(t')dt' = 0. \quad (4.33)$$

Hence, the integral resumes to

$$\sigma(t) = \int_{t_0-\epsilon}^{t_0} \Phi(t-t')\dot{\gamma}(t')dt', \quad (4.34)$$

which, associated to the obtained result (4.30), one obtains that:

$$\sigma(t) = \frac{\gamma_0}{\epsilon} \int_{t_0-\epsilon}^{t_0} \Phi(t-t')dt'. \quad (4.35)$$

Evaluating the limit when $\epsilon \longrightarrow 0$ and applying the theorem of L'Hôpital, one obtains:

$$\sigma(t) = \lim_{\epsilon \rightarrow 0} \gamma_0 \left[\frac{\frac{d}{d\epsilon} \int_{t_0-\epsilon}^{t_0} \Phi(t-t')dt'}{\frac{d}{d\epsilon} \epsilon} \right], \quad (4.36)$$

based on this, the stress tensor for a viscoelastic fluid subjected to a step-strain is given by:

$$\sigma(t) = \gamma_0 \Phi(t - t_0) \quad (4.37)$$

The equation (4.37) corroborates the fact that a viscoelastic fluid, due to its elastic characteristics, is not instantaneous, since the stress responds with a delay in relation to the applied deformation. In addition, it allows experimentally to obtain the stress relaxation function $\Phi(t - t')$ of a given complex fluid by simply deforming the material within a short time and compute the variation of the stress $\sigma(t)$ as a function of a given time interval, then applying the equation (4.37) to the experimental data. The stress relaxation function $\Phi(t - t')$ is of utmost importance because from it, much important information about the fluid is obtained, such as its relaxation time and its elastic and viscous modules.

4.5 Empirical correlations for material functions

In this section, it will be described two empirical rules used in the correlation of linear viscoelastic properties, obtained via experiments in the regime of small amplitude

oscillatory shear flow, and the viscometric functions observed arising from the permanent simple shear flows. Their importance relies in the fact that they allow the indirect determination of a material function from the measurement of the viscoelastic modules and vice-versa.

4.5.1 Cox-Merz's rule

One way to correlate the viscous modulus $\eta'(\omega)$ and the fluid apparent viscosity η is through the Cox-Merz rule (COX; MERZ, 1959), which has an empirical origin and predicts that the apparent viscosity η is equal to the magnitude of the complex viscosity $|\eta^*(\omega)|$, for corresponding values of frequency ω and shear-rate $\dot{\gamma}$,

$$\eta(\dot{\gamma}) = |\eta^*(\omega)|_{(\omega=\dot{\gamma})} = \eta'(\omega) \left[1 + \left(\frac{\eta''(\omega)}{\eta'(\omega)} \right)^{0,5} \right]_{(\omega=\dot{\gamma})}^2. \quad (4.38)$$

However, this rule is suitable only in the linear viscoelasticity regime.

It is easy to show from equations (3.107) and (3.108) that, at the limit where ω tends to zero, i.e. when the system goes into steady-state, the rule of Cox-Merz simplifies to the fact that $\eta'(\omega)$ tends to the dynamic viscosity η_0 , as shown in the equation (4.39).

$$\lim_{\omega \rightarrow 0} \eta'(\omega) = \eta_0 \quad (4.39)$$

The Cox-Merz rule also applies to the elastic properties of complex fluids. In this case, it relates the elastic modulus $G'(\omega)$, obtained from the small amplitude oscillatory shear, and the first normal stress difference N_1 , obtained from the permanent shear flow tests, as follows:

$$G'(\omega) = \frac{N_1(\dot{\gamma})}{2}. \quad (4.40)$$

4.5.2 Laun's rule

Laun (1986) proposes a correlation between the first normal stress difference $N_1(\dot{\gamma})$ measured using steady shear flow and the storage $G'(\omega)$ and loss modulus $G''(\omega)$ measured in oscillatory shear, which is:

$$N_1(\dot{\gamma})|_{\dot{\gamma}=\omega} = 2G'(\omega) \left(1 + \left(\frac{G'(\omega)}{G''(\omega)} \right)^2 \right)^n. \quad (4.41)$$

As the Cox-Merz rule, this ad-hoc expression comes from extensive experimental observations, being found to be usable for many complex fluids, such as polymer melts and concentrated solutions. From such analysis, the power index n was found to lay in between (0.5,0.7). It is important to remark that in the case of a complex fluid that presents a much bigger the loss modulus $G''(\omega)$ in comparison to the storage modulus $G'(\omega)$, it can be easily shown, by a binomial expansion of the term between parenthesis on equation (4.41), that Laun's rule corresponds to the Cox-Merz rule.

5 MATERIALS AND METHODS

5.1 Experimental apparatus

5.1.1 Rheometer

The rheological properties of the fluids under analysis in this work are obtained using a high performance Physica Modular Compact Rheometer - MCR 301 (Anton Paar GmbH, Germany), illustrated in figure (14). As its name states, this rheometer works based on modules, a feature that makes this device really versatile. Each module is composed by a measuring system and a measuring cell, which combined permit the user to measure several material functions of both, Newtonian and non-Newtonian fluids, in a variety of shear flow conditions (permanent and transient). Depending on the module mounted on the rheometer, not only flow-related effects on the rheological behavior of a given fluid can be measured, but also, one can measure the dependence of the material functions on different external variables, like temperature and magnetic field.

The MCR 301 rheometer is very robust. The measuring system is powered by a permanent magnet synchronous drive motor placed on the measuring head, which is able to apply torques from $0.1\mu\text{N.m}$ to 200 mN.m with resolution of $0.001\mu\text{N.m}$ and accuracy of $0.2\mu\text{N.m}$. The capability of the device to apply a wide range of torques is the key factor that allows the measurement of several rheological properties of a considerable variety of fluids. The motor can also apply oscillations in a range from 0.0001 to 100 Hz. Those characteristics can only be achieved due to the fact that the shaft of the measuring system is sustained by an pressurized air bearing, what strongly reduces the friction between the components of the drive system. The pressurized air is provided by an oil-free MSV6 compressor (Schulz S.A., Brazil), with operating pressure of 8.3 bar, this device is shown in figure (15a). Besides that, the pneumatic system of the rheometer requires high quality air, what is obtained using a setup composed by a dehumidifier and filters of oil and solid particles, as depicted in figure (15b).

Temperature greatly influences the rheological behavior of almost all substances (BIRD et al., 1987; BARNES; HUTTON; WALTERS, 1989). As a result, it is of high importance, for obtaining significant measurements, that rheometric devices could provide means of effectively control the temperature of samples under analysis. In this context,

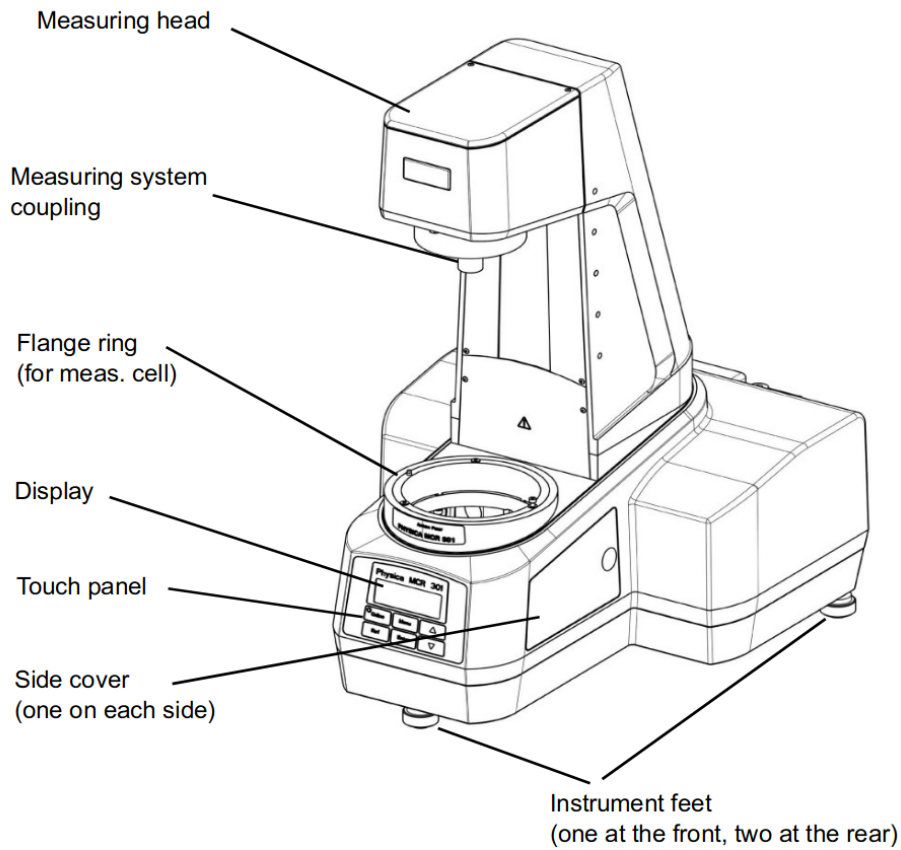
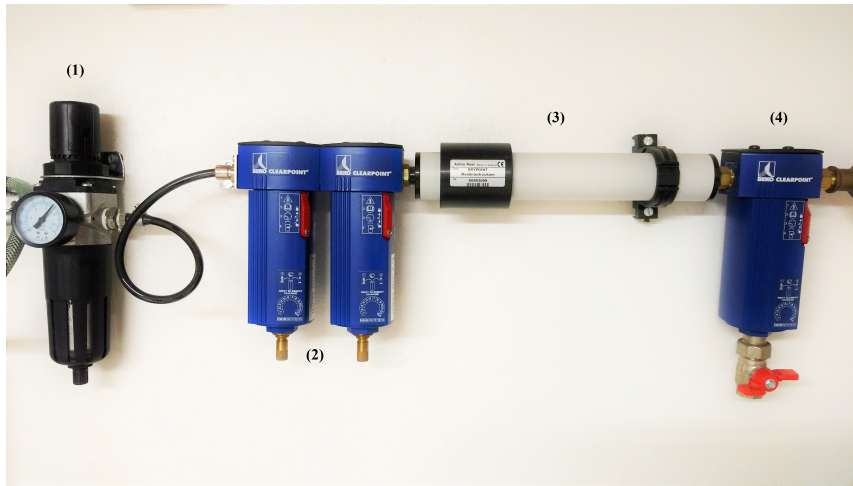


Figure 14 – Rheometer Anton Paar - model Physica MCR 301.



(a) Oil-free MSV6 compressor (Schulz S.A., Brazil)

The Physica MCR 301 rheometer presents different systems of temperature control, also called environmental systems, whose utilization depend on the measuring cell mounted on the flange ring of the device. It is important to note that the temperature control systems are highly accurate, with minimal thermal gradients. In addition, traceable automatic temperature calibration sensors are available to ensure that the system is always operating



(b) Air treatment system: (1) - water filter with manometer, (2) - solid particle filters, (3) - dehumidifier, (4) - oil filter.

Figure 15 – Pressurized air: production and treatment devices.

within specifications.

An environmental system designed to work with all the measuring cells is the liquid temperature control, which operates based on the flow of a liquid with controlled temperature through the measuring cell. The fluid exchange heat with the metal disk, where the material sample is placed. When thermal equilibrium is reached, the temperature of the sample under analysis tends to the temperature of flowing fluid (despite a small uncertainty). The refrigeration/heating fluid must have a well controlled temperature and flow with a high mass flux in order to fulfill the heat exchange needs for keeping the sample at a prescribed temperature. These properties of the flowing fluid are provided by an external Ecoline Staredition RE104 thermal bath (Lauda GmbH, Germany), which is coupled to the rheometer. This device is capable of working with water or oil as circulating fluid. The choice of which fluid to use must take into account their freezing and boiling points, due to the fact that this device can provide controlled temperatures from -30° up to 180°C .

Other environmental system available is the Peltier temperature control. In this technical solution, the temperature of the sample is controlled by a Peltier thermoelectric plate, that is attached to the fixed disk of the measuring cell. This system operates based on the Peltier effect, characterized by maintaining a temperature difference in the union of two conductors (or semiconductors) of distinct materials in a closed circuit when it is passed through by an electric current. This device allows fast, precise and active control of the sample temperature in a range from -40 to 200°C . It is interesting to note that the Peltier system cannot be used in applications where external magnetic fields are applied to the sample. In this case, temperature control is only done using the thermal bath.

Figure (17) summarizes the systems involved in the acquisition of the data concerning the rheological properties of a fluid sample. Despite the pneumatic control system already discussed in this section, the referred schematic representation shows that the



Figure 16 – Ecoline Staredition RE104 thermal bath (Lauda GmbH, Germany)

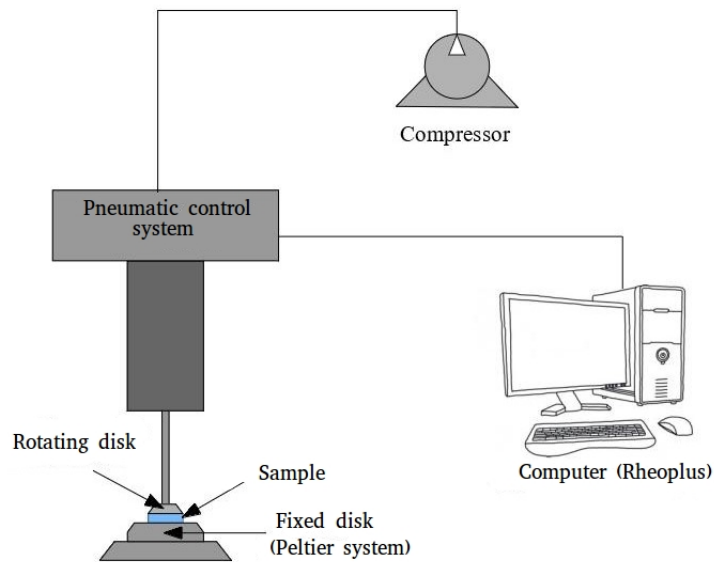


Figure 17 – Schematic.

rheometer is connected to a microcomputer, through which it is operated with the help of the software Rheoplus (Anton Paar GmbH, Germany). In this software, all conditions necessary for performing different types of rheological experimental trials are defined, such as the shear rate, the oscillation frequency, the amplitude of strain, the magnetic field intensity, the temperature of the sample or the heating-rate profile, among other parameters. Additionally, the software presents in real-time the collected data arranged in the form of graphs and tables. Several *ad-hoc* rheological models are available and automated in its database, what enables a preliminary post-processing analysis and, as a result, a previous verification of the adequacy of theoretical models to the data obtained from measurements. Figure (18) shows a typical image of the Rheoplus program interface during data collection.

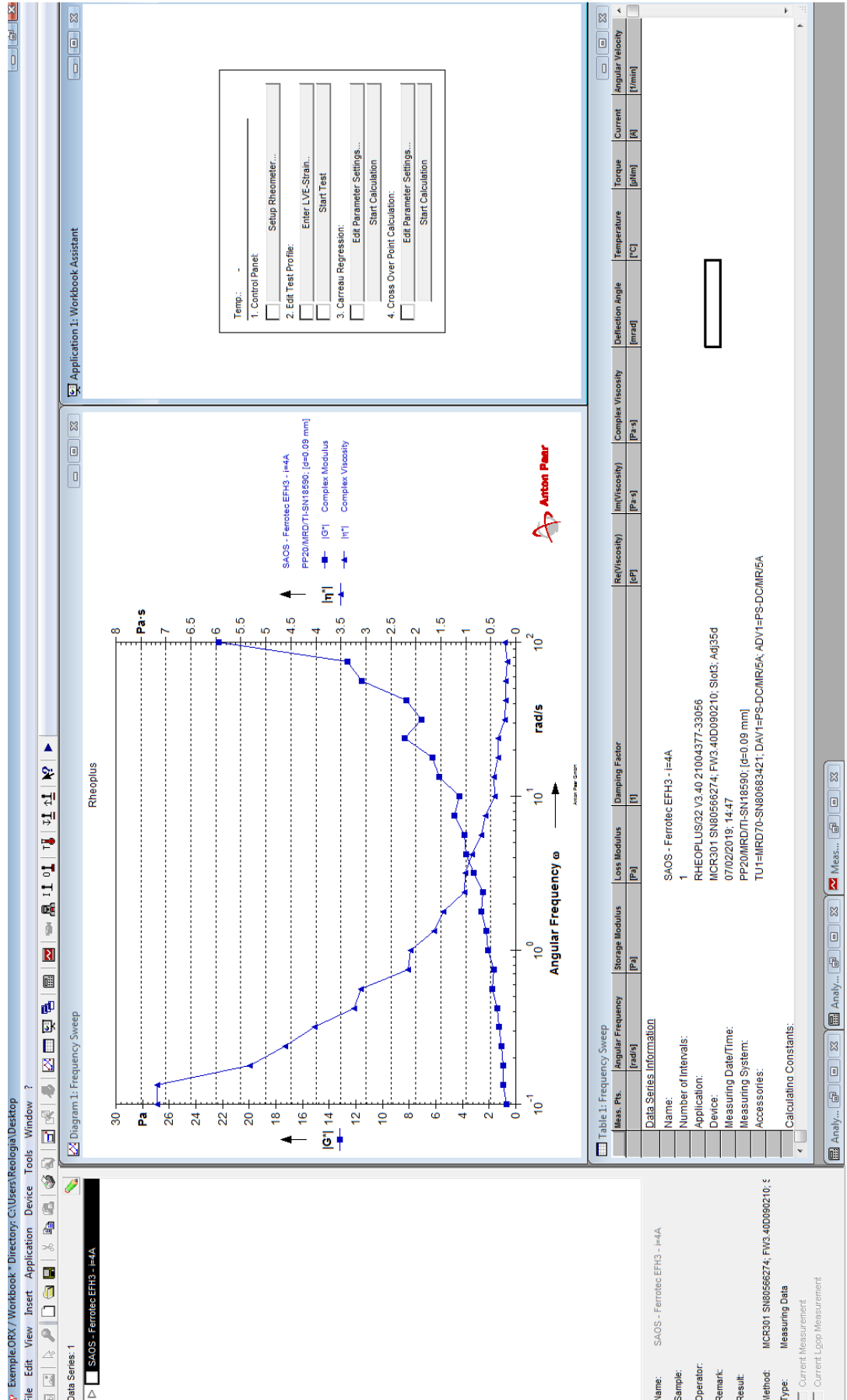


Figure 18 – Interface of the program Rheoplus during data acquisition of the complex modulus and viscosity of a ferrofluid in a small amplitude oscillatory shear flow under a strong magnetic field.

The assemblies of the rheometer used in this work are all of the parallel plate type. They are characterized by the fact that its test region, in which the fluid under analysis is placed, is a fictitious cylinder delimited by two discs, one mobile (measuring system) and the other fixed (measuring cell). The height of this cylinder, which is also the gap between the discs is a function of the fluid viscosity and should be optimized for each type of fluid under analysis. It is important to note that the device is equipped with the TruGap technology (Anton Paar GmbH, Germany), which permits the precise adjustment of the gap between the parallel plates to the value prescribed by the operator, independently of the temperature and thermal expansion of the assembly components. With this feature, small gaps (< 0.5 mm) can be achieved with micrometric precision. The volume of the fluid sample required to obtain a consistent experimental trial can be approximated by the volume of the fictitious cylinder, however it is a good practice to use a slightly larger volume to ensure that the space between the plates is fully filled during data collection.

In order to obtain meaningful measurements, the gap of the rheometer have been calibrated through the measurement of the viscosity of a series of different Newtonian fluids. Figure (19) shows the result of the measurement of the viscosity of water, at a constant temperature of 25°C , when subjected to a fixed shear rate of 100 s^{-1} . The gap used in the referred measurement was 0.08 mm, that resulted on a viscosity of 0.89 ± 0.01 mPa.s. This result is in agreement with the consolidated value presented for the viscosity of water at the referred temperature, what can be easily verified on (TANNER, 2000). As a result, such value of gap is the ideal for performing rheological measurements on fluids whose viscosities are of the same order of magnitude of the one observed for water.

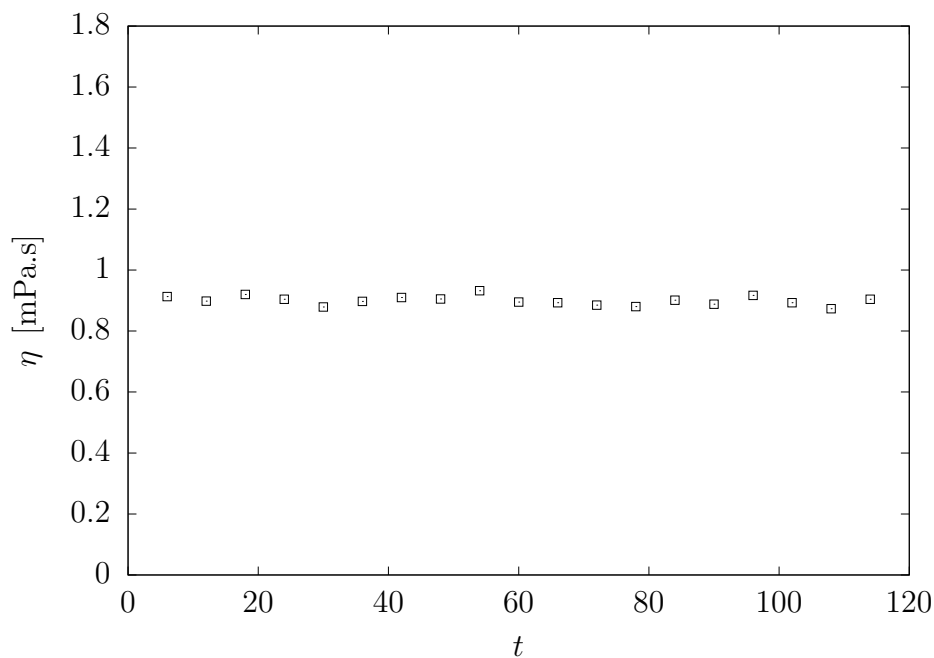


Figure 19 – Viscosity of distilled water as a function of time, measured on the rheometer of parallel plates Physica MCR-301. The shear rate is fixed at 100 s^{-1} and the temperature, at 25°C . The gap between the parallel plates is 0.8 mm.

Using the same methodology, it was possible to establish a reference of optimal gaps to be used in the measurement of the rheological properties of fluids with a wide range of viscosity. The results of this calibration are summarized on table (1).

Table 1 – Optimal gaps for carrying out rheological experiments, on fluids, as a function of the order of magnitude of their kinematic viscosity

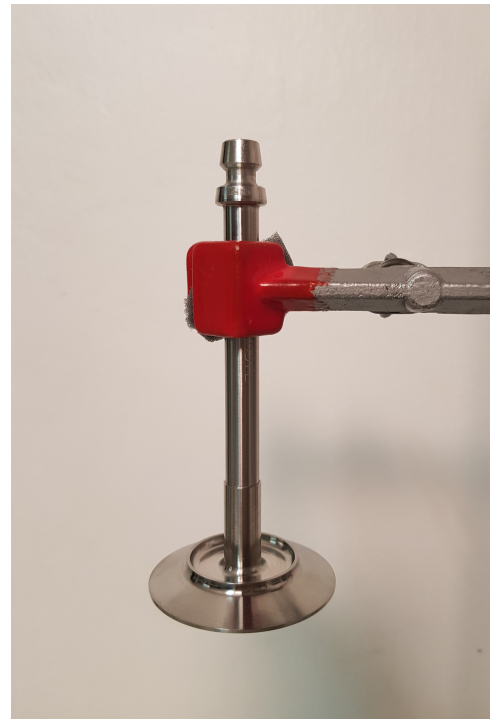
| Fluid | Viscosity [mPa.s] (order of magnitude) | Optimal gap |
|-----------------|---|-------------|
| Water | 1 | 0.08 |
| Ethylene glycol | 10 | 0.1 |
| Mineral oil | 100 | 0.3 |
| Glycerin | 1000 | 0.5 |
| Silicon oil | > 10000 | 0.8 |

5.1.1.1 Standard assembly

This mounting is presented in figure (20a). Its measuring system is denominated PP-50, which is a stainless steel rod that in one of its ends presents a disk with a diameter of 49.963 ± 0.005 mm.



(a)



(b)

Figure 20 – (a) Physica MCR 301 rheometer: standard Assembly. (b) Detail of the measuring system PP50.

The measuring cell in this assembly is a Peltier-temperature-controlled bottom plate. This assembly is used to measure rheological properties of Newtonian and non-Newtonian fluids in regimes of permanent and transient shear. Those properties can be

assessed as functions of time, shear-rate and, especially of temperature, due to the fact that this parameter is precisely controlled in this assembly.

5.1.1.2 Magneto-rheology assembly

This assembly is used to investigate the effects caused by the application of an external homogeneous magnetic field on the rheological behavior of a given magnetizable fluid. Generally, ferrofluids and magneto-rheological suspensions are investigated utilizing this apparatus. In this assembly, the measuring system is denominated PP-20, which is shown in figure (21a). It has the same geometry of PP-50, differing only in the diameter of the disk, that in this device measures $19.946 \pm 0.005\text{mm}$.

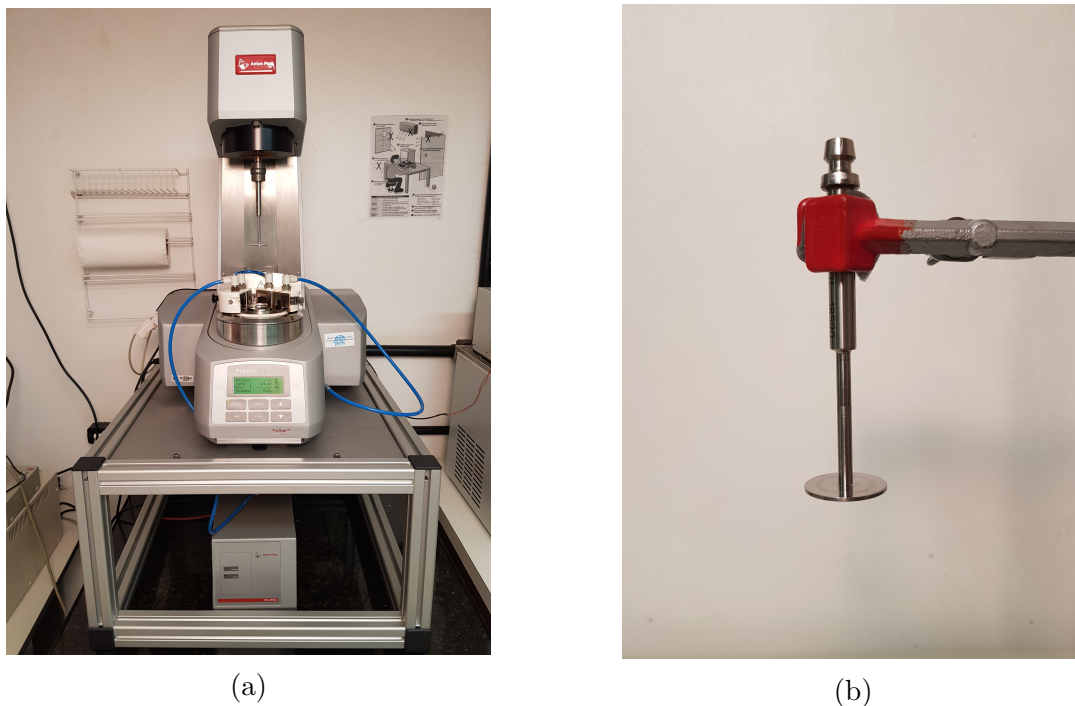


Figure 21 – (a) Physica MCR 301 rheometer: Magneto-rheology assembly. (b) Detail of the measuring system PP20.

In this assembly, the measuring cell is denominated MRD (magneto-rheological device) and it consists of a liquid-temperature-controlled bottom plate with built-in coils that produce magnetic field. A magnetic yoke covers the plate to ensure a homogeneous field and perpendicular field lines with respect to the plate. The parallel-plate system is made of non-magnetized metal, preventing radial forces acting on the shaft. The yoke can be temperature-controlled up to 70°C with the liquid used in the bottom plate. It is important to note that the Peltier temperature controller cannot be used in this assembly owing to the fact that it works based on an electric circuit, that would be certainly damaged by the external magnetic field applied by the coils located under the bottom plate. The MRD is fully integrated in the rheometer's software, which controls the magnetic field and records all important parameters. Measurements of the magnetic field are made using an external Hall sensor. All the features summarized here are displayed on figure (22).

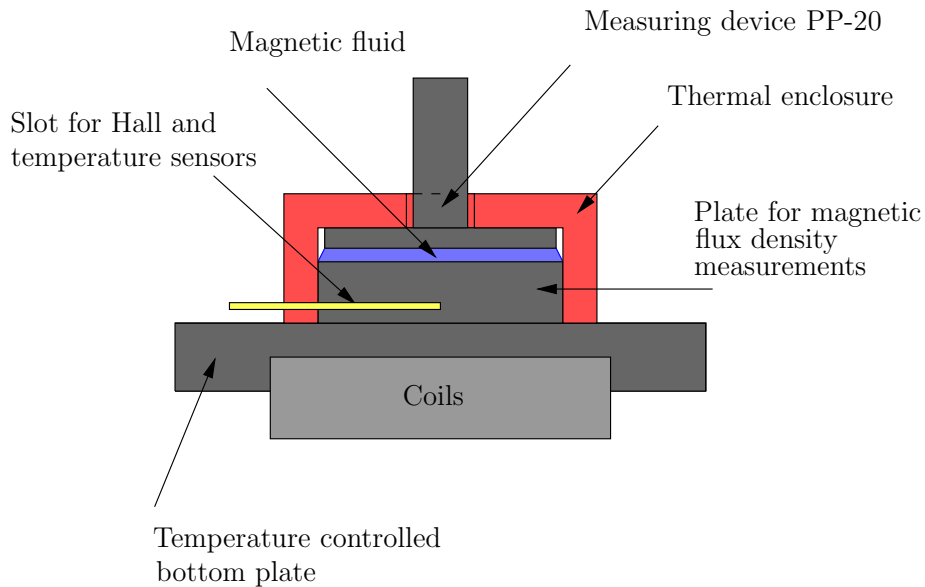


Figure 22 – MRF assembly: schematic of the measuring cell.

The continuous current needed to generate the magnetic field by the coils of the measuring cell is provided by a PS-MRD DC power supply (Anton Paar GmbH, Germany), which is shown in figure (23). This device can furnish continuous currents up to 5A between its terminals. In this maximum condition of operation, the coils produce an magnetic field of up to 1.3 Tesla in the air gap between the parallel disks.



Figure 23 – PS-MRD DC power supply (Anton Paar GmbH, Germany).

5.2 Fluids under analysis

In this dissertation, the rheological behavior of two ferrofluids is described: EFH1 and EFH3, which are produced by the Ferrotec Corporation (USA). Those fluids are examples of the EFH product series, which is a class designed to be used on educational

applications. Regarding this context, they feature strong magnetic properties, such as the magnetization of saturation, in order to make easy the visualization of magnetic patterns that result from the interaction between the fluid and an external magnetic field. These ferrofluids are suspensions of nanoparticles of magnetite (Fe_3O_4) dispersed on a base fluid composed of synthetic hydrocarbons, possessing very low volatility and high thermal stability. The average particle diameter on both ferrofluids is 10nm.

The characteristics regarding the ferrofluids EFH1 and EFH3, according to technical data obtained from the producer, are summarized on table (2).

Table 2 – Properties of the ferrofluids EFH1 and EFH3.

| Ferrofluid | M_s (kA/m) | ϕ | η_0 (cP) (27°C) | ρ (g/ml) (25°C) | Base fluid |
|------------|--------------|--------|----------------------|----------------------|--------------|
| EFH-1 | 35.0 | 7.9% | 6.0 | 1.21 | hydrocarbons |
| EFH-3 | 52.5 | 11.8% | 12.0 | 1.42 | hydrocarbons |

5.3 Rheometry

5.3.1 Measurement of the apparent viscosity on a parallel plate rheometer

In a parallel disk system, whose schematic representation is show at figure (24), when the upper disk is rotated with constant angular velocity, the torque \mathcal{T} required to achieve this rotation, the total force \mathcal{F} required to maintain the disks at a separation H and the pressure distribution $(p + \sigma_{zz})|_{z=0}$ across one of the plates can be measured. From this measurements, one can obtain expressions for some material functions of a given complex fluid, such as for its apparent viscosity $\eta(\dot{\gamma})$, which will be done in the rest of this section.

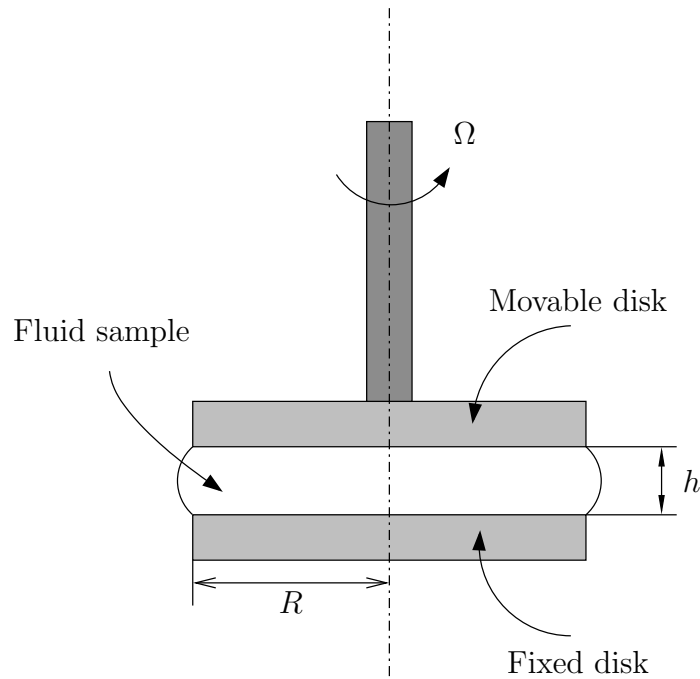


Figure 24 – Schematic representation of a parallel disk rheometer, where R is the maximum radius of the disks and H their spacing.

We begin by considering the shearing surfaces as fluid planes of constant z , each one rotating with an angular velocity $\Omega(z)$, that depends on its position between the parallel disks. Under these conditions and considering a cylindrical coordinate system, as shown in figure (25), it is reasonable to assume that the velocity field is $u_r = u_z = 0$ and $u_\varphi \neq 0$, that is:

$$\mathbf{u} = \begin{bmatrix} 0 \\ u_\varphi \\ 0 \end{bmatrix}_{r\varphi z}. \quad (5.1)$$

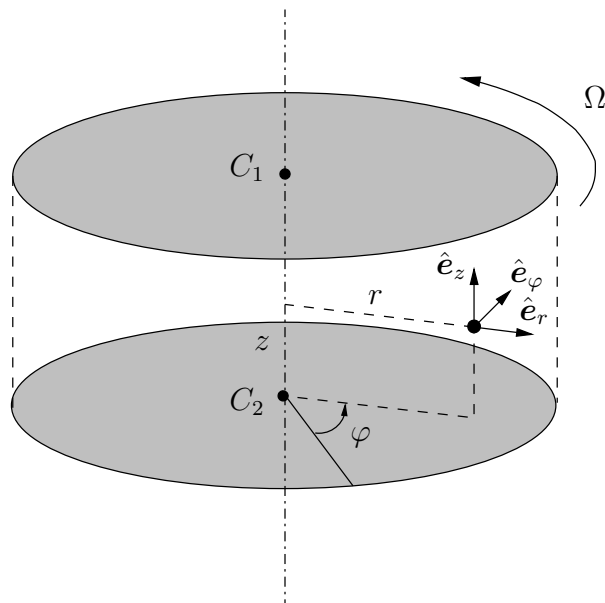


Figure 25 – Parallel plates with cylindrical coordinate system.

With the referred velocity field and assuming that the fluid is incompressible, the application of the continuity equation leads to:

$$\nabla \cdot \mathbf{u} = 0 \quad \longrightarrow \quad \frac{\partial u_\varphi}{\partial \varphi} = 0. \quad (5.2)$$

Now, assuming that a simple shear flow develops in the φ direction, with velocity gradient in the z direction, that is, the velocity profile is linear on z , it can be written that:

$$u_\varphi = A(r)z + B(r), \quad (5.3)$$

where $A(r)$ and $B(r)$ are unknown functions of r . Looking at the cylindrical coordinate system shown in the figure (25), it comes that the boundary conditions for the velocity field are given by: $u_\varphi = 0$ in $Z = 0$ and $u_\varphi = r\Omega$ at $Z = h$, in which $h = ||C_1 - C_2||$ is the spacing between the two disks (C_1 and C_2 are points located, respectively, at the center of the upper and the lower disk). Applying these conditions to the equation (5.3), one obtains:

$$u_\varphi = \frac{r\varphi z}{h}. \quad (5.4)$$

After the determination of the velocity field, the rate of strain tensor \mathbf{D} can be calculated as follows:

$$\mathbf{D} = \frac{\nabla \mathbf{u} + (\nabla \mathbf{u})^T}{2} = \frac{1}{2} \begin{bmatrix} 0 & \frac{\partial u_\varphi}{\partial r} - \frac{u_\varphi}{r} & 0 \\ \frac{\partial u_\varphi}{\partial r} - \frac{u_\varphi}{r} & 0 & \frac{u_\varphi}{z} \\ 0 & \frac{u_\varphi}{z} & 0 \end{bmatrix}_{r\varphi z} = \begin{bmatrix} 0 & 0 & 0 \\ 0 & 0 & \frac{r\Omega}{2h} \\ 0 & \frac{r\Omega}{2h} & 0 \end{bmatrix}_{r\varphi z} \quad (5.5)$$

Thus, the shear-rate $\dot{\gamma}$, calculated from its definition, is given by:

$$\dot{\gamma} = ||2\mathbf{D}|| = (2\mathbf{D} : \mathbf{D})^{\frac{1}{2}} = \frac{r\Omega}{h}. \quad (5.6)$$

At the extremity of the moving disk ($r = R$), the shear-rate is given by: $\dot{\gamma} = \dot{\gamma}_R$. Therefore, regarding the hypothesis that the velocity profile in z is linear, the shear-rate for any given r may be expressed as a function of $\dot{\gamma}_R$ as follows:

$$\dot{\gamma} = \dot{\gamma}_R \frac{r}{R}, \quad (5.7)$$

where, $\dot{\gamma}_R = R\Omega/h$. Based on this, it is now possible to calculate an expression for the angular strain, having in mind that it is also a function of r , what is done by:

$$\gamma(0, t) = \int_0^t \dot{\gamma}(t') dt' = \int_0^t \frac{R\Omega}{h} dt' = \frac{R\Omega t}{h} \quad (5.8)$$

Looking at the equations (5.4) and (5.5), one realizes that the effect of curvature in the φ direction was ignored. This was so, due to the fact that, according to Morrison (2001), the effects coming from the referred curvature on simple shear flows are insignificant and, therefore, the flow can be considered unidirectional in φ , having the form

$\mathbf{u} = \dot{\gamma}z\hat{\mathbf{e}}_\varphi$. This hypothesis of unidirectional flow applies more effectively to the disk end, where $r = R$, what justifies the calculation of viscosity from the following relationships:

$$\sigma_{12} = \sigma_{z\varphi}|_{r=R}, \quad (5.9)$$

$$\dot{\gamma}_0 = \frac{R\Omega}{h} = \dot{\gamma}_R, \quad (5.10)$$

$$\eta = \frac{\sigma_{21}}{\dot{\gamma}_0} = \frac{\sigma_{z\varphi}}{\dot{\gamma}_r}. \quad (5.11)$$

The equation (5.11) implies that, to calculate the viscosity, it is necessary to know $\sigma_{z\varphi}$ in $r = R$, which is done by observing that the flow is axisymmetric in z and, therefore, the stress tensor in cylindrical coordinates assumes the following form:

$$\boldsymbol{\sigma} = \begin{bmatrix} \sigma_{rr} & 0 & 0 \\ 0 & \sigma_{\varphi\varphi} & \sigma_{z\varphi} \\ 0 & \sigma_{z\varphi} & \sigma_{zz} \end{bmatrix}_{r\varphi z}. \quad (5.12)$$

In order to write the equations of motion using this form of the stress tensor, we assume by hypothesis:

1. Steady, laminar, isothermal flow;
2. Negligible body forces;
3. Cylindrical edge.

Under those conditions, the components of the equation of motion (Cauchy's equation) can be written as:

$$r - \text{component} : \quad \frac{\rho u_\varphi^2}{r} = \frac{1}{r} \frac{\partial}{\partial r} (r\sigma_{rr}) - \frac{\sigma_{\varphi\varphi}}{r}, \quad (5.13)$$

$$\varphi - \text{component} : \quad 0 = \frac{\partial \sigma_{z\varphi}}{\partial z}, \quad (5.14)$$

$$z - \text{component} : \quad 0 = \frac{\partial \sigma_{zz}}{\partial z}. \quad (5.15)$$

The torque \mathcal{T} required to rotate the upper disk (or to keep the lower disk stationary) is given by:

$$\mathcal{T} = \int_A -\sigma_{z\varphi}(r, z = h)(2\pi r dr). \quad (5.16)$$

Also, viscosity at any value of r can be written as follows:

$$\eta = \frac{-\sigma_{21}}{\dot{\gamma}_0} = \frac{-\sigma_{z\varphi}}{\dot{\gamma}(r)} = \eta(r), \quad (5.17)$$

which, substituted on equation (5.16), results in:

$$\mathcal{T} = 2\pi \int_0^R \eta(r) \dot{\gamma} r^2 dr. \quad (5.18)$$

The equation (5.18) implies that the torque is given as a function of an integral over the viscosity and shear rate, however, for practical reasons, it is more usual to express viscosity as a function of torque, given that the latter is the truly experimentally obtained parameter. For this, an approach similar to the Weissenberg-Rabinowitsch correction factor (MORRISON, 2001), which was originally proposed to determine viscosity as a function of shear rate from experimental data, obtained from capillary tube tests. In the context of the flow under study, which is performed between parallel disks, the approach is to differentiate the equation (5.18) with respect to the the-shear rate. In order to do that, one first eliminates r in equation (5.18), using the following change of variables: $\dot{\gamma} = \dot{\gamma}_R r/R$. This results on:

$$\mathcal{T} = \frac{2\pi R^3}{\dot{\gamma}_R^3} \int_0^{\dot{\gamma}_R} \eta \dot{\gamma}^3 d\dot{\gamma}. \quad (5.19)$$

Next, using the rule of Leibniz (ARIS, 2012), one differentiates both sides of equation (5.19) with respect to $\dot{\gamma}_R$, obtaining:

$$\frac{\mathcal{T}}{2\pi R^3} \dot{\gamma}_R^3 = \int_0^{\dot{\gamma}_R} \eta \dot{\gamma}^3 d\dot{\gamma}, \quad (5.20)$$

$$\frac{d}{d\dot{\gamma}_R} \left[\frac{\mathcal{T}}{2\pi R^3} \dot{\gamma}_R^3 \right] = \int_0^{\dot{\gamma}_R} \frac{\partial}{\partial(\dot{\gamma}_R)} (\eta \dot{\gamma}^3) d\dot{\gamma} + \eta(\dot{\gamma}_R) \dot{\gamma}_R^3. \quad (5.21)$$

The first term on the right side of the equation is zero, so, by rearranging the terms, one obtains an equation for the apparent viscosity measured on a torsional rheometer of parallel disks, which is:

$$\eta(\dot{\gamma}_R) = \frac{\mathcal{T}}{2\pi R^3 \dot{\gamma}_R} \left[3 + \frac{d \log\left(\frac{\mathcal{T}}{2\pi R^3}\right)}{d \log \dot{\gamma}_R} \right]. \quad (5.22)$$

Therefore, to measure the apparent viscosity of any given fluid on a parallel disk rheometer based on the shear-rate evaluated on the border of the disk $\dot{\gamma}_R$, it is necessary to obtain experimental data of the viscosity for multiple values of $\dot{\gamma}_R$, that is, for a wide range of Ω , so that the torque derivative shown in equation (5.22) can be calculated. Based on this, one can finally apply the correction represented by the bracketed term in this equation to each pair of data $(\mathcal{T}, \dot{\gamma}_R)$.

It is important to note that the material particles do not experience the same angular deformation (γ) because it varies with the radius, as shown in equation (5.8). On the other hand, the torque \mathcal{T} is an integral quantity and, as a result, it represents the contribution of all fluid elements subjected to shear, which is also verified for viscosity, since it is obtained from the measurement of the torque. Therefore, this property represents an average viscosity that would be calculated for each element subjected to a different shear

rate. This only poses a problem for fluids that are very sensitive to angular deformation, such as liquid crystals and multiphase fluids.

The formula (5.22) permits the obtainment of the viscosity as a function of torque for any fluid in a parallel disc rheometer. Therefore, it is also applicable to Newtonian fluids, for which it is considerably simpler. By developing the exact differentials of the numerator and denominator on the right side of the equation (5.22), we obtain that:

$$d \left[\log \left(\frac{\mathcal{T}}{2\pi R^3} \right) \right] = \frac{2\pi R^3}{\ln(10)} d \left(\frac{\mathcal{T}}{2\pi R^3} \right), \quad (5.23)$$

and

$$d [\log(\dot{\gamma}_R)] = \frac{1}{\ln(10)\dot{\gamma}_R} d(\dot{\gamma}_R). \quad (5.24)$$

Dividing equations (5.23) and (5.24), we obtain that:

$$\frac{d \log \left(\frac{\mathcal{T}}{2\pi R^3} \right)}{d \log \dot{\gamma}_R} = \frac{2\pi R^3 \dot{\gamma}_R}{\mathcal{T}} \frac{d \left(\frac{\mathcal{T}}{2\pi R^3} \right)}{d(\dot{\gamma}_R)}. \quad (5.25)$$

For a Newtonian fluid, it is easily shown that the applied torque on a parallel disks configuration (Couette flow) is given by:

$$\mathcal{T} = \pi \dot{\gamma}_R \eta \frac{R^3}{2}. \quad (5.26)$$

Replacing this result on equation (5.25), it comes that:

$$\frac{d \log \left(\frac{\mathcal{T}}{2\pi R^3} \right)}{d \log \dot{\gamma}_R} = \frac{4}{\eta} \frac{d \left(\frac{\dot{\gamma}_R \eta}{4} \right)}{d(\dot{\gamma}_R)}. \quad (5.27)$$

Since viscosity η is constant with respect to shear-rate variations for a Newtonian fluid, one obtains:

$$\frac{d \log \left(\frac{\mathcal{T}}{2\pi R^3} \right)}{d \log \dot{\gamma}_R} = \frac{d(\dot{\gamma}_R)}{d(\dot{\gamma}_R)} = 1. \quad (5.28)$$

Because of this result, it can be shown that equation (5.22) for a Newtonian fluid reduces to:

$$\eta(\dot{\gamma}_R) = \frac{\mathcal{T}}{2\pi R^3 \dot{\gamma}_R} [3 + 1] = \frac{2\mathcal{T}}{\pi R^3 \dot{\gamma}_R}. \quad (5.29)$$

Substituting expression (5.10) on equation (5.29), one obtains:

$$\eta(\dot{\gamma}_R) = \frac{2\mathcal{T}h}{\pi \Omega R^4}. \quad (5.30)$$

6 RESULTS: RHEOLOGY OF FERROFLUIDS

6.1 Permanent shear analysis

In this section, it will be shown and discussed the experimental results concerning the rheological behavior of the apparent viscosity η as a function of the magnetic field intensity H and of the shear flow intensity $\dot{\gamma}$. As a result, it will be discussed the magnetoviscous effect, which is the elevation of the viscosity of a ferrofluid when it is placed under the influence of an external magnetic field and the pseudoplastic effect, which is the shear rate dependence of the ferrofluid's viscosity, which also appears when it is subjected to an external magnetic field.

In order to focus on the physical meaning of the material functions and the variables on which they depend, they are going to be denoted by nondimensional parameters. Regarding this context, the intensity of the effective applied magnetic field is expressed by the magnetic parameter α , defined as:

$$\alpha = \frac{\mu_0 m H}{k_B T}, \quad (6.1)$$

where, μ_0 is the vacuum magnetic permeability, m is the intensity of the magnetic dipole momentum of a magnetic particle, H is the modulus of the effective magnetic field, k_B is the Boltzmann constant and T is the absolute temperature. Besides that, the intensity of the magnetic dipole of a single-domain particle can be expressed in terms of its magnetization of saturation by

$$m = v_p M_d, \quad (6.2)$$

in which, $v_p = 4\pi a^3/3$ is the volume of a magnetic particle of radius a and M_d is the magnetization of the material that composes the particles. Replacing equation (6.2) into (6.1) one obtains:

$$\alpha = \frac{\mu_0 v_p M_d H}{k_B T}. \quad (6.3)$$

It is important to remark that this parameter is a ratio between the magnetic and the Brownian forces.

Other important parameter is the ratio between the magnetic dipolar force and the Brownian force, named parameter of dipolar interaction,

$$\lambda = \frac{\mu_0 \pi v_p M_d^2}{24 k_B T} \quad (6.4)$$

It is important to note that this parameter is intrinsically related to the formation of particles chains. Big values of λ indicate that the magnetic force is much intenser than the Brownian one, making it possible for aggregates to form. The particles which compose the ferrofluids used in the experiments have the same average diameter (10 nm) and are formed by the same material, magnetite, whose magnetization M_d is 440 kA/m. Besides that, the experiments were carried out at a constant temperature of 300 K. Regarding this context, in this work, the parameter of dipolar interaction is constant for both ferrofluids and equals to 1.3.

The intensity of the flow, measured by its shear-rate, is referred in this work by the number of Peclet. This nondimensional parameter is defined as a ratio between two characteristic times, one related to Brownian diffusion τ_d and other to the flow's convection τ_f , that is:

$$Pe = \frac{\tau_d}{\tau_f}. \quad (6.5)$$

As the particles that make up the ferrofluids have a mean characteristic length of approximately 10^{-9} m, its movement, in the absence of flow or external magnetic field, is dominated by the Brownian motion. Because of that, the characteristic time of diffusion can be modeled as the inverse of the Stokes-Einstein coefficient of diffusion D (EINSTEIN et al., 1905),

$$\tau_d = \frac{a^2}{D} = \frac{6\pi\eta a^3}{k_B T}. \quad (6.6)$$

Following the same idea, the characteristic time of the flow can be defined as:

$$\tau_f = \frac{1}{\dot{\gamma}}. \quad (6.7)$$

Replacing equations (6.6) and (6.7) into equation (6.5), one obtains:

$$Pe = \frac{6\pi\eta a^3 \dot{\gamma}}{k_B T}. \quad (6.8)$$

The apparent viscosity of a ferrofluid is composed, when in the presence of an external magnetic field, by Einstein's viscosity η_ϕ , which is a correction to the viscosity of the base fluid originated from the presence of the rigid particles in the suspension, by a correction of the viscosity of the base fluid due to hydrodynamic interactions η_h between the particles, by the rotational viscosity η_r , induced by the external magnetic field and also, by a correction to the viscosity of the suspension owing to dipolar interactions between the magnetic particles, η_d . This apparent viscosity function is made nondimensional by defining its characteristic scale η^* as the viscosity of the ferrofluid in the absence of external magnetic field η_0 , which is the viscosity of the suspension, describe above, removing the

effect of the magnetic field, that is, excluding the rotational viscosity η_r . As a result, the nondimensional viscosity is given by:

$$\tilde{\eta} = \frac{\eta}{\eta^*} = \frac{\eta}{\eta_0}. \quad (6.9)$$

6.1.1 Magnetoviscous effect

In this subsection, it is presented the magnetoviscous effect of the ferrofluids EFH1 and EFH3, that is, the increase of their viscosity in response to an elevation on the intensity of the applied magnetic field.

6.1.1.1 Experimental procedure

The magneto viscous effect of a sample of ferrofluid is evaluated by fixing the shear flow intensity and applying a continuous increase of magnetic field intensity H^1 , which is varied, in the experiments here detailed, from 0 to 2.07×10^5 A/m, considering three fixed intensities of the shear flow $\dot{\gamma}$: 100, 2500 and 5000s^{-1} .

The determination of the optimized gap between the disks of the rheometer, which is used in the experimental trials must be chosen carefully, due to the fact that both ferrofluids present a severe change on their viscosity as the intensity of the magnetic field strengthens. For each of the three flow intensities, the process of choosing the optimal gap for each ferrofluid was carried out following these steps:

1. In the absence of external magnetic field, the viscosity of EFH1, at 25°C , is lower than 6 cP. For EFH3, at the same temperature, the value of this property is lower than 12 cP. The usual gap to measure the viscosity of water, which is 0.89cP at the referred temperature, is 0.08mm. As a result, by comparison, a gap of 0.1mm is a good choice to measure the viscosity of both ferrofluids in the referred condition. This gap value was considered the bottom limit for choosing the optimal gap;
2. For a condition of medium magnetic field intensity, $H= 2.07 \times 10^5$, six gaps were tried for both ferrofluids, 0.2, 0.3, 0.4, 0.5, 0.6 and 0.7. The ones that resulted in a lower variation of the viscosity were chosen;
3. The same process was repeated for the highest intensity of magnetic field applied. Gaps that implicated on lower variability of the viscosity being measured were chosen as alternatives for the optimized gap;
4. Regarding the results obtained in the last two steps, one chooses an intermediate gap for each fluid that, when applied to the limit conditions of low and high magnetic field intensities, generates variability in the viscosity results lower than 5%.

¹ The intensity of the magnetic field is a part of the intensity of the induced magnet field B, generated by the application of a current to the coils located under the lower fixed disk of the rheometer.

For each of the flow intensities, the gaps chosen for the ferrofluids are displayed on table (3)

Table 3 – Optimal gaps used in the experimental evaluations of the magnetoviscous effect of the ferrofluids EFH1 and EFH3, for different flow intensities.

| $\dot{\gamma}$ | EFH1 | EFH3 |
|----------------|------|------|
| 100 | 0.4 | 0.6 |
| 2500 | 0.2 | 0.3 |
| 5000 | 0.2 | 0.3 |

Having chosen the optimal gap, the experimental evaluation of the magnetoviscous effect, for each fixed condition of flow intensity (constant shear rate), presented by both ferrofluids was done by applying the following experimental protocol:

1. The volume of ferrofluid needed to fulfill the optimum gap is calculated and, after, this quantity is pipetted in the testing area;
2. The upper disk is lowered until the prescribed gap is achieved between the two disks. The gap is visually inspected in order to identify possible leakages of the sample, which, if found, must be cleaned due to the fact that they can severely increase the experimental error;
3. The magnetic yoke is placed around the measuring device. A demagnetization procedure is applied to the sample, in order to free the ferrofluid of any previous magnetic effects;
4. The temperature of the experiment, 25°C, is set on the thermal bath attached to the rheometer. After this, enough time is waited for the temperature of the sample, here defined as the temperature of the lower plate, which is measured by the rheometer, to reach the target temperature;
5. Using the software *Rheoplus*, the flow condition is set, which is resumed to define a constant value of shear-rate for the experimental trial;
6. Using the software *Rheoplus*, the magnetic field conditions are programmed indirectly by controlling the electric current that the power supply (PS-MRD) provides to the coils located under the bottom disk of the rheometer (see figure 5.8). The current is programmed to vary from 0 to 5A, following a linear increase ramp. Between these limits, 15 data points are collected, each one with a variable time of measurement, due to the fact that the option "*no time setting*" is active during the data acquisition. This feature ensures that enough time is being waited at each data acquisition in order to guarantee that the steady state has been achieved when the data collection is done.

7. The viscosity and the shear stress are acquired as a function of the magnetic field intensity for a given constant condition of shear rate.

This process was carried out 10 times, for each ferrofluid, at every condition of flow intensity prescribed. The experimental errors were calculated using the methodology presented on appendix (A.1).

6.1.1.2 Discussion

The first insights on the physical process behind the increase of viscosity on magnetic colloids by the action of applying an external magnetic field were drawn considering the experimental works of [McTague \(1969\)](#), [Hall and Busenberg \(1969\)](#). The authors reported an increase of about 40 % in the viscosity of a ferrofluid, composed by hard Cobalt spherical particles with a diameter of about 10 nm and volume fraction of 0.05%, when subjected to a weak flow in the presence of an orthogonal external homogeneous magnetic field with intensity varying from 0 to 8 kG. In other words, it can be said that the ferrofluids evaluated on these works are highly diluted suspensions composed by small spheres, which are considered to be magnetically hard, that is, its characteristic length scale (e.g. diameter) is big enough for its Néel time τ_N to be much greater than its Brownian time τ_B . This guarantees that the magnetic moment m is fixed in the particle and. As a result, when the magnetic dipole is rotated by the magnetic torque in order to align itself with the external field, the whole particle rotates with it. It is important to remark that, since the suspensions are diluted, the particles do not interact neither hydrodynamically, nor magnetically.

Based on those assumptions, the referred authors explain that the magnetoviscous effect arises from a hindrance of rotation perpetrated by the suspended magnetic particles due to the action of the magnetic field. That is, the particles are no longer free to rotate by the action of the flow-induced mechanical torque, because when an external magnetic field is applied, the magnetic moment m of the particles will try to align with the magnetic field direction by the action of the magnetic torque, that arises from the misalignment between m and H promoted by the mechanical torque. Such competition between mechanic and magnetic torque increases the local viscous dissipation of energy in each particle, what is translated in an increase of the suspension's viscosity.

Regarding this context, a rigorous theoretical analysis of this phenomenon was firstly addressed by [Shliomis \(1971\)](#), which considering the Brownian motion of the particles, derived an expression to model the change of viscosity as a function of the strength and direction of the applied magnetic field, which is given by

$$\eta_r = \Delta\eta = \eta(\alpha) - \eta_0 = \frac{3}{2}\eta_0\phi_h\alpha\frac{L(\alpha)}{2 + \alpha L(\alpha)}, \quad (6.10)$$

where, η_r is called the rotational viscosity, $\eta(\alpha)$ is the viscosity of the ferrofluid for a given intensity of magnetic field α , η_0 is the viscosity of the ferrofluid in the absence of an

external magnetic field, ϕ_h is the volume concentration of the magnetic particles including surfactant and $L(\alpha) = \coth(\alpha) - \alpha^{-1}$ is the Langevin function. It is important to note that for diluted suspensions, the viscosity of magnetic colloids of nanoparticles, in the absence of magnetic field, is composed by the viscosity of the base fluid η_b enhanced by the presence of the suspended particles, that is $\eta_0 = \eta_b(1 + 2.5\phi_h)$, which is Einstein's viscosity.

Considering a microscopic approach, using the kinetic theory and defining the ferrofluid as an ideal suspension of non-interacting magnetic dipoles subjected to magnetic field, Brownian motion and the vorticity of the flow, [Martsenyuk, Raikher and Shliomis \(1974\)](#) predicted, for weak flows, the following relation for the dependence of the rotational viscosity on the intensity of the magnetic field:

$$\eta_r = \Delta\eta = \frac{3}{2}\eta_0\phi_h\frac{\alpha L^2(\alpha)}{\alpha - L(\alpha)}. \quad (6.11)$$

This model is generally referred as the non-interacting model ([ODENBACH, 2009](#)).

Figure (26) presents the increase in the relative viscosity as a function of α . The black squares present the results obtained for the ferrofluid EFH1 at a condition of weak flow ($Pe = 4.64 \times 10^{-4}$). This ferrofluid is composed by magnetite hard particles at a volume fraction of 7.9%. The insert presents other results: the circles are experimental data obtained from [Odenbach and Thurm \(2002\)](#) for a ferrofluid composed by magnetite hard particles at a volume concentration of 7.2% in a similar condition of weak flow ($Pe = 1.85 \times 10^{-2}$). Besides that, it is also shown a curve, which was generated applying the properties of EFH1 to equation (6.11). It is immediate from figure (26) and from its insert that the dependence of the viscosity increment on the intensity of the magnetic field is much stronger than the non-interacting model was able to predict. According to [Odenbach \(2009\)](#), the discrepancies between ideal and real ferrofluids arises from the fact that the ideal ones are considered high diluted and, as a result, its particles do not interact. However, real ferrofluids, which generally have volumetric fractions of particles in the range of 7–10%, cannot be considered diluted and, therefore, the effect of interparticle interactions must be considered. In concentrated ferrofluids, those interactions, such as the dipolar interactions, lead to formation of particles chains and agglomerates which produce a much severe hindrance of rotation, leading to a much intenser increase on viscous dissipation and, as a result on overall viscosity of the fluid. [Odenbach and Thurm \(2002\)](#) argue that, as in other complex fluids, the transport and rheological properties of ferrofluids are strongly influenced by their internal, flow- and field-induced structures.

It is interesting to observe that the increment on the viscosity of saturation $\Delta\eta/\eta_0(\infty)$ of EFH1 is harshly different from the one obtained in the work of [Odenbach \(2009\)](#), even though both fluids are subjected to very similar weak-flow conditions. This effect comes from the difference in the volume concentration of the fluids. Since more particles per volume of fluid are available on EFH1, induction of particle aggregates formation can be done on a wider range of α in comparison to the fluid tested in the work

of Odenbach (2009). That is, the field-induced microstructure of EFH1 can structurally responds to a wide range of field intensities and, reaching its maximum complexity (bigger length scale of the chains and agglomerates) for a high value of α , regarding a fixed weak-flow condition.

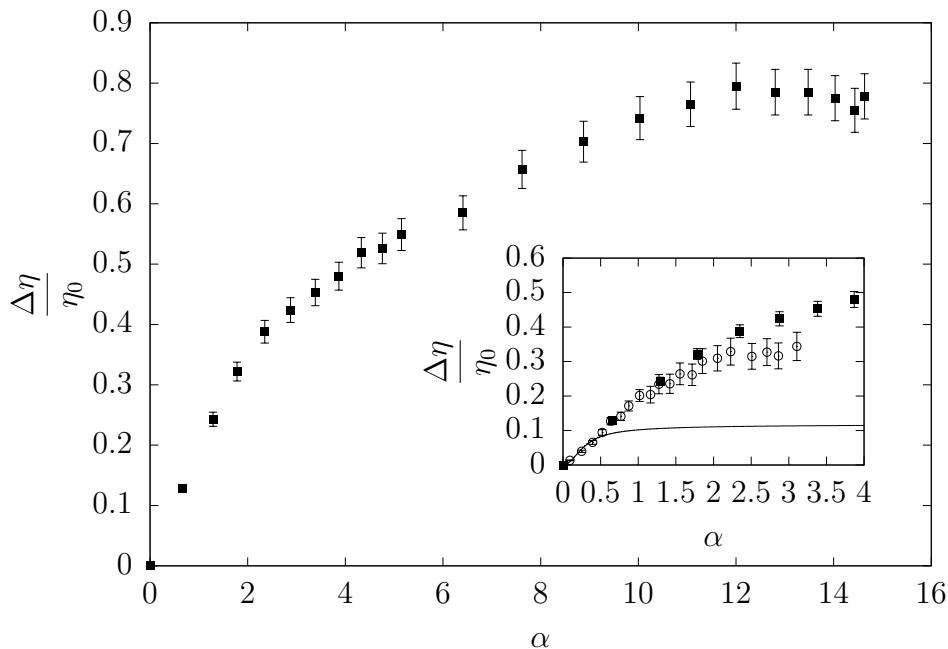


Figure 26 – Relative viscosity increment $\Delta\eta/\eta_0$ as a function of the non-dimensional magnetic field strength α subjected to a weak flow, $Pe = 4.64 \times 10^{-4}$ (■). In the insert, it is shown a comparison of the behavior of $\Delta\eta/\eta_0$ as a function of α for two magnetic fluids: (■) represents, as previously, the data obtained for the ferrofluid EFH1, which is a colloidal suspension of magnetite particles with mean diameter of 10 nm and $\phi = 7.9\%$ subjected to $Pe = 4.64 \times 10^{-4}$, (○) speaks for the data presented on the work of Odenbach (2009) for a colloidal suspension of magnetite particles with mean diameter of 10 nm and $\phi = 7.2\%$ subjected to a similar weak flow, $Pe = 1.85 \times 10^{-2}$). The curve is theoretically predicted behavior by equation (6.11), considering $\phi = 7.9\%$. The viscosity in the absence of magnetic field η_0 is constant and, at $25^\circ C$, equals to 0.94×10^{-2} Pa.s.

Figures (27) and (28) respectively show the behavior of the relative viscosity increase $\Delta\eta/\eta_0$ of the ferrofluids EFH1 and EFH3 as functions of the intensity of the applied magnetic field, here denoted by the magnetic parameter α . For each fluid, the referred viscosity variation was obtained considering three intensities of shear flow: a weak-flow ($\mathcal{O}(Pe) \sim 10^{-4}$), a medium-flow ($\mathcal{O}(Pe) \sim 10^{-2}$) and a strong-flow ($\mathcal{O}(Pe) \sim 10^{-2}$). Both ferrofluids under analysis presented an increase on the viscosity provoked by the application of an orthogonal homogeneous magnetic field. EFH3, for all applied flow intensities, showed viscosity increments superiors than EFH1. In fact, figure (27) shows that the ferrofluid EFH1, in a condition of weak-flow ($Pe = 4.64 \times 10^{-4}$), presents an increase of its viscosity increment of almost 80% as α rises from 0 to 15. On the other hand, regarding

the same flow intensity² ($Pe = 1.01 \times 10^{-3}$) and magnetic conditions applied to EFH1, it follows from figure (28) that the viscosity increment of the ferrofluid EFH3 increased 140%. These results are much higher when compared to the 40% of increase on $\Delta\eta/\eta_0$ reported by McTague (1969) for a diluted ferrofluid. This discrepancy comes from the fact that both ferrofluids, EFH1 and EFH3, have high volume fractions of particles, respectively 7.9% and 11.8%, which implies that both hydrodynamic and, mainly, magnetic interactions occur between the particles. Under the influence of a magnetic field, Odenbach and Thurm (2002) argue that those interactions lead to the formation of chains and clusters of particles, which generate a hindrance of rotation much more intense than the one produced by single particles. The bulk effect of the viscous dissipation caused by the hindrance of rotation of the agglomerates gives rise to the severe increase of viscosity of the ferrofluids as the magnetic field strengthens. Based on this theory, the fact that the ferrofluid EFH3 has a much stronger magnetoviscous effect when compared to the ferrofluid EFH1 is explained by the fact that the volume fraction of EFH3 is bigger and, as a result, the formation of chains and clusters is more pronounced in this fluid when subjected to an external magnetic field.

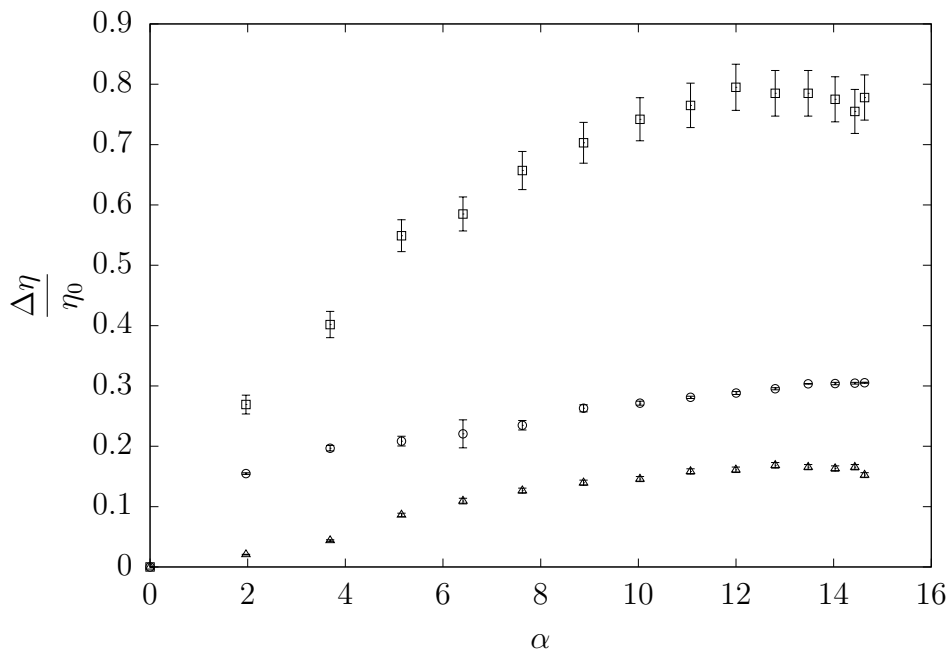


Figure 27 – EFH1: Relative viscosity increment $\Delta\eta/\eta_0$ as a function of the non-dimensional magnetic field strength α for different flow intensities: $Pe = 4.64 \times 10^{-4}$ (\square), $Pe = 1.18 \times 10^{-2}$ (\circ), $Pe = 2.32 \times 10^{-2}$ (\triangle). The viscosity in the absence of magnetic field η_0 is constant and, at $25^\circ C$, equals to $0.94 \times 10^{-2} Pa.s$.

² The same flow condition is related to the fact that the same constant shear-rate was applied to both ferrofluids, $\dot{\gamma} = 100s^{-1}$. The difference on the resulting values of Pe comes from the fact that the viscosity in the absence of magnetic field η_0 is slightly different for both ferrofluids, as shown at table (2).

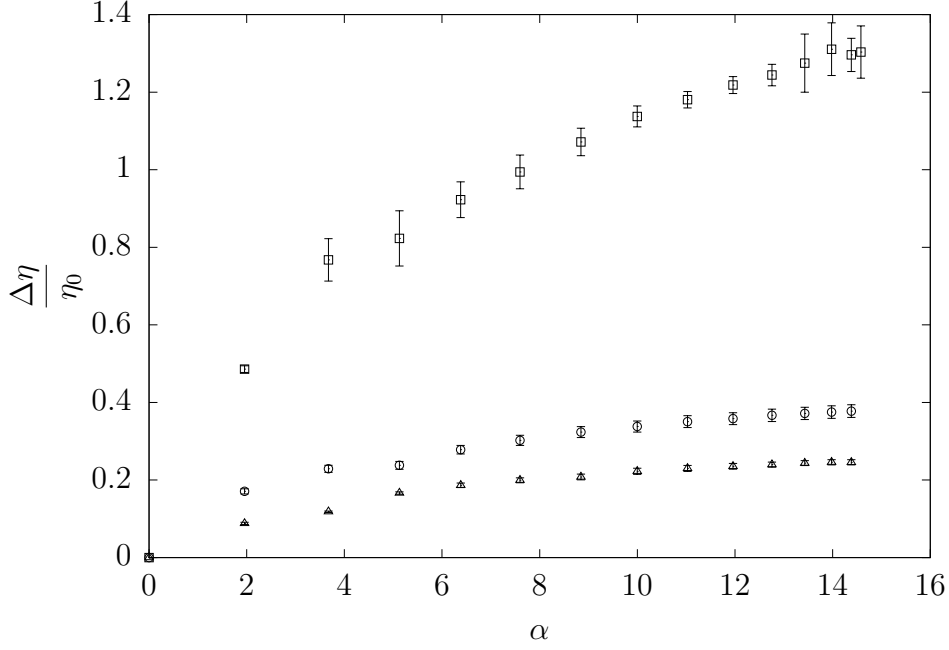


Figure 28 – EFH3: Relative viscosity increment $\Delta\eta/\eta_0$ as a function of the non-dimensional magnetic field strength α for different flow intensities: $Pe = 1.01 \times 10^{-3}$ (\square), $Pe = 2.57 \times 10^{-2}$ (\circ), $Pe = 5.02 \times 10^{-2}$ (\triangle). The viscosity in the absence of magnetic field η_{nf} is constant and, at $25^\circ C$, equals to $1.80 \times 10^{-2} Pa.s$.

As the magnetic field gets stronger, that is, as α rises, the relative viscosity increment tends to a constant value, named relative viscosity increment of saturation $\Delta\eta(\infty)/\eta_0$. This is due to the fact that when α reaches a critical value, the magnetization saturates at its maximum, which is characterized by a condition in which all magnetic moments of dipole are fully aligned with the direction of the magnetic field. In the saturation range, the field-induced microstructure of the fluid has reached a maximum complexity, that is, the mean length size of the chains and agglomerates no longer increase following increments on α . This property clearly depends on the intensity of the flow, being higher the lower that Pe is, what is explained by the fact that a stronger flow subjects the magnetic field induced structures to much stronger shear stresses, leading to their rupture and, as a result, decreasing the fluid's viscosity. It can be said that each value of $\Delta\eta(\infty)/\eta_0$ indicates that a dynamical equilibrium is achieved between the rate of structures being formed by the action of the magnetic field and those being broken by the action of the flow. The values of $\Delta\eta(\infty)/\eta_0$ obtained for both ferrofluids at each condition of Pe are summarized on table (4)

Table 4 – Viscosity increment of saturation $\Delta\eta(\infty)/\eta_0$ obtained, for each ferrofluid, as a function of Pe .

| Ferrofluid EFH1 | | |
|----------------------|-----------------------|---|
| $\dot{\gamma}$ [1/s] | Pe | $\Delta\eta(\infty)/\eta_0$ |
| 100 | 4.64×10^{-4} | $7.68 \times 10^{-1} \pm 3.73 \times 10^{-2}$ |
| 2550 | 1.18×10^{-2} | $3.04 \times 10^{-1} \pm 1.23 \times 10^{-3}$ |
| 5000 | 2.32×10^{-2} | $1.63 \times 10^{-1} \pm 4.40 \times 10^{-3}$ |
| Ferrofluid EFH3 | | |
| 100 | 1.01×10^{-3} | $1.30 \times 10^0 \pm 5.94 \times 10^{-2}$ |
| 2550 | 2.57×10^{-2} | $3.75 \times 10^{-1} \pm 1.62 \times 10^{-2}$ |
| 5000 | 5.02×10^{-2} | $2.44 \times 10^{-1} \pm 6.58 \times 10^{-3}$ |

Figures (27) and (28) also show that the growth of the apparent viscosity is different depending on the intensity of the applied flow. In both figures, one can easily see that, in the condition of weak flow, that is $Pe = 4.64 \times 10^{-4}$ for the EFH1 and $Pe = 1.01 \times 10^{-3}$ for the EFH3, the viscosity of both ferrofluids increases strongly as α rises. On the other hand, for medium and high intensities of flow, that is $Pe > 1.18 \times 10^{-2}$ for the EFH1 and $Pe > 2.57 \times 10^{-2}$ EFH3, the viscosity increases slowly and reaches values much smaller in comparison to those obtained in the condition of weak flow. This is due to the fact that when a magnetic field is applied to a concentrated ferrofluid, a microstructure of chains and clusters of particles is developed, turning the viscosity of this complex fluid dependent on the intensity of the flow, that is, the fluid becomes pseudoplastic. This effect will be discussed in details on subsection (6.1.2).

6.1.2 Pseudo-plasticity

In this subsection, it is discussed the experimentally observed pseudoplastic behavior of the ferrofluids EFH1 and EFH3. This effect appears when those fluids flow in the presence of an external magnetic field, being characterized by an intense decrease on their apparent viscosity η when subjected to the action of a strengthening shear flow.

6.1.2.1 Experimental procedure

The pseudoplastic effect of a ferrofluid sample is evaluated by fixing the magnetic field intensity and applying a continuous increase of shear rate. Both ferrofluids were tested in three conditions of magnetic field intensity: $H = 0$ (absence of magnetic field), $H = 6.87 \times 10^4$ A/m ($i = 1$ A) and $H = 1.61 \times 10^5$ A/m ($i = 3$ A). The shear rate was varied from 10 to 5000s⁻¹. As both ferrofluids present shear rate dependence when they are in the presence of a magnetic field, it is important to choose an appropriate length of gap to obtain consistent results from the experiments. The process of choosing the optimal gap is similar to the one described on subsection (6.1.1.1) for dealing with the

same issue on the analysis of the magnetoviscous effect. This process, for each ferrofluid followed these steps:

1. In the absence of external magnetic field, both ferrofluids are Newtonian and present viscosity similar to water, as can be seen on table (2), thus a gap of 0.1mm is an appropriate choice for this condition;
2. For the first non-zero magnetic field condition applied, that is, $H = 6.87 \times 10^4$ A/m, the viscosity was evaluated for the minimum and the maximum values of $\dot{\gamma}$, which are, respectively, 10 and 5000s^{-1} . This tests are carried out for six values of the gap: 0.1, 0.2, 0.3, 0.4, 0.5 and 0.6 mm. A value of gap that permits the evaluation of the viscosity in both conditions is searched. This process resulted on the choice of 0.2 mm as the optimal gap for EFH1 and of 0.3 mm for EFH3;
3. Repeating the last step, but considering the highest value of magnetic field intensity, $H = 1.61 \times 10^5$ A/m, the choosing process resulted on the choice of the following gaps: 0.3 mm for EFH1 and 0.4 mm for EFH3.

Having chosen the optimal gap, the experimental evaluation of the magnetoviscous effect, for each fixed condition of flow intensity (constant shear rate), presented by both ferrofluids, was done by applying the following experimental protocol:

1. The volume of ferrofluid necessary to fulfill its optimum gap is calculated and, then, this quantity is pipetted in the testing area;
2. The upper disk is lowered until the prescribed gap is achieved between the two disks. The gap is visually inspected in order to identify possible leakages of ferrofluid, which, if found, must be trimmed and cleared;
3. The magnetic yoke is placed around the measuring rod and a process of demagnetization is applied in order to free the magnetic fluid of any previous influences of external magnetic fields;
4. The temperature of the experiment, 25°C , is set on the thermal bath attached to the rheometer. After this, enough time is waited for the temperature of the sample, here defined as the temperature of the lower plate, which is measured by the rheometer, to reach the target temperature;
5. Using the software *Rheoplus*, the magnetic field intensity condition is set. It is resumed to define a constant value of current in order to provide a constant magnetic field intensity when passing through the coils underneath the bottom plate of the measuring device (see figure 5.8);
6. Using the software *Rheoplus*, the shear rate is programmed to vary from 1 to 5000s^{-1} according to a logarithmic ramp, with increase rate of 10 points per decade.

Each data point has a variable time of collection due to the fact that the option "*no time setting*" is active during the data acquisition process. This feature ensures that enough time is being waited at each data acquisition, what aims to guarantee that the steady state has been achieved while data collection is being done.

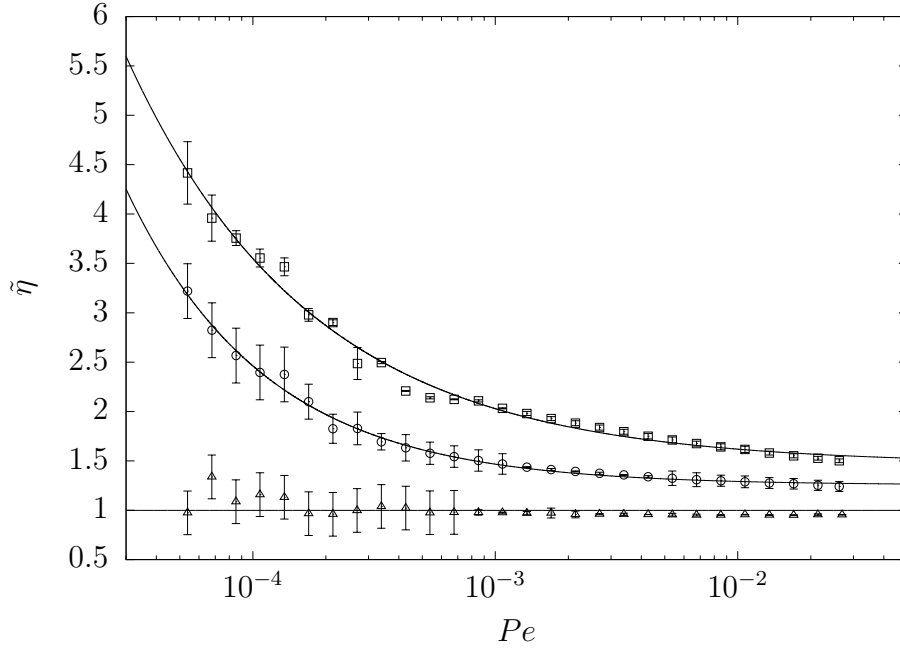
7. The viscosity and the shear stress are acquired as a function of shear rate for a given constant magnetic field intensity.

This process was carried out 10 times, for each ferrofluid, at every condition of magnetic field intensity prescribed. The experimental errors were calculated using the methodology presented on appendix (A.1).

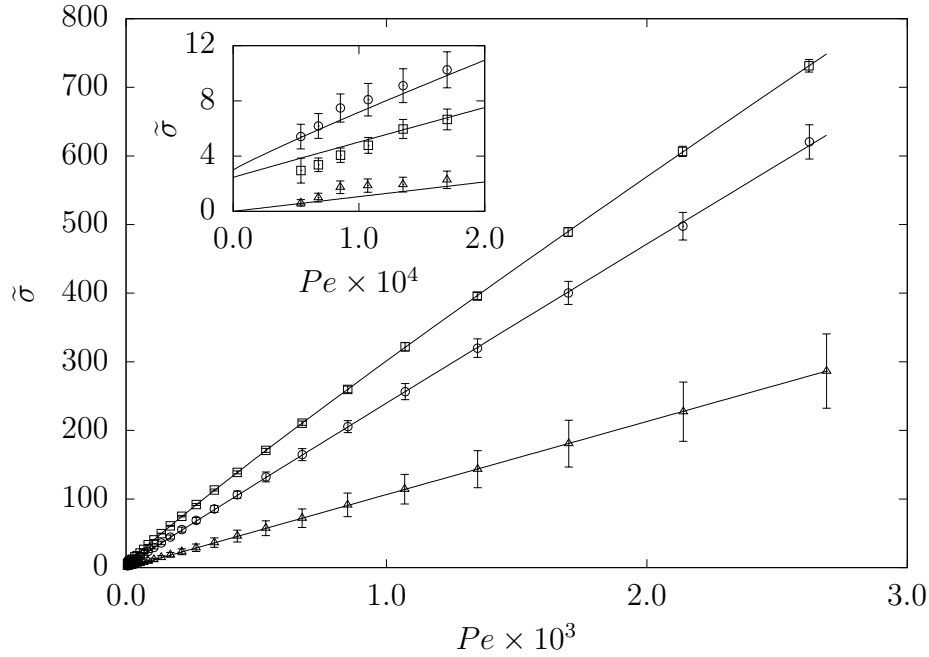
6.1.2.2 Discussion

Another effect caused by the application of an external effective magnetic field on a ferrofluid is the appearance of pseudo-plasticity, which is intimate related to the magnetoviscous effect analyzed on the previous subsection. Figures (29) and (30) depict that the apparent viscosity of both ferrofluids presents two behaviors: in the absence of magnetic field, the viscosity of the samples remains constant (independent of Pe variations), that is, the fluid presents a Newtonian behavior. Nonetheless, when an external magnetic field is applied and its intensity is held constant, the apparent viscosity $\tilde{\eta}$ of the ferrofluid under analysis is observed to strongly decreases as Pe strengthens, characterizing both ferrofluids, EFH1 and EFH3, as shear-thinning.

Shear-thinning behavior is generally associated with microstructure changes caused by modifications on the intensity of the flow, that is, on its shear rate. In the case of the ferrofluids EFH1 and EFH3 this is also verified, but it is of high importance to remark that the formation and resultant complexity of the microstructure of those fluids is strongly dependent on the intensity of the applied magnetic field α . In the absence of an external magnetic field, those ferrofluids, whose particles' length scale is nanometric, do not present a microstructure of equilibrium due to the fact that, in this condition, the Brownian motion tends to randomize the particles in the suspension (ROSENSWEIG, 2013). However, when an external magnetic field is applied, as commented in the previous subsection, the nanoparticles align with the field, what is followed by a process in which dipolar interactions promote the formation of anisotropic chains and clusters. From equation (6.4), it can be seen that an increase on the length scale of the particles has a severe influence on the intensity of the dipolar interaction between them. Since chains of aligned particles are formed, the length scale of the resulting structure increases rapidly, implicating that the dipolar interactions also strengthens. As the fluids are concentrated, this process go even further and stronger dipolar interactions between big structures take place, leading the formation of even bigger, stiffer and stabler structures.

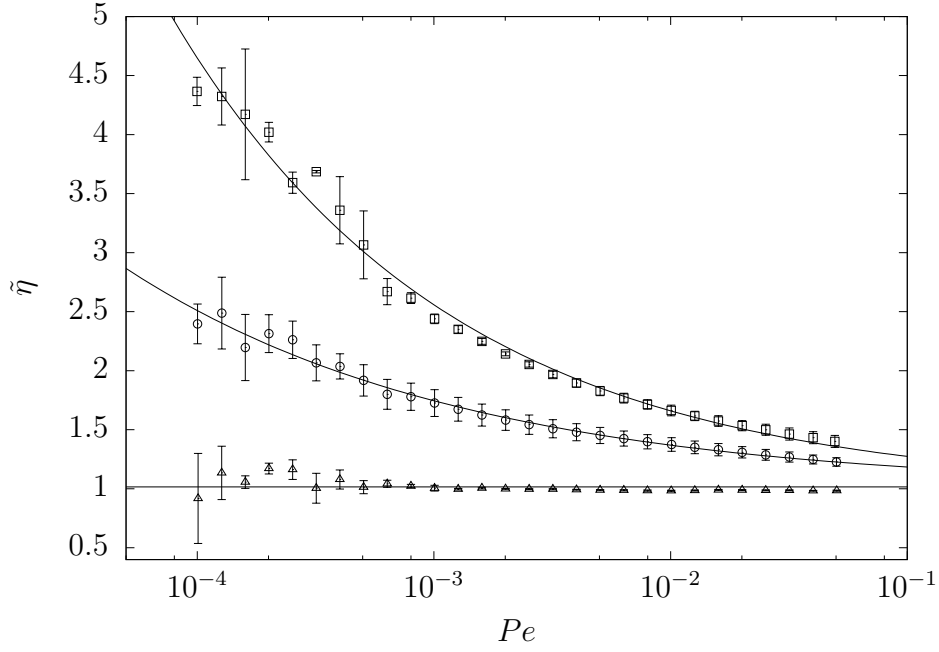


(a) Non-dimensional apparent viscosity.

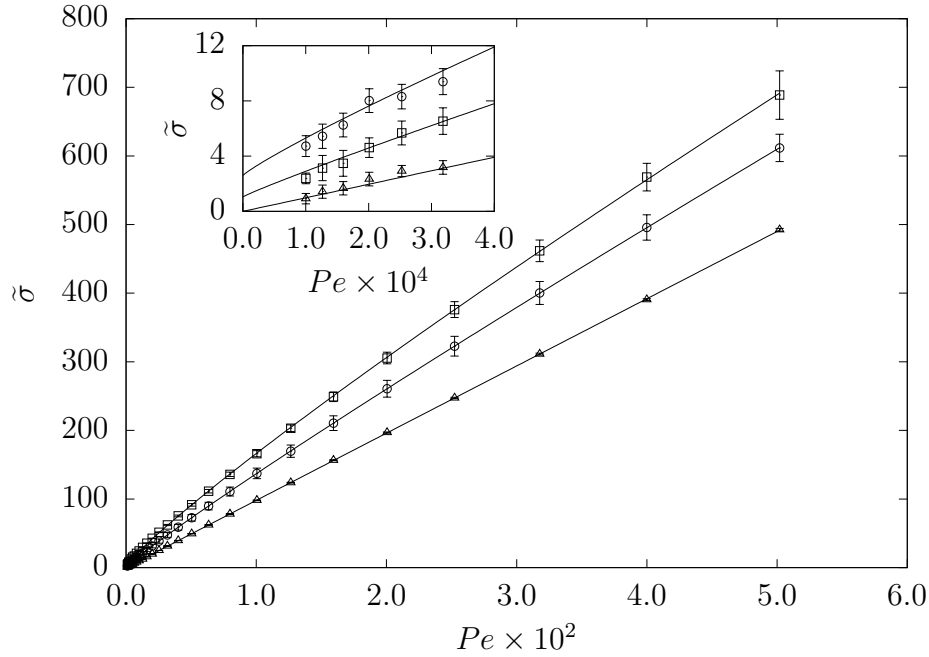


(b) Non-dimensional shear stress

Figure 29 – Ferrofluid EFH1: (a) Relative viscosity $\tilde{\eta}$ as a function Pe for three values of the magnetic parameter: $\alpha = 0$ (\triangle), $\alpha = 4.85 \times 10^0$ (\square) and $\alpha = 1.14 \times 10^1$ (\circ). The curves are fits of the experimental data by the generalized fluid model denoted by equation (6.12). (b) Nondimensional shear-stress as a function of Pe for the same values of α . The curves are fits of the experimental data by the generalized fluid model denoted by equation (6.14). (The viscosity in the absence of magnetic field η_{nf} , at $25^\circ C$, which is equals to 0.94×10^{-2} Pa.s.) The fitting parameters obtained for the referred models are displayed on table (5).



(a) Non-dimensional apparent viscosity.



(b) Non-dimensional shear stress

Figure 30 – Ferrofluid EFH3: (a) Relative viscosity $\tilde{\eta}$ as a function Pe for three values of the magnetic parameter: $\alpha = 0$ (\triangle), $\alpha = 4.84 \times 10^0$ (\circ), $\alpha = 1.14 \times 10^1$ (\square). The curves are fits of the experimental data by the generalized fluid model denoted by equation (6.12). (b) Nondimensional shear-stress as a function of Pe for the same values of α . The curves are fits of the experimental data by the generalized fluid model denoted by equation (6.14). (The viscosity in the absence of magnetic field η_{hf} , at 25°C , which is equals to 1.80×10^{-2} Pa.s.). The fitting parameters obtained for the referred models are displayed on table (5).

Table 5 – Parameters obtained from nonlinear regressions of the data, collected on experiments performed on permanent simple shear flow regime, for the ferrofluids EFH1 and EFH3 by the proposed generalized fluid model, which is described by equations (6.12) and (6.14).

| Ferrofluid | Fitting Parameter | $H = 0$ | $H = 6.87 \times 10^4$ [A/m] | $H = 1.61 \times 10^5$ [A/m] |
|------------|-----------------------|---------|---|---|
| EFH1 | $\tilde{\sigma}_0$ | 0 | $1.83 \times 10^0 \pm 3.00 \times 10^{-2}$ | $2.35 \times 10^0 \pm 1.69 \times 10^{-2}$ |
| | $\tilde{\eta}_\infty$ | 1 | $1.19 \times 10^0 \pm 2.13 \times 10^{-3}$ | $1.32 \times 10^0 \pm 1.98 \times 10^{-3}$ |
| | K | 0 | $2.07 \times 10^4 \pm 3.70 \times 10^2$ | $2.12 \times 10^4 \pm 2.80 \times 10^2$ |
| | n | 0 | $7.69 \times 10^{-1} \pm 4.70 \times 10^{-3}$ | $8.89 \times 10^{-1} \pm 2.31 \times 10^{-3}$ |
| EFH3 | $\tilde{\sigma}_0$ | 0 | $2.18 \times 10^0 \pm 1.42 \times 10^{-2}$ | $3.63 \times 10^0 \pm 8.27 \times 10^{-3}$ |
| | $\tilde{\eta}_\infty$ | 1 | $1.23 \times 10^0 \pm 1.84 \times 10^{-2}$ | $1.98 \times 10^0 \pm 4.70 \times 10^{-3}$ |
| | K | 0 | $1.00 \times 10^4 \pm 3.60 \times 10^1$ | $9.82 \times 10^3 \pm 1.60 \times 10^1$ |
| | n | 0 | $7.23 \times 10^{-1} \pm 2.00 \times 10^{-3}$ | $9.34 \times 10^{-1} \pm 1.82 \times 10^{-3}$ |

Figures (29a) and (30a) display that, in a condition of Pe approaching zero, the viscosity is higher for more intense magnetic fields, what corroborates the fact that stronger magnetic fields induce the formation of bigger and stiffer agglomerates of particles. This kind of microstructure, when subjected to a flow field, generates a high local energy dissipation, due to the fact that they produce a more intense local drag when compared to single particles owing to their bigger characteristic length scales. Besides that, those structures, due to their anisotropic shape, present a much bigger rotational inertia, what increases their already high magnetic-induced rotational hindrance and, therefore, the local energy dissipation. The bulk effect of those energy dissipation mechanisms is traduced by the high value of viscosity in the presence of an external magnetic field in a condition of weak-flow.

Still considering a situation in which the external magnetic field is held constant, the apparent viscosity is observed to strongly decrease as the flow intensifies. This observation can be explained considering two mechanisms: the first one is related to the fact that the strengthening shear flow tries to align the magnetic field induced chains and clusters of particles with the stream lines, reducing the drag produced by them and leading to an overall reduction of the suspension's viscosity. The second mechanism takes place on much stronger flow regimes, in which the magnetic field induced microstructure of the fluid is gradually broken by the action of the increasingly intense shear-stresses that arises from the strengthening of Pe. This latter process leads to a microstructure formed by ever smaller agglomerates of particles, resulting on a continuous reduction of the intensity of local drag and also, of the particle hindrance effects in the flow. This mitigation of energy dissipation mechanisms is observed macroscopically as the severe decrease on the apparent viscosity, especially in the region of medium and high values of Pe depicted on figures (29a) and (30a). It is important to note that, in the limit of high values of Pe, that is, for strong flows, the apparent viscosity tends to its value in the case of absence of magnetic field η_0 . This happens because, in a regime of extremely strong flow, the magnetic field-induced microstructure is almost completely broken, resembling

the situation characterized by the absence of external magnetic field.

Figures (29b) and (30b) respectively present the behavior of the shear stress of the ferrofluids EFH1 and EFH3. As it is expected, in the case of $\alpha = 0$, that is, when no external magnetic field is applied, the relation between the shear stress $\tilde{\sigma}$ and Pe is perfectly linear, confirming that, in this condition, both ferrofluids behave as Newtonian fluids. In the cases in which α is different from zero, a non-linear relation between $\tilde{\sigma}$ and Pe is observed. Besides that, both fluids have presented yield stress $\tilde{\sigma}_0$ when subjected to an external magnetic field ($\alpha \neq 0$).

From the discussions above presented, it can be concluded that the ferrofluid present yield stress $\tilde{\sigma}_0$, and, when flowing, display a shear-thinning behavior. It has also been noted that, for high values of Pe , their viscosities tend to a constant plateau, named infinity-shear viscosity η_∞ . Because of these characteristics, the following constitutive model has been proposed:

$$\tilde{\sigma}(Pe) = \begin{cases} \tilde{\sigma}_0 + \eta_\infty Pe + KPe^n, & \text{if } |\tilde{\sigma}| > |\tilde{\sigma}_0| \\ \infty, & \text{if } |\tilde{\sigma}| \leq |\tilde{\sigma}_0|, \end{cases} \quad (6.12)$$

in which, K is a consistency coefficient and n is the power-law index. The experimental data presented on the graphs of figures (29b) and (30b) have been adjusted to this model and the resulting constants of fit are displayed on table (5).

Considering the fundamental constitutive relation for the generalized Newtonian fluids,

$$\tilde{\sigma}(Pe) = \eta(Pe)Pe, \quad (6.13)$$

one can derive, based on (6.12), a constitutive relation for the dependence of the apparent viscosity on Pe , which is given by:

$$\tilde{\eta}(Pe) = \begin{cases} \tilde{\eta}_\infty + \frac{\tilde{\sigma}_0}{Pe} + KPe^{n-1}, & \text{if } \alpha \neq 0, \\ 1, & \text{if } \alpha = 0. \end{cases} \quad (6.14)$$

The values obtained by non-linear regression of the experimental data presented on the graphs of figures (29a) and (30a) to equation (6.14) for the constants $\tilde{\eta}_\infty$, K_s and n are presented on table (5).

From table (5), it can be seen that, when an external magnetic field is applied, the non-Newtonian characteristics of both ferrofluids arise due to the appearance of anisotropic magnetic field induced microstructure. In this regime, and based on the information presented on table (5), the following conclusions can be drawn about the rheological behavior of the ferrofluids EFH1 and EFH3:

- For the ferrofluid EFH1, the values for the infinity-shear viscosity parameter $\tilde{\eta}_\infty$ are very close considering the two intensities of external magnetic field applied, rising just 10.9% when H increases from 6.87×10^4 to 1.61×10^5 A/m (increase of 135%).

The proximity of the values for this parameter comes from the fact that in regimes of strong flow, the microstructure created by the action of the magnetic field is being forced to align with the streamlines of the flow and, also, is successively being broken by the intense shear stresses applied by the flow. This process is carried out until a theoretical limit is reached, in which no cluster or chain remains formed, independently of the intensity of the applied magnetic field. On the other hand, the infinite-shear viscosity η_∞ of EFH3 increases 61% for the same variation of magnetic field intensity applied to EFH1. That is, even the condition of the flow being very strong, the magnetic field still can change appreciably the viscosity of this fluid, what comes from the fact that this fluid has a much higher volume fraction of magnetic particles and, also, a greater magnetization of saturation than EFH1.

- The power-law index n of the proposed model, for EFH1, increased approximately 15% following the increase on the intensity of the external magnetic field, whereas, for EFH3, this variation was around 30%. This indicates that, when subjected to a higher magnetic field, the fluid becomes less shear-thinning, that is, the decrease of its viscosity when the flow gets stronger is much less pronounced when compared to the situation in which a less intense magnetic field is applied. This is physically explained by the fact that an intense magnetic field leads to the formation of bigger and stabler structures of magnetic particles, which are much more difficult to be aligned, by the flow, with its streamlines and also harder to break.
- For the ferrofluid EFH1, the yield stress $\tilde{\sigma}_0$ increased almost 28% following the enhance of α , whereas for EFH3 the referred growth was of 67%. The increase of the yield stress following a strengthening of the applied magnetic field comes from the fact that stronger magnetic fields induce the formation of more complex microstructure (chains, clusters and aggregates of particles). As a result, microstructure resulting from the action of intense magnetic fields are more rigid and well consolidated at equilibrium, resulting on a much intenser initial resistance to flow. Since the volume fraction of magnetic particles of EFH3 is higher and, regarding the fact that yield stress arises from microstructure-related effects, the increase of this property as a function of the magnetic field intensity must be bigger than the one observed for EFH1.

6.2 Transient shear analysis

Experimental trials have been executed in the regime of transient shear flow in order to evaluate how the shear stress relaxes when the fluid is subjected to different conditions of external magnetic field intensities α and angular strains γ_0 . Those experiments have made possible the determination of the spectrum of relaxation times of each

ferrofluid and also the measurement of their residual stresses as functions of the applied magnetic field and of the shear flow intensities.

6.2.1 Step-strain part I: Magnetic field influence

Step-strain experiments were used in this section to evaluate the dependence of the stress relaxation function $\Phi(s)$ ³ of both ferrofluids on the intensity of the applied magnetic field. Based on the time behavior of the referred material function, it was possible to determine the spectrum of times of relaxation for each fluid at each condition of magnetic field intensity. Besides that, the residual stress relaxation parameter $\tilde{\Phi}_R$ was also obtained as function of the magnetic field intensity for both ferrofluids.

6.2.1.1 Experimental procedure

The step-strain experiment is used to obtain the stress relaxation function $\Phi(s)$ of a given complex fluid. Based on this material function, it is possible to determine the spectrum of relaxation times characteristic of the fluid.

This experimental protocol is composed by the following steps:

1. For each ferrofluid, the optimized gap between the disks of the rheometer is chosen based on the viscosity exhibited by them on each of the four magnetic field intensities applied. The gaps used on this experiment are displayed on table (6);
2. The volume of ferrofluid needed to fulfill the gap is calculated and, after, this quantity is pipetted and placed in the test area;
3. The upper disk is lowered until the precise gap between the disks is reached. Eventual leakages of fluid from the gap are trimmed and cleaned;
4. The magnetic yoke is placed around the measuring rod and a process of demagnetization is applied in order to free the magnetic fluid of any previous influences of external magnetic fields;
5. Through the software *Rheoplus* a fixed current is set to be provided by the PS-MRD DC power supply to the coils in the magneto-rheology assembly, which generate a homogeneous magnetic field in the gap, where the ferrofluid is located;
6. The temperature of the experiment, 25°C, is set on the thermal bath attached to the rheometer. After this, enough time is waited for the temperature of the sample, here defined as the temperature of the lower plate, which is measured by the rheometer, to reach the target temperature;

³ It is important to remember that s is the time shift, defined as $s = t - t'$, in which t is the actual time and t' is a reference time, usually the instant in which the instantaneous strain is applied to the fluid on a step-strain experiment. Further details are given on subsection (3.4.3).

7. A step-strain with a fixed angular strain γ_0 is applied to the sample. It is important to note that the angular strain, which is applied instantaneously to the fluid, should be as small as possible to ensure that the flow regime is linear viscoelastic. However, it should be noted that the smaller this parameter is, the smaller the applied torque will be. Therefore, one can easily enter a torque condition lower than the minimum torque required for meaningful measurements to be made. Regarding this context, for both ferrofluids, EFH1 and EFH3, γ_0 was set as 0.5⁴;
8. The data concerning the stress relaxation function is acquired as a function of time every 0.01s.

Table 6 – Gaps chosen for each ferrofluid considering four different conditions of magnetic field intensity, which are here denoted by its originating electric current.

| Current [A] | EFH1 - h [mm] | EFH3 - h [mm] |
|-------------|---------------|---------------|
| 1 | 0.2 | 0.3 |
| 2 | 0.3 | 0.5 |
| 3 | 0.5 | 0.7 |
| 4 | 0.5 | 0.7 |

The experimental errors were calculated using the methodology presented on appendix (A.1).

6.2.1.2 Discussion

In this subsection, it will be analyzed and discussed the results obtained by applying a step-strain reometric flow to samples of the ferrofluids EFH1 and EFH3, in the presence of a constant homogeneous magnetic field. The realization of this kind of experiments, led to the obtainment of the stress relaxation functions $\Phi(s)$ for different intensities of the external magnetic field H .

The results are presented here on their dimensionless form. The magnetic field intensity is traduced, as usually, by the magnetic parameter α . Regarding this context, the stress relaxation function, for a fixed intensity of external magnetic field, $\Phi(s)|_\alpha$ was made dimensionless using the following time and viscosity characteristic scales:

$$t^* \sim \tau_m, \quad (6.15)$$

$$\eta^* \sim \eta_0, \quad (6.16)$$

where τ_m is the principal time of relaxation of the fluid evaluated in the presence of the lowest magnetic field intensity applied, η_0 is the viscosity of the ferrofluid, at 25°C, in

⁴ This value was chosen based on strain-sweep experiments, in the regime of small amplitude oscillatory shear, carried out for both ferrofluids, at each fixed condition of magnetic field intensity applied. From the experiments, it was identified a range of γ_0 for which the storage modulus G' is constant. For each ferrofluid, and external magnetic field intensity, the value of γ_0 used on the step-strain experiments was selected among the referred range.

the absence of external magnetic field. Using those scales, the typical scale of the stress relaxation function, which has unit of stress is given by:

$$[\Phi|_\alpha]^* \sim \frac{\eta_0}{\tau_m}. \quad (6.17)$$

Besides that, the time shift, $s = t - t'$, has the following typical scale:

$$s^* \sim t^* \sim \tau_m. \quad (6.18)$$

Therefore, the nondimensional form of the stress relaxation function, considering a fixed condition of α , is given by:

$$\tilde{\Phi}(\tilde{s})|_\alpha = \frac{\Phi(s/s^*)|_\alpha}{[\Phi|_\alpha]^*} = \frac{\Phi(s/\tau_m)\tau_m}{\eta_0} = \frac{\Phi(\tilde{s})\tau_m}{\eta_0}, \quad (6.19)$$

where \tilde{s} is the nondimensional time shift.

Analyzing the graphs presented on figures (31) and (32), it can be observed that both ferrofluids presented a long-time stress relaxation process after the application of the step-strain (almost instantaneous shear flow), which was done under the permanent action of a series of external magnetic field intensities. The fact that those fluids are non-instantaneous, in the presence of an external magnetic field, indicates that their rheology changed towards a viscoelastic behavior. Bird et al. (1987) affirms that the time retardation on the stress relaxation of complex fluids are intimately related to elastic effects arising from its microstructure. Borin et al. (2014) argue that the relaxation process of ferrofluids, when subjected to an external magnetic field, strongly depends on its magnitude and that the stress decreases over time in a close exponential fashion, what is also verified for the stress relaxation function. This context strongly suggests the utilization of a viscoelastic constitutive model for describing the relaxation of the shear stress on these fluids. As a result, it has been used Maxwell's generalized viscoelastic model, due to the fact that it predicts the stress relaxation function behavior as a summation of exponentials, which are pondered by the a series of characteristics viscosities and times, that simulate the effects of relaxation due to viscous dissipation and elastic energy storage.

The constitutive equation for Maxwell's generalized viscoelastic model is presented on (3.87). In order to obtain its dimensionless form, expression (3.87) will be substituted on equation (6.19), which leads to

$$\tilde{\Phi}(\tilde{s})|_\alpha = \frac{\Phi(\tilde{s})\tau_m}{\eta_0} = \sum_{j=1}^N \frac{\eta_j/\eta_0}{\tau_j/\tau_m} \exp\left(-\frac{\tilde{s}}{\tau_j/\tau_m}\right) = \sum_{j=1}^N \frac{\tilde{\eta}_j}{\tilde{\tau}_j} \exp(-\tilde{s}/\tilde{\tau}_j). \quad (6.20)$$

Defining,

$$A_j = \frac{\tilde{\eta}_j}{\tilde{\tau}_j}, \quad (6.21)$$

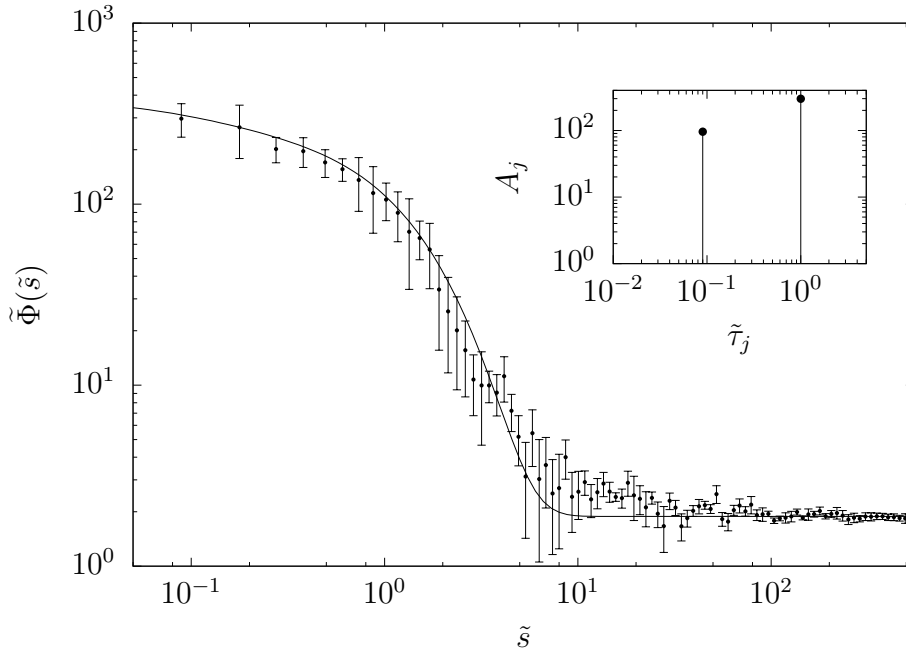
equation (6.20) can be rewritten as

$$\tilde{\Phi}(\tilde{s})|_\alpha = \sum_{j=1}^N A_j \exp(-\tilde{s}/\tilde{\tau}_j), \quad (6.22)$$

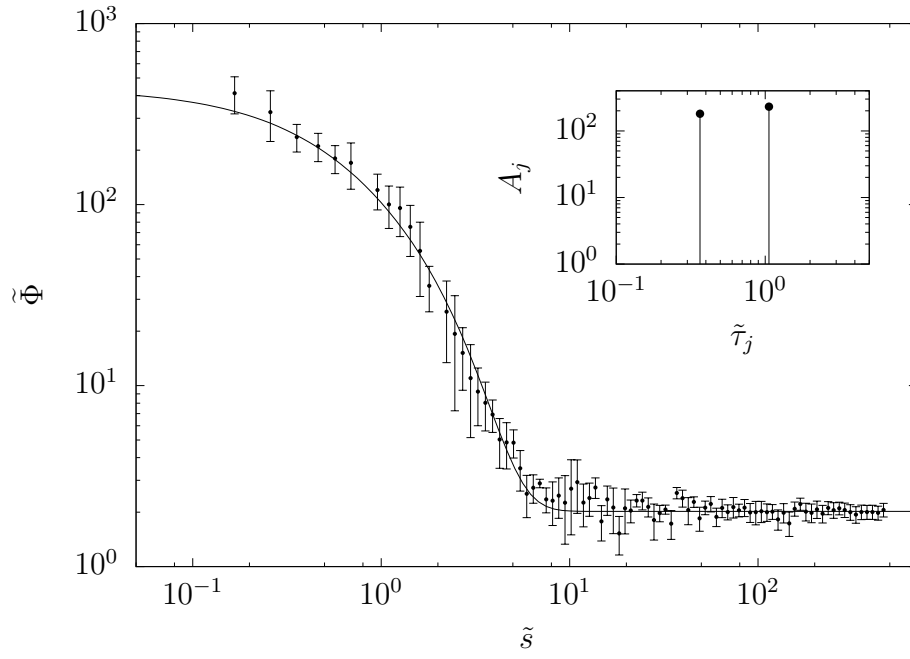
where, $\tilde{\Phi}(\tilde{s})|_\alpha$ is the nondimensional stress relaxation function, considering a fixed α , for a generalized Maxwell's fluid, A_j is the j-th amplitude of nondimensional shear stress, \tilde{s} is the nondimensional time shift and τ_j is the nondimensional time associated to the j-th Maxwell's element. However, analyzing carefully the results present on figures (31) and (32), it can be seen that the stress relaxation function does not reaches zero for long times, as predicted by equation (6.22). Instead of this, the referred material function relaxes for a constant non-zero value, which was named, in this work, residual stress relaxation parameter $\tilde{\Phi}_R|_\alpha$. From this observation, an adaptation of the constitutive equation (6.22) was proposed in order to take into account $\tilde{\Phi}_R|_\alpha$, which resulted in:

$$\tilde{\Phi}(\tilde{s})|_\alpha = \tilde{\Phi}_R|_\alpha + \sum_{j=1}^N A_j \exp(-\tilde{s}/\tilde{\tau}_j). \quad (6.23)$$

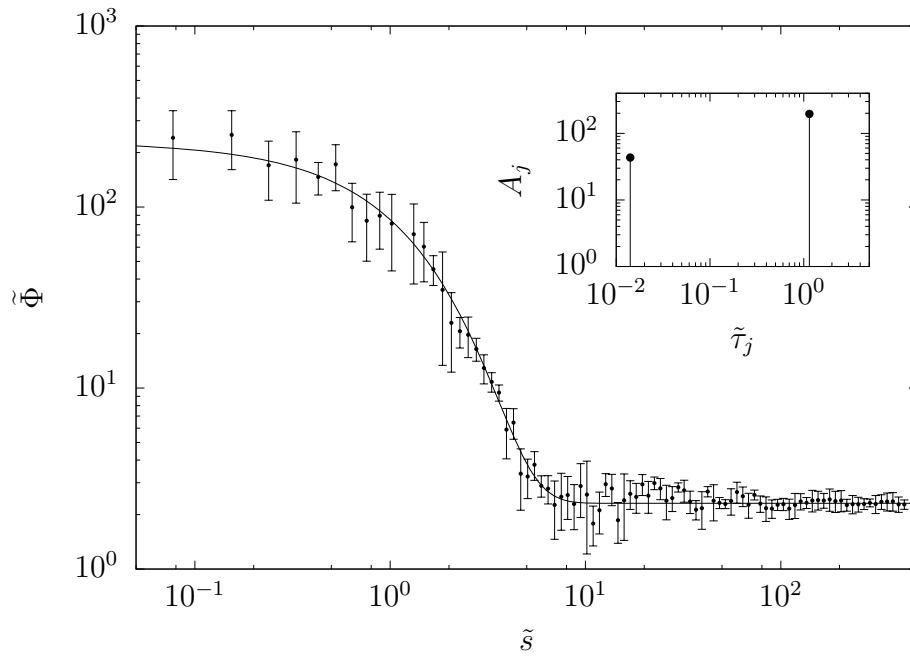
Using equation (6.23) to fit the experimental data obtained for each ferrofluid, at four different conditions of magnetic field intensity α , it was possible to determine the dimensionless times of relaxation $\tilde{\tau}_j$ and nondimensional shear stress amplitudes A_j . It is important to note that the main time of relaxation $\tilde{\tau}_1$ for each value of α was obtained previously by numerical integration of equation (3.126). As a result, the fitting process have been carried out already considering defined the referred parameter. The constant obtained from the fitting process are displayed, for the ferrofluid EFH1 on table (7) and for the ferrofluid EFH3 on table (8).



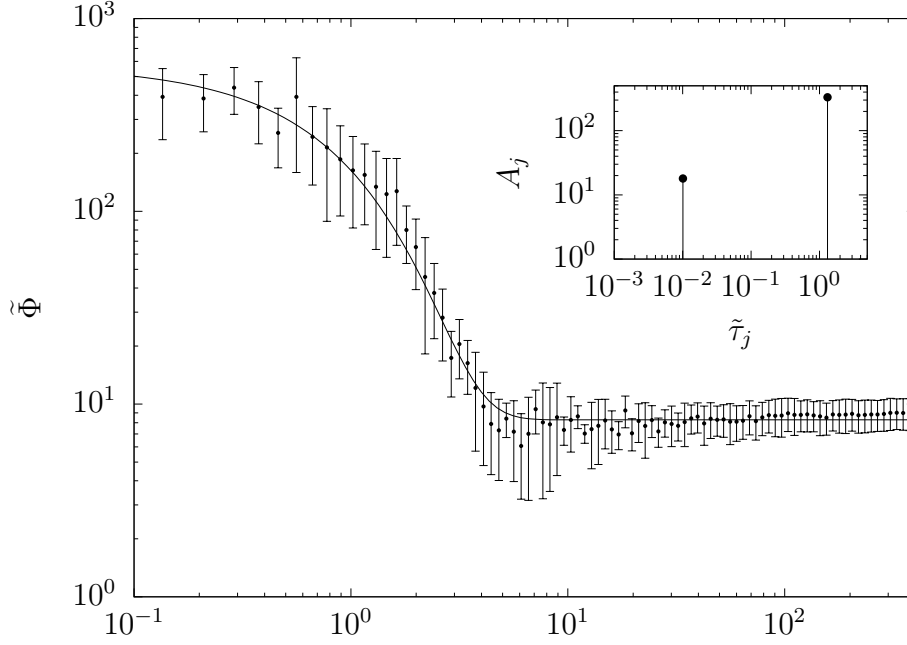
(a) $\alpha = 4.85 \times 10^0$.



(b) $\alpha = 8.37 \times 10^0$.



(c) $\alpha = 1.14 \times 10^1$.

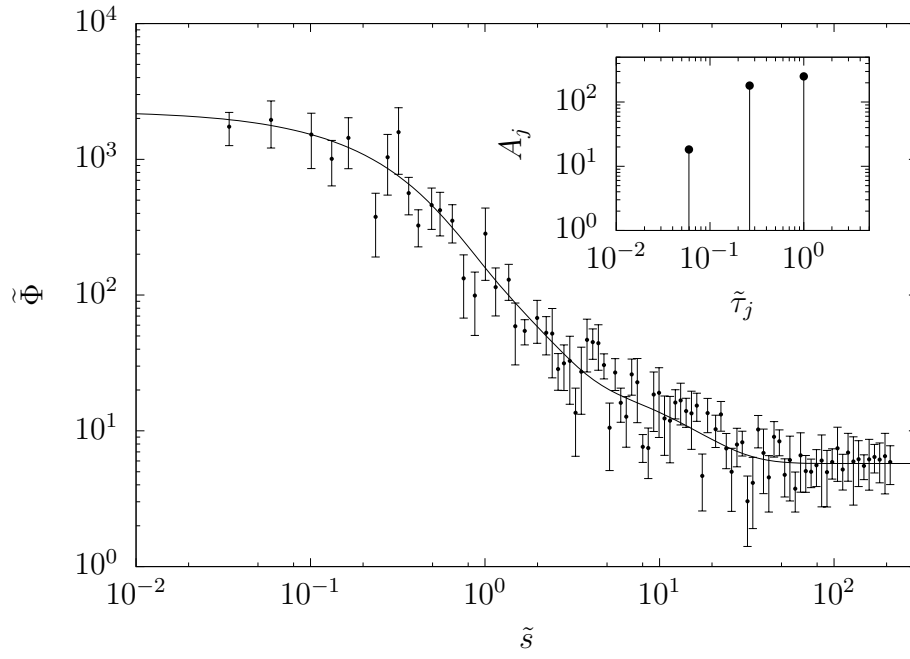


(d) $\alpha = 1.36 \times 10^1$.

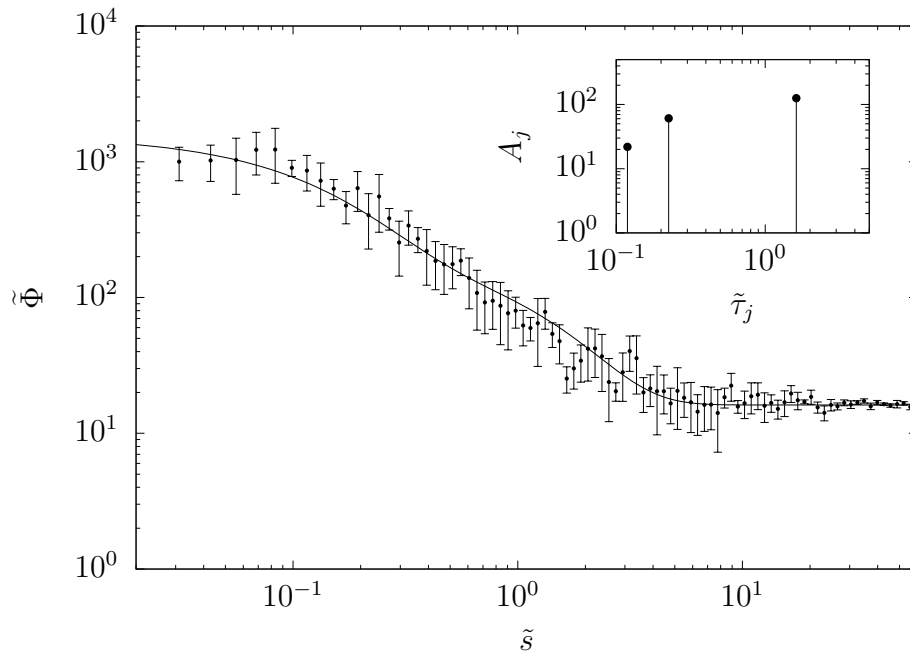
Figure 31 – Ferrofluid EFH1: Dimensionless stress relaxation function $\tilde{\Phi}$ in terms of the nondimensional time shift \tilde{s} for different values of α . The curves are fits of the experimental data by an adaptation of the generalized Maxwell’s model, given by equation (6.23). The parameters for each curve are shown in table (7). The viscosity in the absence of magnetic field η_0 , at 25°C , is 0.94×10^{-2} Pa.s and the main time of relaxation for the lowest magnetic field applied τ_m is 1.24×10^{-1} s. In the inserts, it is shown a plot of the amplitude of the stress A_j as a function of the characteristic times $\tilde{\tau}_j$ involved in the process of stress relaxation at each condition of magnetic field strength α .

Table 7 – Material parameters obtained for the ferrofluid EFH1 via non-linear regression of the experimental data to the model represented by equation (6.23). Four intensities of the external magnetic field are considered.

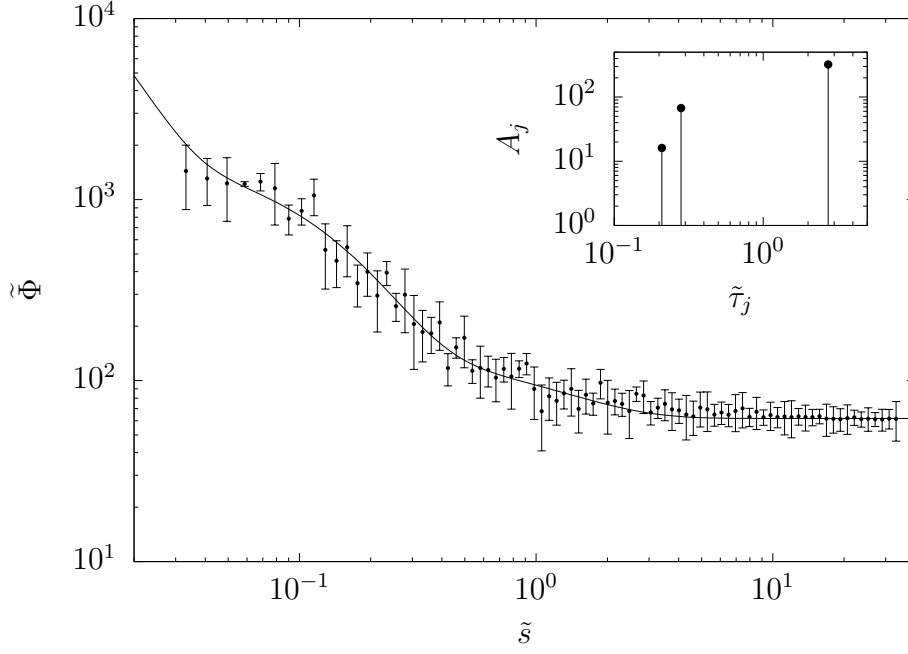
| i [A] | α | τ_1 [s] | $\tilde{\Phi}_R$ | j | $\tilde{\eta}_j$ | $\tilde{\tau}_k$ |
|-------|--------------------|-----------------------|--------------------|---|-----------------------|-----------------------|
| 1 | 4.85×10^0 | 1.24×10^{-1} | 1.88×10^0 | 1 | 2.99×10^2 | 1.00×10^0 |
| | | | | 2 | 8.63×10^0 | 9.00×10^{-2} |
| 2 | 8.37×10^0 | 1.32×10^{-1} | 2.01×10^0 | 1 | 2.45×10^2 | 1.06×10^0 |
| | | | | 2 | 6.59×10^1 | 3.65×10^{-1} |
| 3 | 1.14×10^1 | 1.42×10^{-1} | 2.31×10^0 | 1 | 2.25×10^2 | 1.15×10^0 |
| | | | | 2 | 6.10×10^{-1} | 1.41×10^{-2} |
| 4 | 1.36×10^1 | 1.62×10^{-1} | 8.28×10^0 | 1 | 4.35×10^2 | 1.31×10^0 |
| | | | | 2 | 1.82×10^{-1} | 1.01×10^{-2} |



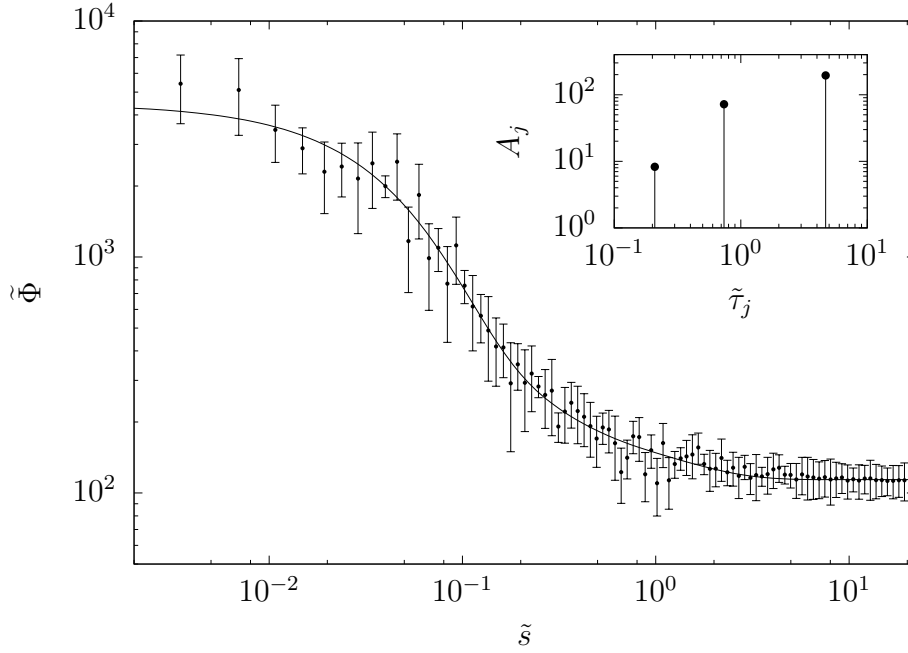
(a) $\alpha = 4.84 \times 10^0$.



(b) $\alpha = 8.35 \times 10^0$.



(c) $\alpha = 1.14 \times 10^1$.



(d) $\alpha = 1.35 \times 10^1$.

Figure 32 – Ferrofluid EFH3: Dimensionless stress relaxation function $\tilde{\Phi}$ in terms of the nondimensional time shift \tilde{s} for different values of α . The curves are fits of the experimental data by an adaptation of the generalized Maxwell's model, given by equation (6.23). The parameters for each curve are shown in table. The viscosity in the absence of magnetic field η_0 , at 25°C , is 0.18×10^{-1} Pa.s and the main time of relaxation for the lowest magnetic field applied τ_m is 6.73×10^{-1} s. In the inserts, it is shown a plot of the amplitude of the stress A_j as a function of the characteristic times $\tilde{\tau}_j$ involved in the process of stress relaxation at each condition of magnetic field strength α .

Table 8 – Material parameters obtained for the ferrofluid EFH3 via non-linear regression of the experimental data to the model represented by equation (6.23). Four intensities of the external magnetic field are considered.

| i [A] | α | τ_1 [s] | $\tilde{\Phi}_R$ | k | $\tilde{\eta}_j$ | $\tilde{\tau}_j$ |
|---------|--------------------|-----------------------|--------------------|-----|--------------------|-----------------------|
| 1 | 4.84×10^0 | 6.73×10^{-1} | 5.75×10^0 | 1 | 2.51×10^2 | 1.00×10^0 |
| | | | | 2 | 4.80×10^1 | 2.66×10^{-1} |
| | | | | 3 | 1.09×10^0 | 5.97×10^{-2} |
| 2 | 8.35×10^0 | 1.09×10^0 | 1.62×10^1 | 1 | 2.03×10^2 | 1.62×10^0 |
| | | | | 2 | 1.37×10^1 | 2.25×10^{-1} |
| | | | | 3 | 2.60×10^0 | 1.19×10^{-1} |
| 3 | 1.14×10^1 | 1.84×10^0 | 6.18×10^1 | 1 | 8.81×10^2 | 2.73×10^0 |
| | | | | 2 | 1.84×10^1 | 2.81×10^{-1} |
| | | | | 3 | 3.37×10^0 | 2.09×10^{-1} |
| 4 | 1.35×10^1 | 3.16×10^0 | 1.14×10^2 | 1 | 9.13×10^2 | 4.69×10^0 |
| | | | | 2 | 5.29×10^1 | 7.37×10^{-1} |
| | | | | 3 | 1.67×10^0 | 2.02×10^{-1} |

According to Borin et al. (2011), Borin et al. (2014), the total stress achieved by the magnetic fluid just after the cessation of the flow is determined by the presence of linear chains and bulk, dense aggregates (clusters) due to the action of dipolar interactions between the particles. It is important to remark that they are formed by the action of the external magnetic field, vanishing when α is zero. Regarding this context it is important to note that the volumetric fraction of magnetic particles plays an important role on the stress relaxation due to the fact that it influences directly the complexity of the microstructure formed when a magnetic field is applied. Ferrofluids with higher ϕ produce bigger and stiffer linear chains and clusters, that form the field induced microstructure when a given α is applied. According to Borin et al. (2014), the linear chains are responsible for the stress relaxation at short time scales, that is, in the initial part of the process, whereas the bulk clusters are involved on the final long part of the process.

From tables (7) and (8), it can be observed that for the fluid EFH1, it has been possible to describe its stress relaxation function, for every condition of α applied, using two Maxwell's elements. On the other hand, for the ferrofluid EFH3, it was necessary to use three elements. In the case of the fluid EFH1, it can be said that it presents a simpler stress relaxation process than EFH3, that is, its relaxation involves less characteristic times. Bird, Armstrong and Hassager (1987) emphasize that, in a relaxation process, each characteristic time is intimately related to a physical relaxation mechanism. As a result, it can be concluded that the stress relaxation of the ferrofluid EFH1 involves less physical mechanisms than the one of the ferrofluid EFH3, that is, EFH3 has a more complex memory. This observation is related to the fact that the volume fraction of magnetic particles of EFH3 is higher in comparison to EFH1, which means that the magnetic field induces more efficiently the formation of chains and clusters of particles in this fluid. That is, EFH3 presents more magnetic particles per unit of volume, what makes it easier for the dipolar interactions to promote the formation of particle chains.

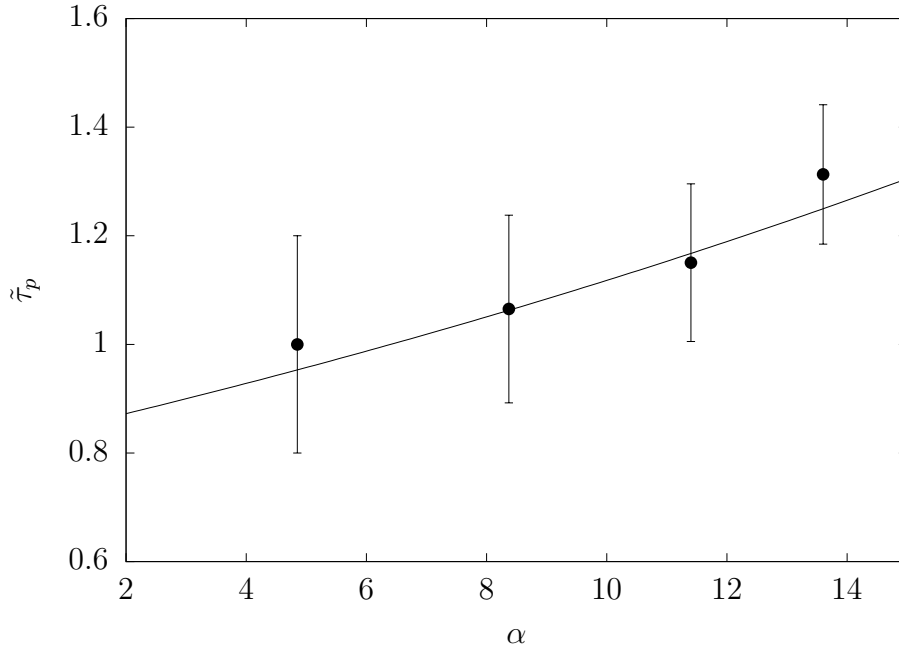
These structures can interact magnetically on a much more intense fashion, due to their larger length scale, leading to the formation of even bigger particles aggregates. Due to this process, EFH3 presents a much more complex, coherent and well-settled magnetic induced microstructure, composed by bigger chains and aggregates when compared to the ones formed when the same magnetic field conditions are applied to EFH1. In the inserts presented on the graphs of figures (31) and (32), it is shown the amplitude of the stress being dissipated during each characteristic time, it is immediate from all the graphs that the most part of the shear stress is relaxed by the main relaxation time $\tilde{\tau} = 1$ due to the fact that this characteristic time reflects the dominant mechanism of stress relaxation.

Regarding the data concerning the experimentally obtained stress relaxation functions, presented on figures (31) and (32), it was possible to determine the main time of relaxation, for each intensity of the applied magnetic field, by using equation (3.126), on a process of numerical integration. Those results are presented for the ferrofluids EFH1 and EFH3, respectively, on figures (33a) and (33b). It is immediate from those graphs, that the main time of relaxation of both ferrofluids depends on the intensity of the applied magnetic field. Since the field-dependent time of relaxation is made nondimensional using the time of relaxation obtained in the condition of lowest α , the principal time of relaxation $\tilde{\tau}_p(\alpha)$ always starts at one on the graphs of figures (31) and (32). Regarding this context, one can see that, when α increases from its lower to its higher value (increase of almost 180%), the time of relaxation of EFH1 increases 31.3%, while in the case of the ferrofluid EFH3, this increase is of 369.2%. This severe difference in the growth of the main time of relaxation is also due to the fact that EFH3 has a bigger volume fraction of magnetic particles than EFH1. Therefore, the magnetic field induces the formation of bigger and more complex structures on EFH3, leading to a more substantial increase in the overall elastic behavior of this ferrofluid when compared to EFH1.

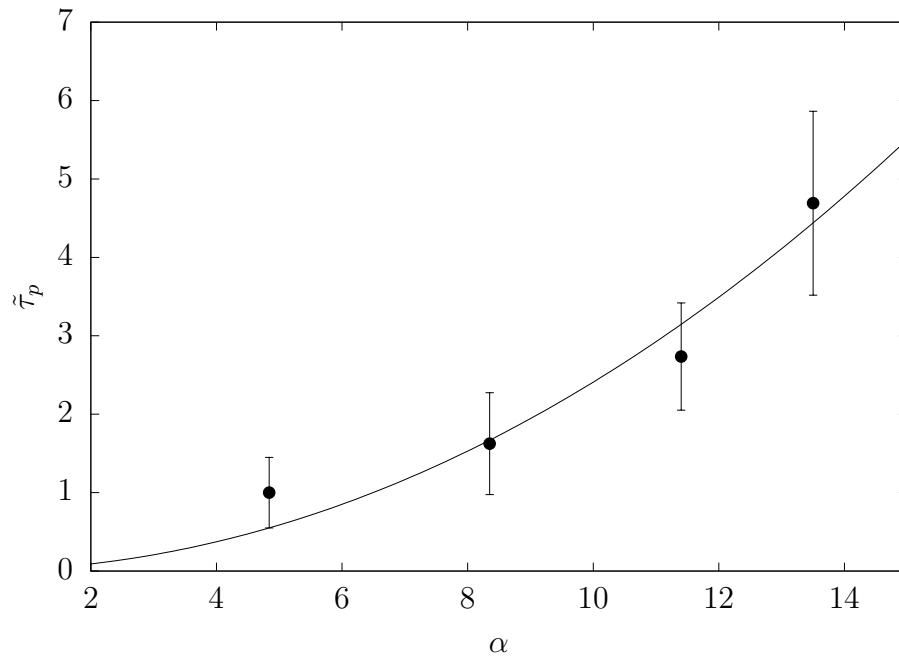
Analyzing the data displayed on figures (33a) and (33b), and also regarding the variations on the main time of relaxation with respect to the intensity of the applied magnetic field, the following equation has been proposed to model such behavior:

$$\tilde{\tau}_p(\alpha) = c_1 \exp(c_2 \alpha), \quad (6.24)$$

where c_1 and c_2 are constants obtained from a non-linear regression of the experimental data to the model. The values obtained for these constants are shown on table (9).



(a) EFH1



(b) EFH3

Figure 33 – Nondimensional time of relaxation $\tilde{\tau}$ as a function of the magnetic field intensity parameter α . The curves are fits of the experimental data to equation (6.24). The fitting parameters are displayed on table (9).

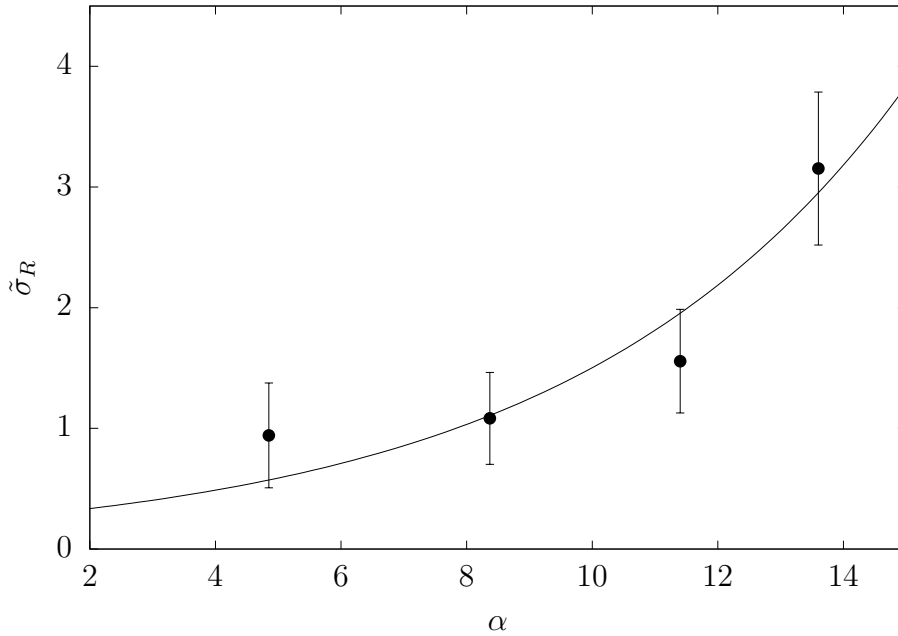
From the constant value towards the stress relaxation function tends, that is, the residual stress relaxation parameter $\tilde{\Phi}_R$, it can be defined a nondimensional residual stress $\tilde{\sigma}_R$ by applying equation (4.37):

$$\tilde{\sigma}_R = \tilde{\Phi}_r \gamma_0; \quad (6.25)$$

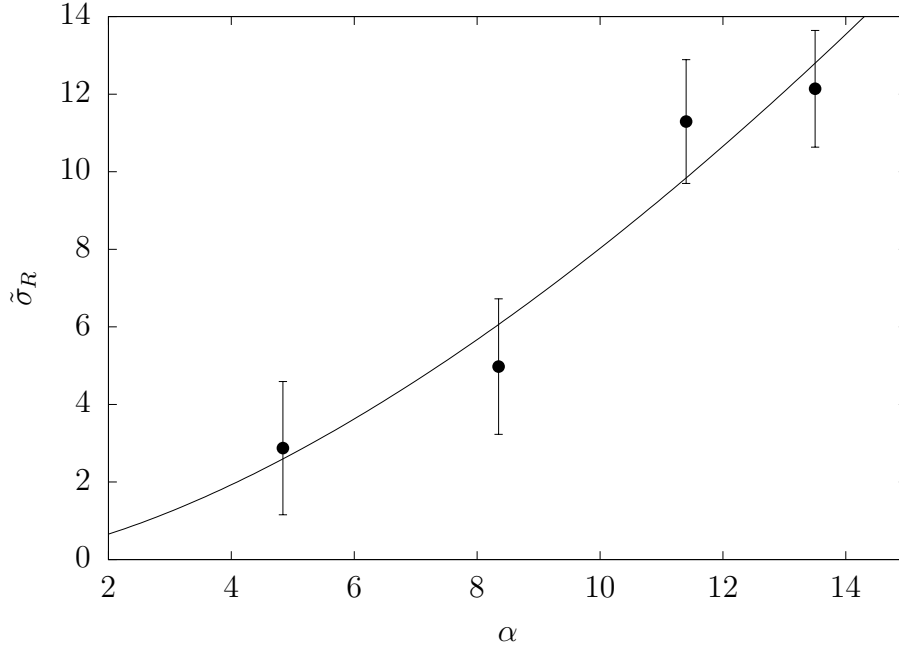
where, γ_0 is the angular strain. Therefore, regarding the results displayed on figures (31) and (32), it can be said that a residual stress $\tilde{\sigma}_R$ is observed for both fluids at each constant intensity of magnetic field applied. For the two ferrofluids, the residual stress was observed to increase as the intensity of the magnetic field strengthened. According to Borin et al. (2014), this increase is related to the enhancement of the size and intensification of the stability of the magnetic field-induced aggregates as the intensity of the magnetic field rises. This effect is stronger on EFH3 than on EFH1, owing to its bigger volume fraction of magnetic particles. Figures (34a) and (34b) show the dependence of the residual stress $\tilde{\sigma}_R$ as a function of the nondimensional magnetic field α . It was proposed a power-law relation to model such dependence, resulting on the following expression:

$$\tilde{\sigma}_R = C_3 \exp(C_2 \alpha), \quad (6.26)$$

where c_1 and c_2 are constants obtained from a non-linear regression of the experimental data to the model. The values obtained for these constants are shown on table (9).



(a) *Ferrotec EFH1.*



(b) *Ferrotec EFH3*.

Figure 34 – Dimensionless residual stress $\tilde{\sigma}_R$ as a function of the non-dimensional magnetic field α . The curves are fits of the experimental data to equation (6.26). The fitting parameters are displayed on table (9).

Table 9 – Fitting parameters obtained for the non-linear regression of the data concerning the magnetic field-dependent time of relaxation and the magnetic field-dependent residual stress, respectively, to the models represented by equations (6.24) and (6.26).

| Constants | EFH1 | EFH3 |
|-----------|---|---|
| C_1 | $6.5 \times 10^{-1} \pm 4.32 \times 10^{-2}$ | $3.53 \times 10^{-4} \pm 7.68 \times 10^{-4}$ |
| C_2 | $7.0 \times 10^{-3} \pm 3.22 \times 10^{-3}$ | $2.02 \times 10^0 \pm 4.74 \times 10^{-1}$ |
| C_3 | $2.29 \times 10^{-1} \pm 1.63 \times 10^{-2}$ | $1.58 \times 10^0 \pm 8.40 \times 10^{-1}$ |
| C_4 | $2.35 \times 10^{-2} \pm 7.09 \times 10^{-3}$ | $1.98 \times 10^{-2} \pm 5.51 \times 10^{-3}$ |

6.2.2 Step-strain part II: Effects of the magnitude of the applied strain

Step-strain experiments were used, in this section, to evaluate the dependence of the stress relaxation function $\Phi(s)$, of both ferrofluids, on the intensity of the applied shear-flow. Based on the time behavior of the referred material function, it was possible to determine the residual stress relaxation parameter $\tilde{\Phi}_R$, for both fluids, at different values of Pe. From this parameter, it was determined the behavior of the residual stress $\tilde{\sigma}_R$, of both ferrofluids, as a function of Pe.

6.2.2.1 Experimental procedure

The experimental protocol used to obtain the results presented in this section is composed by the following steps:

1. An intensity of electric current is selected to be constant throughout the experimental trials. For the tests on both ferrofluids, it has been selected 2 and 4A, which correspond to effective magnetic fields with intensities of 1.18×10^5 and 1.92×10^5 A/m, respectively;
2. Having defined a current intensity, the volume of ferrofluid needed to fulfill the gap between the disks of the rheometer is calculated regarding the usable gaps displayed on table (6). Following this, the referred quantity is pipetted and placed in the test area;
3. The upper disk is lowered until the precise gap between the disks is reached. Eventual leakages of fluid from the gap are trimmed and cleaned. A final visual check is carried out in order to verify that the gap is completely filled by the ferrofluid being tested;
4. The magnetic yoke is placed around the measuring rod and a process of demagnetization is applied in order to free the magnetic fluid of any previous influences of external magnetic fields;
5. A constant magnetic field is applied orthogonal to the sample. Its intensity is kept constant through all the experimental trials;
6. The temperature of the experiment, 25°C , is set on thermal bath attached to the rheometer. After this, enough time is waited for the temperature of the sample, here defined as the temperature of the lower plate, which is measured by the rheometer, to reach the target temperature. This step must be done after applying the magnetic field due to the fact that the process of induction of the magnetic field by the coils below the bottom plate, produces heat, that must be compensated by the thermal bath, in order to keep the temperature, of the fluid in the gap, constant at 25°C ;
7. A series of step-strains, with different values of angular strain γ_0 , is applied to the sample, while the magnetic field intensity is kept constant;
8. The data concerning the stress relaxation function, for each value of γ_0 applied, is acquired as a function of time. The frequency of data collection was of 1 point every 0.01s.

6.2.2.2 Discussion

Following the steps described on the previous subsection, for each of the two constant magnetic field intensities, it has been obtained the behavior of the nondimensional

stress relaxation function $\tilde{\Phi}(\tilde{s})$ as a function of the intensity of the nondimensional time shift \tilde{s} , for different intensities of shear flow, here denoted by Pe . As commented on section (6.1), Pe is defined by:

$$Pe = \frac{6\pi\eta a^3 \dot{\gamma}}{k_B T}. \quad (6.27)$$

Considering that the fluid characteristics and its temperature defined, this parameter can only be varied by changing the shear rate of the flow $\dot{\gamma}$. It is important to remember that, from equation (4.30), the shear-rate applied by a step-strain is given by:

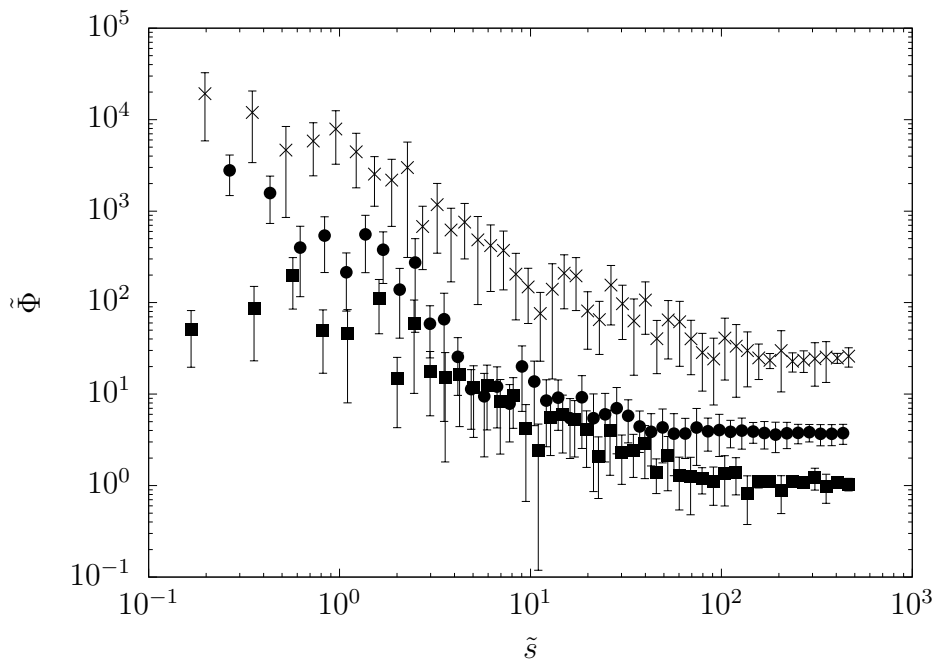
$$\dot{\gamma} = \frac{\gamma_0}{\epsilon}, \quad (6.28)$$

where, γ_0 is a defined angular strain and ϵ is a small time interval in which γ_0 is applied. The time interval ϵ is fixed in all the experiments describe on this section. Therefore, to vary Pe it is necessary to change γ_0 , to which it is related by:

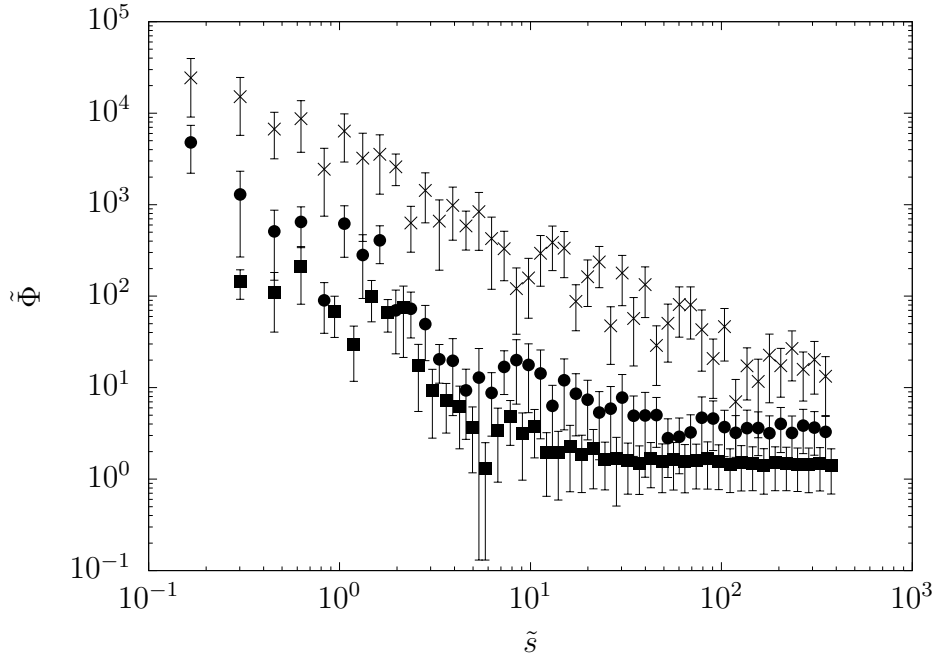
$$Pe = \frac{6\pi\eta a^3 \gamma_0}{k_B T \epsilon}. \quad (6.29)$$

In the experiments, for both conditions of constant external magnetic field explored, the ferrofluids were subjected to nine conditions of γ_0 , in order to apply a wide range of flow intensities.

For the ferrofluid EFH1, when subjected to a constant magnetic field intensity H of 1.18×10^5 A/m (induced by a current of 2A), figure (35a) displays the temporal behavior of its stress relaxation function for only three intensities of shear flow in order to facilitated the visualization of the data. Those intensities are: Pe equals to 2.15×10^{-6} , 2.15×10^{-5} and 8.61×10^{-5} . Figure (35b) presents the same results, but obtained for a condition of a much intenser magnetic field, with intensity H of 1.92×10^5 A/m (related to a current of 4A).



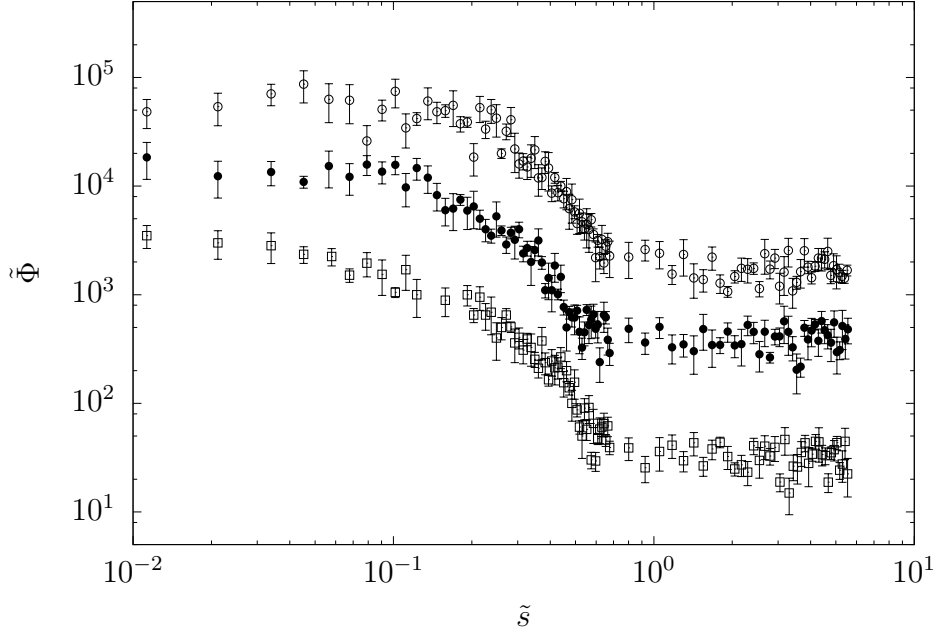
(a) $\alpha = 8.37 \times 10^0$



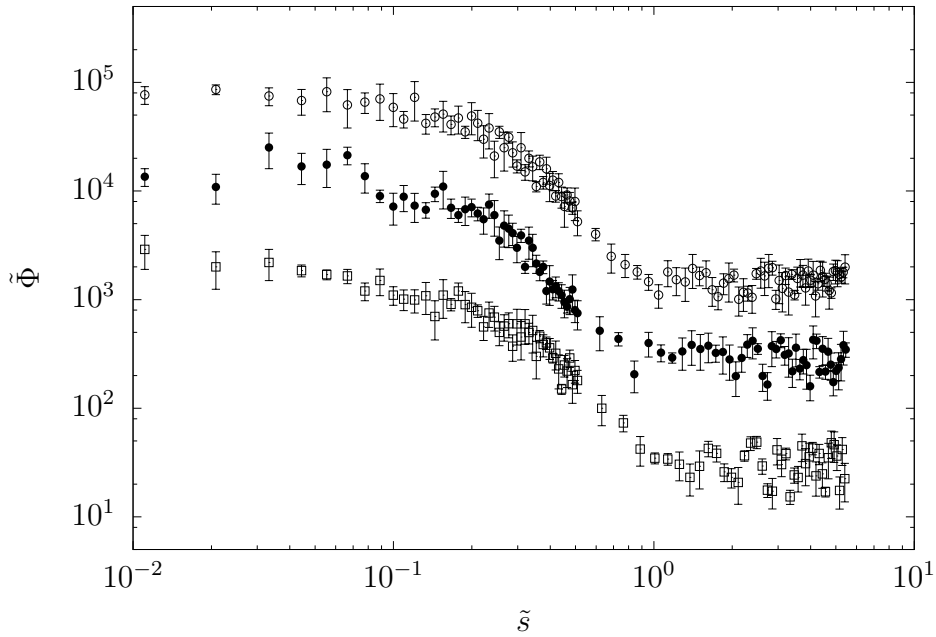
(b) $\alpha = 1.14 \times 10^1$

Figure 35 – EFH1: Nondimensional stress relaxation $\tilde{\Phi}$ as a function of \tilde{s} for different values of γ_0 : (\times) - $\text{Pe} = 1.69 \times 10^{-5}$ ($\gamma_0 = 0.02$), (\bullet) - $\text{Pe} = 1.69 \times 10^{-4}$ ($\gamma_0 = 0.2$), (\blacksquare) - $\text{Pe} = 6.74 \times 10^{-4}$ ($\gamma_0 = 0.8$).

Figure (36) is the analogous of figure (35), but concerning the ferrofluid EFH3. When this ferrofluid is subjected to a constant magnetic field intensity H of 1.18×10^5 A/m (induced by a current of 2A), figure (36a) displays the temporal behavior of its stress relaxation function for only three intensities of shear flow: Pe equals to 4.03×10^{-6} , 4.03×10^{-5} and 1.61×10^{-4} . Figure (36b) presents the same results, but obtained for a condition of a much intenser magnetic field, with intensity H of 1.92×10^5 A/m (related to a current of 4A).



(a) $\alpha = 8.35 \times 10^0$



(b) $\alpha = 1.35 \times 10^1$

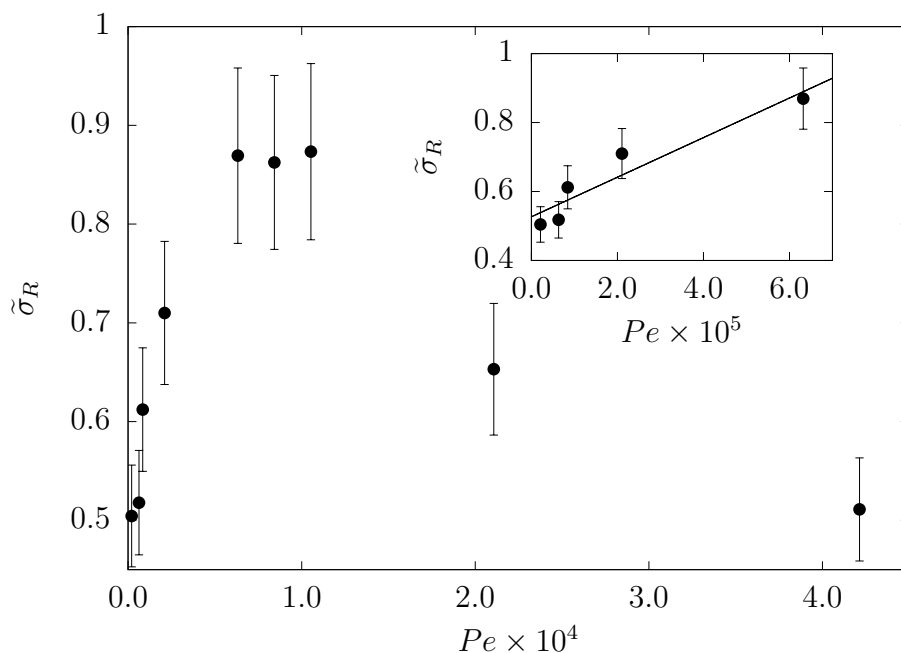
Figure 36 – EFH3: Nondimensional stress relaxation $\tilde{\Phi}$ as a function of \tilde{s} for different values of γ_0 : (o) - $\text{Pe} = 4.03 \times 10^{-6}$ ($\gamma_0 = 0.02$), (●) - $\text{Pe} = 4.03 \times 10^{-5}$ ($\gamma_0 = 0.2$), (□) - $\text{Pe} = 1.61 \times 10^{-4}$ ($\gamma_0 = 0.8$).

Figures (35) and (36) shows that for the two conditions of fixed magnetic field intensity, the shear stresses applied to both ferrofluids did not relaxes for zero as the time passes. The reasons behind this behavior have been extensively discussed on section (6.2.1). The new information comes from the fact that the constant non-zero plateau, to which the stress relaxation function tends for high time intervals, presents a dependence

on Pe . The referred constant value defines the Pe -dependent residual stress relaxation parameter $\tilde{\Phi}_R$, which, as a result, can be used to determine the Pe -dependent residual stress $\tilde{\sigma}_R$, by applying equation (4.37):

$$\tilde{\sigma}_R = \tilde{\Phi}_R \gamma_0. \quad (6.30)$$

For the ferrofluid EFH1, the dependence of its $\tilde{\sigma}_R$ on Pe is shown, for the two conditions of external magnetic field intensities, in the graphs of figure (37). The same is depicted for the ferrofluid EFH3 in the graphs of figure (38). The data displayed on figure (37a) and (38a) are obtained by maintaining the intensity of the magnetic field constant at $H = 1.18 \times 10^5$ A/m, whereas the ones displayed on figures (37b) and (38b), by maintaining $H = 1.92 \times 10^5$. It can be observed in both figures that there are two distinct behaviors of the residual stress as a function of Pe . For small values of Pe , the residual stress is found to increase as Pe enhances, until a critical value of Pe is achieved, from which, the residual stress starts to decrease when Pe is further increased. The second behavior, that is, the decrease of the residual stress as the flow gets more intense is in qualitative agreement with the results presented on Borin et al. (2014). According to those authors, this rheological behavior is motivated by the fact that an increase on shear-rate in this regime leads to a break-up process of the field-induced structures, resulting on lower values of $\tilde{\sigma}_r$. The authors punctuate that their methodology did not permit the application of much lower flow intensities, however, they argue that it would be expected that the value of the residual stress stayed saturated and constant on this regime. Nonetheless, the results obtained in this work strongly disagree with the last assumption. As stated previously, the experiments carried out in this dissertation showed that, in regimes of very small Pe , the residual stress increases following increments on Pe .



(a)

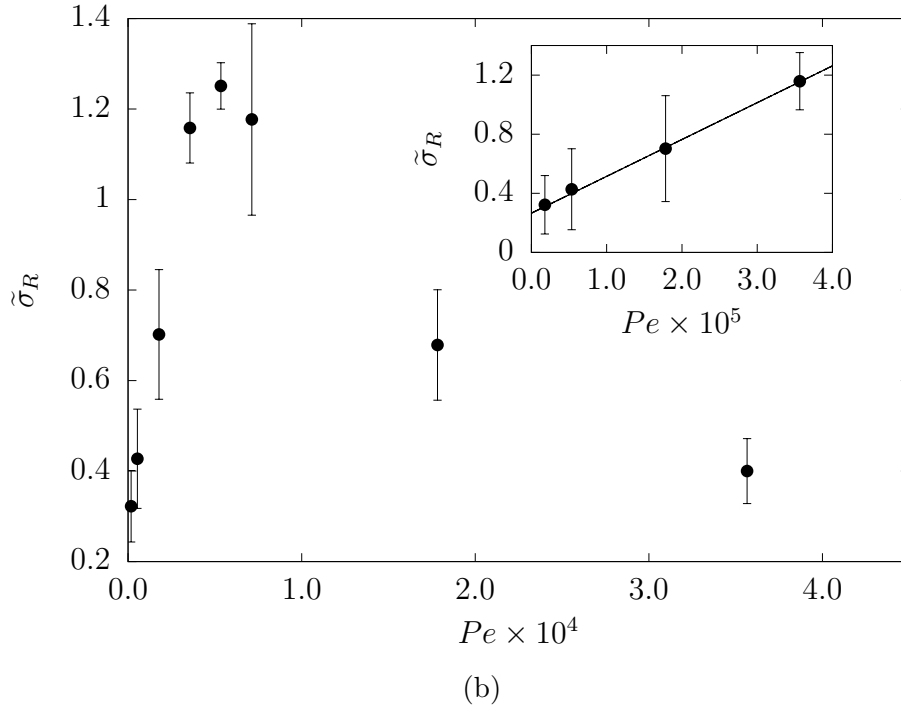
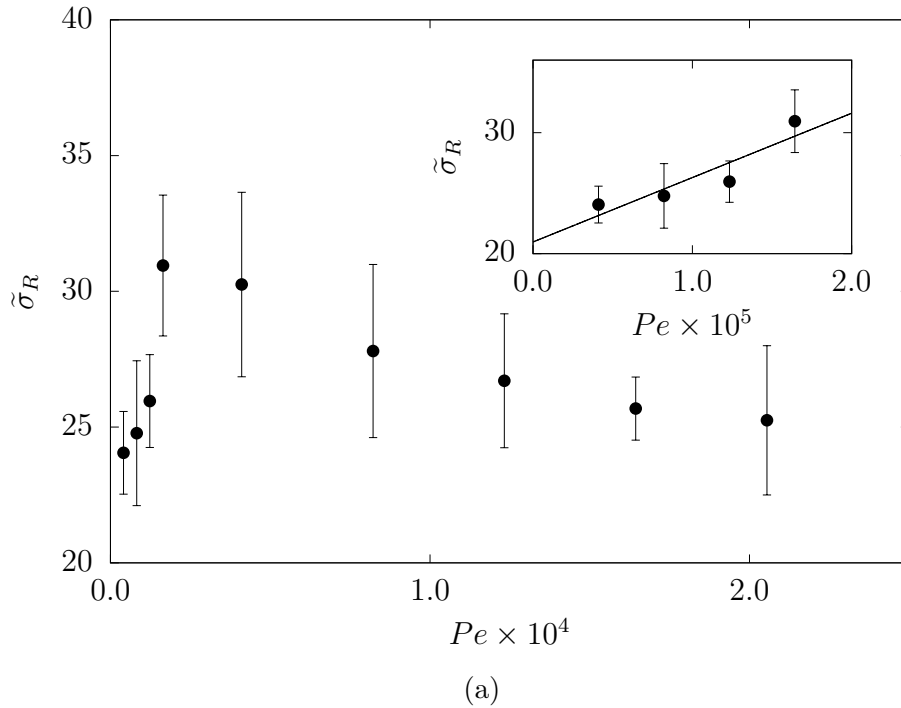


Figure 37 – EFH1: nondimensional residual stress $\tilde{\sigma}_R$ as a function of Pe for two intensities of the external magnetic field: (a) $\alpha = 8.37 \times 10^0$ and (b) $\alpha = 1.14 \times 10^1$. In the inserts is shown a detailed view of the experimental data in the range of small Pe . The lines are fits of experimental data concerning the range of small Pe to $\tilde{\sigma}_r = c_1 Pe$. The constant is, for (a), $c_1 = 5.74 \times 10^3$ and, for (b), $c_1 = 2.49 \times 10^4$.



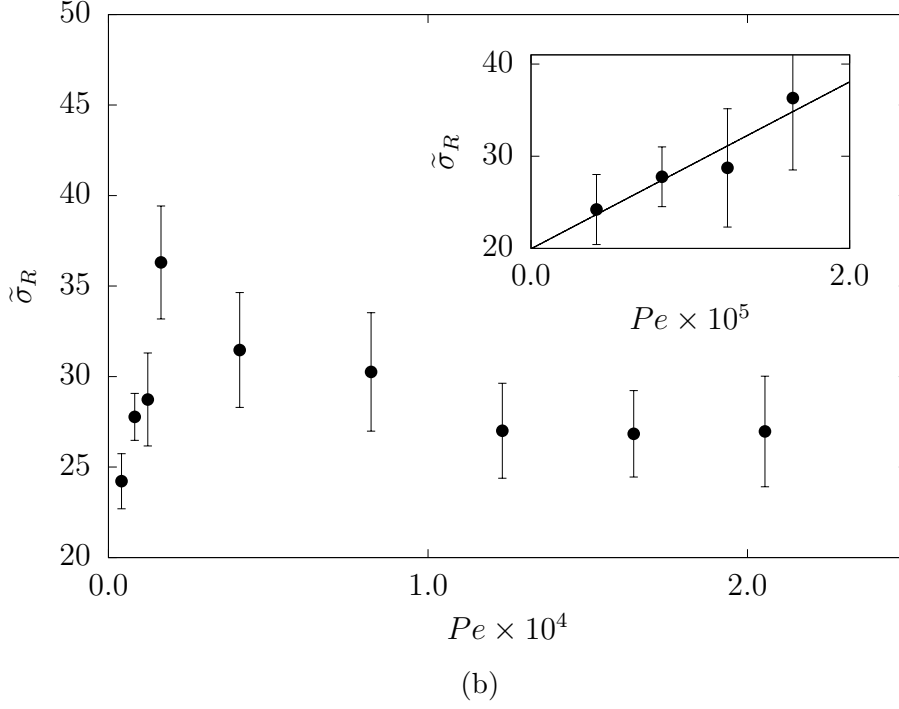


Figure 38 – EFH3: nondimensional residual stress $\tilde{\sigma}_R$ as a function of Pe for two intensities of the external magnetic field: (a) $\alpha = 8.37 \times 10^0$ and (b) $\alpha = 1.14 \times 10^1$. In the inserts is shown a detailed view of the experimental data in the range of small Pe. The lines are fit of experimental data concerning the range of small Pe to $\tilde{\sigma}_r = c_1 Pe$. The constant is, for (a), $c_1 = 5.32 \times 10^5$ and, for (b), $c_1 = 9.06 \times 10^5$.

In order to explain this behavior, firstly, it is important to note that the experimental methodology applied, in this work, to measure the residual stress dependence on the flow intensity, the step-strain, permits the achievement of extreme low values of Pe and, also, the measurement of the shear stress related to it, with good precision. The ascending behavior of the residual stress, in the regime of low values of Pe, indicates that the flow is not strong enough to promote plastic deformations or, even, to breakup magnetic field-induced structures. That is, the shear stress is inferior than the yield stress of the microstructure, which results from the action of the dipolar interactions between the magnetic particles. As a result, in this regime, the effect of the flow is resumed to promote elastic deformations of the elements that compose the microstructure, being the magnetic dipolar interaction the main restoration mechanism. However, when the flow reaches an intensity that produces shear stresses strong enough to surpass the yield stress, the microstructure starts to experience plastic deformations and, as a result, the residual stress is observed to start to decrease. Further increments on Pe lead to the break-up of structures, followed by a strong decrease on $\tilde{\sigma}_R$. In a limit where $Pe \rightarrow \infty$, the residual stress would become zero, as the field-induced microstructure would vanish, due to the high intensity of the shearing flow.

It is important to remark that, in all cases studied, the relation between $\tilde{\sigma}_R$ and Pe was found to be linear in the regime of low Pe, that is, in the range lower than the

yielding point. As Pe is directly related to the angular deformation γ_0 , one can affirm that, in the referred regime of Pe , the shear stress and the angular deformation presents a linear dependence. This is another factor that speaks in favor of the argument that, in the regime of low Pe , the elements of the magnetic field-induced microstructure experience only elastic deformations.

6.2.3 Small amplitude oscillatory shear

The experimental test of small amplitude oscillatory shear is widely used in experimental rheology, because it allows the determination of the viscoelastic response of the most diverse complex fluids, by evaluating the phase difference between the applied oscillatory shear rate and its response, the oscillating stress. This permits, by performing a Fourier analysis of the input and output signals, the determination of viscoelastic modules of the complex fluid.

6.2.3.1 experimental procedure

The experimental protocol is composed by two parts, a preliminary, which is essential for determining the right parameters to be used in the second part, which is effectively the one in which the viscoelastic modules are measured. Both parts are carried out for both ferrofluids at four different conditions of magnetic field intensity, which are: 6.85×10^4 (i=1A)⁵, 1.18×10^5 (i=2A), 1.61×10^5 and 1.93×10^5 A/m (i=4A). In the preliminary part, it is determined the angular strain, γ_0 , which must be used to ensure that the test will be performed under the regime of linear viscoelasticity. This process was carried out, for each ferrofluid, according to the following experimental protocol:

1. According to the fluid and field intensity that will be, respectively, used and applied, an optimized gap is chosen from table (6);
2. Using the value of the chosen gap, the needed volume of ferrofluid to fulfill the gap is calculated. This quantity of ferrofluid is poured in the test area of the rheometer;
3. The upper disk is lowered down until it reaches the exactly prescribed optimal gap. Possible leakages of ferrofluid from the gap are visually searched and, in case of being found, they are trimmed and cleaned;
4. The ferrofluid is demagnetized, using the automatic function of the magnetic cell "demagnetization". This process is essential for freeing the ferrofluid from possible magnetic effects previous to the experiment;

⁵ In parenthesis is displayed the current applied to the coils underneath the bottom plate of the rheometer to generate the referred magnetic field.

5. The thermal bath is set to keep the temperature of the experiment controlled at 25°C;
6. The magnetic field is applied and enough time is waited for the temperature rise, occasioned by the field generation, to be compensated by thermal bath.
7. The execution steps are programmed in the software *Rheoplus*, composed by setting a fixed value of angular frequency ω at the highest value that will be achieved in the second part of the experiments, that is, the maximum value until which the frequency will be varied in the frequency sweep experiments. This value was set to be 100 rad/s for all the cases treated in this experimental work. Besides that, the angular strain γ is programmed to vary from 1×10^{-5} to 1;
8. It is measured the dependence of the storage modulus G' on γ for the fixed value of ω prescribed at each fixed condition of external magnetic field intensity;
9. The optimal angular strain, that is, the one that will guaranty that the experiments of frequency sweep will be carried out in regime of linear viscoelasticity, is chosen between the range of angular strains for which G' is verified to be independent of γ .

From this initial analysis, it has been verified that $\gamma = 0.01$ was sufficient to ensure the linear viscoelastic regime, for both ferrofluids, in all conditions of magnetic field intensity analyzed. After determining this essential parameter, the second part of the experiments, which is focused on the measurement of the viscoelastic modules as functions of frequency, for fixed conditions of magnetic field intensities, could be carried out. The frequency sweep experiments, in the regime of linear viscoelasticity, were carried out, for each condition of magnetic field intensity, through the following protocol:

1. The steps 1 to 6 were the same of the protocol presented above for the strain sweep;
2. In the software *Rheoplus*, it is programmed a variation of the applied angular frequency from 0.1 to 100 rad/s, according to a logarithmic ramp, with an increase rate of 8 points per decade. During this process, the amplitude of angular strain was held constant at $\gamma = 0.01$;
3. The software collects data for viscoelastic modules as functions of the angular frequency and, indirectly, of the magnetic field intensity.

The experimental errors were calculated using the methodology presented on appendix (A.1).

6.2.3.2 Discussion

The oscillatory experiments allows the perception of changes in the rheological behavior of a given fluid complex fluid related to elastic effects arising from its microstruc-

ture. In the experiments, it has been measured, as functions of the frequency of excitation ω and of the intensity of the magnetic field, the complex shear modulus $G_c(\omega, H)$, with its storage $G'(\omega, H)$ and loss $G''(\omega, H)$ parts. Also, it has been measured the complex viscous modulus $\eta_c(\omega, H)$, with its viscous $\eta'(\omega, H)$ and its complex $\eta''(\omega, H)$ parts. These quantities were made nondimensional by using the following characteristic time and viscosity scales:

$$t^* \sim \tau_m, \quad (6.31)$$

$$\eta^* \sim \eta_0, \quad (6.32)$$

where τ_m is the principal time of relaxation for the condition obtained in the presence of the lowest magnetic field intensity applied and η_0 is the viscosity of the ferrofluid, at 25°C, evaluated in a condition of no external magnetic field applied. Using those scales, the typical scales of the referred viscoelastic modules are given by:

$$[G_c]^* \sim [G']^* \sim [G'']^* \sim \frac{\eta_0}{\tau_m}, \quad (6.33)$$

and

$$[\eta_c]^* \sim [\eta']^* \sim [\eta'']^* \sim \eta_0. \quad (6.34)$$

Therefore, the nondimensional form of those material functions are:

$$\tilde{G}_c = \frac{G_c}{[G_c]^*} = \frac{G_c \tau_m}{\eta_0}, \quad (6.35)$$

and

$$\tilde{\eta}_c = \frac{\eta_c}{[\eta_c]^*} = \frac{\eta_c}{\eta_0}. \quad (6.36)$$

It is immediate that the nondimensional form of the material function \tilde{G}' and \tilde{G}'' is the same of \tilde{G}_c , what is also true for the functions $\tilde{\eta}'$ and $\tilde{\eta}''$ in relation to $\tilde{\eta}_c$. In order to make the frequency nondimensional, one defines its characteristic scale as:

$$\omega^* \sim \frac{1}{\tau_m}. \quad (6.37)$$

As a result, the nondimensional frequency, also know as the Deborah number De , is given by:

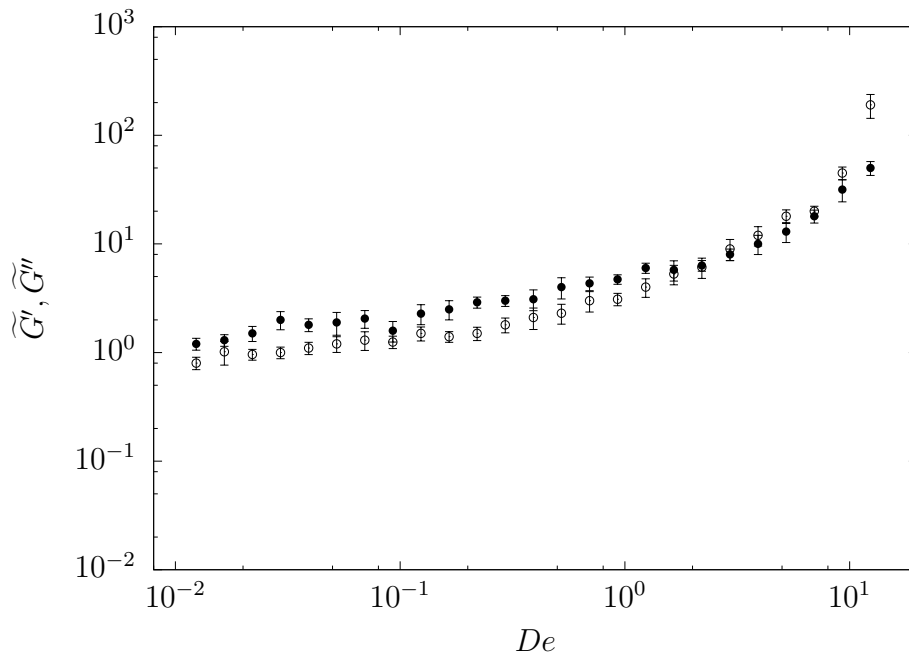
$$De = \tilde{\omega} = \frac{\omega}{\omega^*} = \omega \tau_m. \quad (6.38)$$

It is important remark that for the ferrofluid EFH1, $\eta_0 = 0.94 \times 10^{-2}$ Pa.s and $\tau_m = 1.24 \times 10^{-1}$ s, while, for EFH3, $\eta_0 = 0.18 \times 10^{-1}$ Pa.s and $\tau_m = 6.73 \times 10^{-1}$ s.

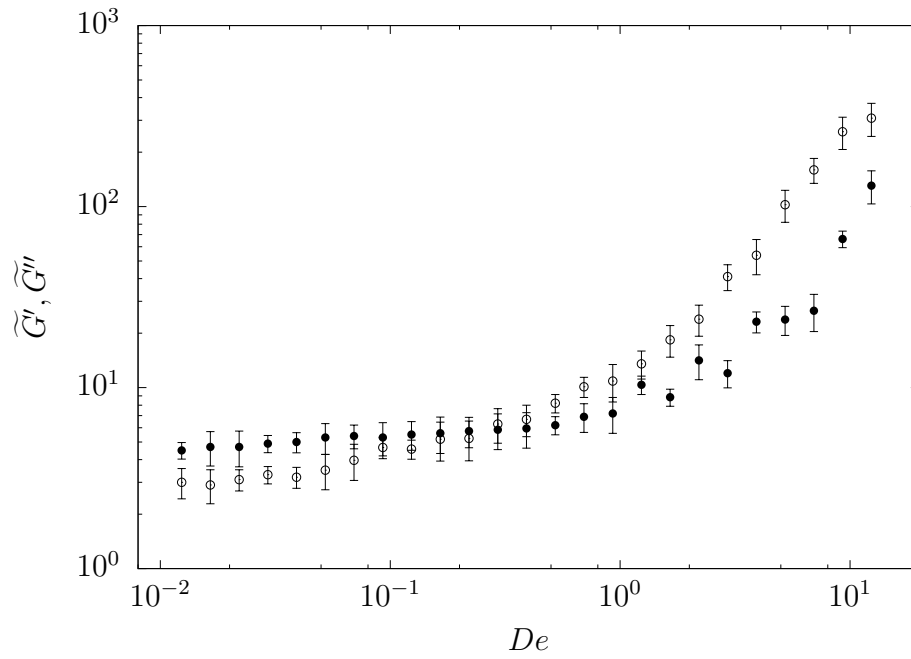
Figures (39) and (40) present, for the fluid EFH1 and EFH3, the behavior of the storage and the loss modulus as a function of De . Figures (39a) and (40a) present results for a condition of weak magnetic field and figures (39b) and (40b) for a condition of strong magnetic field intensity. Due to differences on the ferrofluids' viscosity in the absence of magnetic field η_0 and on their magnetization of saturation M_s , the values of α are different for each ferrofluid, even though the same intensities of magnetic field H are applied. For

EFH1, the conditions of weak and strong magnetic field are, respectively, $\alpha = 4.85 \times 10^0$ and 1.36×10^1 , whereas for EFH3, those conditions are defined by $\alpha = 4.84 \times 10^0$ and 1.35×10^1 .

Figures (39) and (40) show that the application of an external magnetic field has changed completely the rheological behavior of both ferrofluids, due to the fact that they presented, in all conditions of magnetic field applied, an elastic component $G'(De)$ positive, which is an indication that those fluids are viscoelastic. As discussed earlier, this effect is intrinsically related to the fact that both ferrofluids form chains and clusters of particles. That is, the external magnetic field induces the formation of a microstructure on both ferrofluids, via dipolar interactions, what, as a result, injects elasticity in the system of the fluid. Other important observation is that $G'(De)$, for all the range of De , is higher as intenser as the magnetic field intensity is. This can be easily seen by comparing the values of this material functions, on figures (39) and (40), for the higher and lower values of magnetic field intensity. This shows that the complexity of the microstructure formed by strong magnetic fields is much grater than the one formed by weak fields, that is, intense magnetic fields are able to induce the formation of bigger and stabler particle agglomerates, leading to the more pronounced elastic response observe in the referred figures.

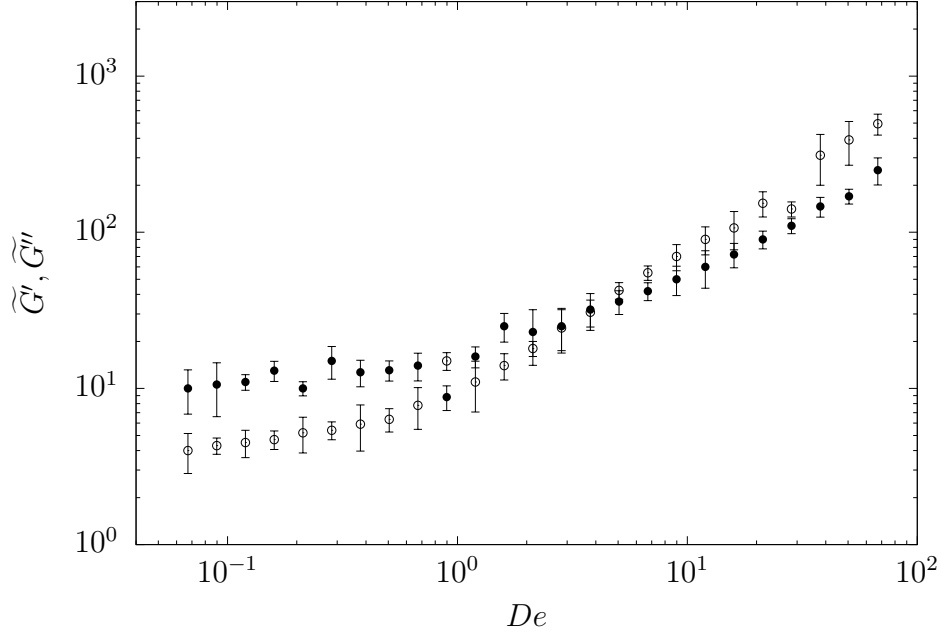


(a) $\alpha = 4.85$

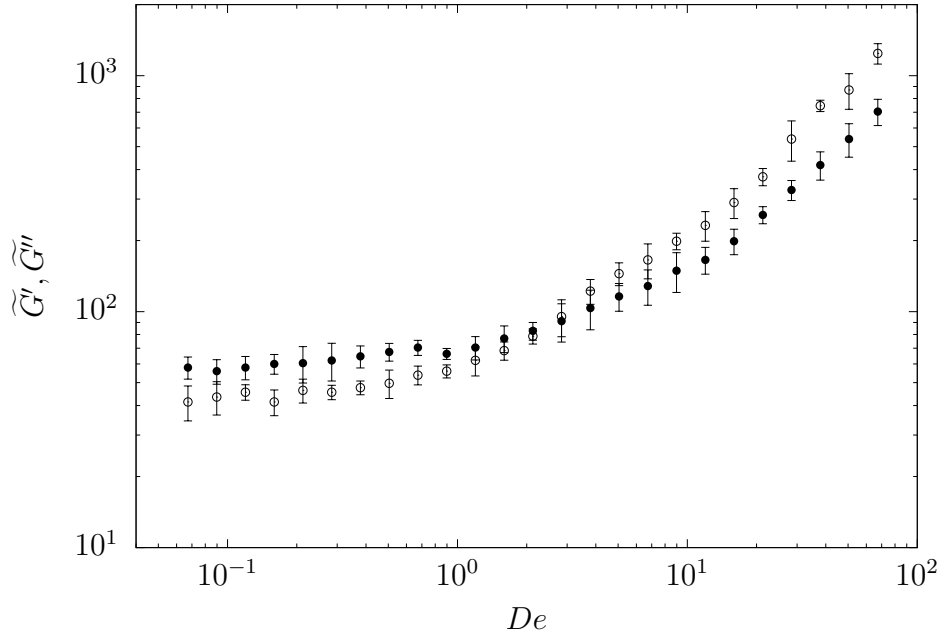


(b) $\alpha = 13.6$

Figure 39 – EFH1: Nondimensional storage modulus \tilde{G}' (○) and nondimensional loss modulus \tilde{G}'' (●) as a function of De , for (a) $\alpha = 4.89$ and (b) $\alpha = 13.5$.



(a) $\alpha = 4.89$



(b) $\alpha = 13.5$

Figure 40 – EFH3: Nondimensional storage modulus \tilde{G}' (\circ) and nondimensional loss modulus \tilde{G}'' (\bullet) as a function of De , for (a) $\alpha = 4.89$ and (b) $\alpha = 13.5$.

Comparing the figures (39a) and (39b) and, also, the figures (40a) and (40b), which are, respectively, representatives of the viscoelastic behavior of the ferrofluid EFH1 and of EFH3, one can observe two slightly different regions at each graph. There is a critic value of De below which, $G' < G''$ and above which, $G' > G''$. Such observation confirms the fact that, at a range of low De , the viscoelastic solution has a more dissipative character, behaving, predominantly, like a viscous liquid. Similarly, for frequencies above the critical value of De , the opposite is true, indicating that the behavior of the solution

is mostly elastic, but the dissipative effect should not be neglected, since the values of \tilde{G}'' are \tilde{G}' very near. The fact that \tilde{G}'' is higher than \tilde{G}' , in the regime of high De, can be understood by taking into account the relationship between the characteristic time scale of the experiment τ_f , defined as the inverse of the excitation frequency, and the one of the material τ_m , which is characterized by its main time of relaxation. In a high frequency regime, τ_f is small compared to τ_m , making the flow perceive the field induced microstructure already deformed, which results on a preponderance of the solid (elastic) character on the dynamical response of the material, given that the field-induced structure tries to relax but is impeded by the flow. Since \tilde{G}' is an indicator of the elasticity of the magnetic suspension, it has a higher value in this situation. The reverse is also true, implying that by subjecting a sample of the viscoelastic suspension to a small range of De relative to the critical, the characteristic flow time will be much longer than that of the fluid. In this condition, the field-induced microstructure is not affected by the flow, that is, the microstructure stays relaxed and, therefore, without adding elasticity to the solution. In this situation, the complex fluid behaves preponderantly like a viscous liquid.

As stated above, for both ferrofluids, at each condition of α , there is a critical value of De in which the curves on \tilde{G}' and \tilde{G}'' intercept. It is immediate, from the graphs on figures (39) and (40), that the critical value of De is a function of the intensity of the applied magnetic field α . It is clear from those graphs that, for small values of α , i.e. weak magnetic fields, the critical De is much higher than that observed for strong magnetic fields. Physically, this observation is explained by observing that, for weak magnetic fields, the main relaxation time of the fluid is considerably shorter than the one observed on stronger fields, given the small amount and length scales of the magnetic field induced structures formed in this condition. Because of this, it is necessary to apply a high excitation frequency in order to the experimental time scale τ_f to be of the same order of magnitude as the fluid relaxation time τ_m , due to the fact that, only after reaching this condition, the microstructure of the complex fluid can interact with the flow and, thus, enabling the alteration of the rheological behavior of the material.

As commented previously, the formation of chains and agglomerates of particles by the action of the magnetic field is the key factor for the appearance of elastic effects on ferrofluids. Regarding this context, (41) display the influence of the magnetic field intensity on the nondimensional storage modulus of both ferrofluids. In order to allow comparison, for each α , \tilde{G}' was evaluated for De=1. It is immediate that, for both ferrofluids, the elastic component has increased as α heightened. This can be explained, according to Borin et al. (2014), by the fact that strong magnetic field induces the formation of larger and stabler structures in the fluid, what, collaterally, means an intenser injection of elasticity in the fluid. This effect is so intense in both ferrofluids that the dependence of \tilde{G}' on α was found to be exponential in the experiments described on this dissertation. Moreover, it can be also observed that, for each value of α , the nondimensional storage modulus is higher for the ferrofluid EFH3 in comparison to EFH1, what can be explained regarding the fact

that the volume fraction of magnetic particles of EFH3 is bigger, which facilitates, due to the bigger availability of particles per unit of volume in this fluid, the action of the dipolar interactions. As a result, when an external magnetic field is applied, bigger and stabler structures are formed in EFH3 in comparison to the ones formed on EFH1, also justifying the faster increase experimented by its \tilde{G}' when the same variation of α is applied to both ferrofluids.

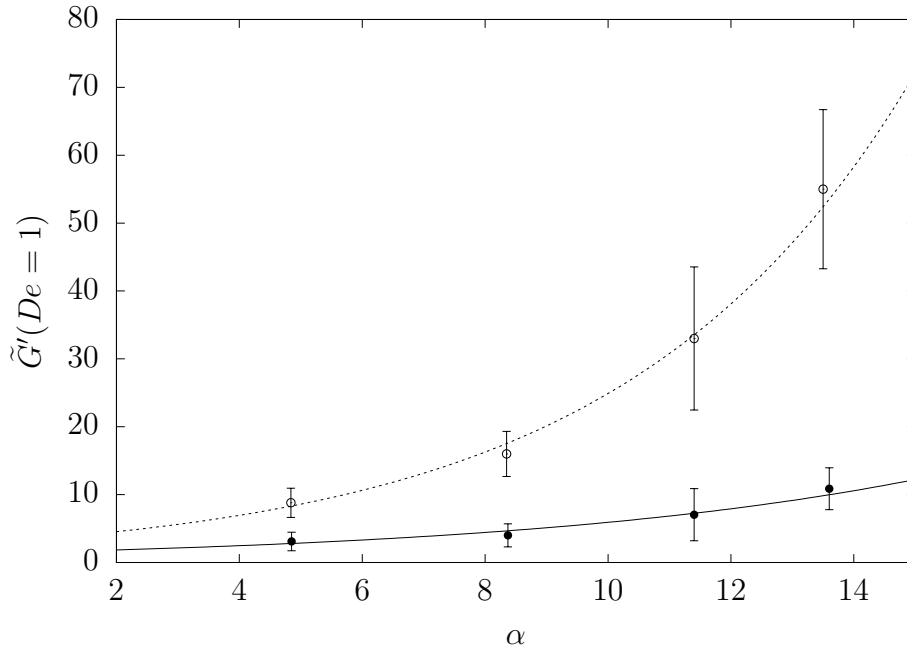


Figure 41 – Non-dimensional storage modulus \tilde{G}' evaluated at $De = 1$ for different values of α for the ferrofluids EFH1 (●) and EFH3 (○). The curves are fits to the experimental data to $\tilde{G}'(De = 1, \alpha) = c_1 \exp(c_2 \alpha)$. The constants for the dashed curve are $c_1 = 2.97$ and $c_2 = 0.21$. For the continuous curve, they are $c_1 = 1.39$ and $c_2 = 0.15$.

The nondimensional viscous modulus $\tilde{\eta}'$ also experimented an intense increase when subjected to an enhancement of the magnetic field intensity. Figure (42) depicts that this variation is exponential, according to our experiments. This is also a reflection of the formation of larger and stabler structures in conditions of strong magnetic fields. Those large structures cause a much intenser hindrance of rotation and also a higher localized drag, which are mechanisms that result on severe local energy dissipation. The bulk effect of those localized dissipation effects is the overall increase of the viscous behavior of the suspension. The higher values obtained for $\tilde{\eta}'$ on EFH3, in comparison to EFH1, is due to the difference of volume fraction of magnetic particles and of magnetization of saturation between both ferrofluids.

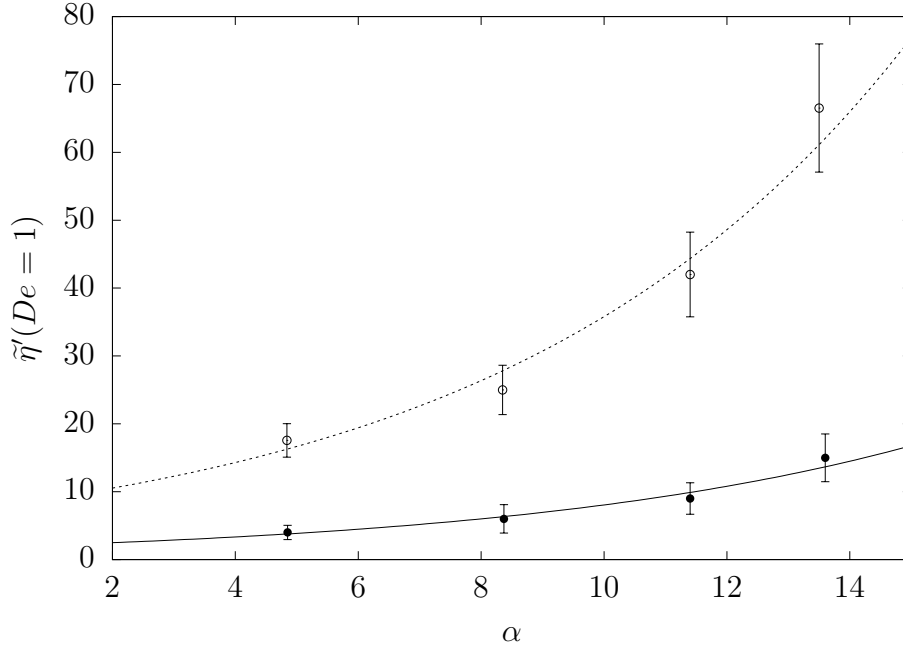


Figure 42 – Nondimensional viscosity modulus $\tilde{\eta}$ evaluated at $De = 10$ for different values of α for the ferrofluids EFH1 (●) and EFH3 (○). The curves are fits to the experimental data to $\tilde{\eta}'(De = 1, \alpha) = c_1 \exp(c_2 \alpha)$. The constants for the dashed curve are $c_1 = 7.76$ and $c_2 = 0.15$. For the continuous curve, they are $c_1 = 1.85 \pm$ and $c_2 = 0.15$.

The determination of the viscoelastic modules of a given complex fluid through experiments in the regime of linear viscoelasticity, which is the case of the small amplitude oscillatory shear experiments carried out in this dissertation, allows the indirect determination of the first normal stress difference N_1 . It is important to remark that this material function can be directly measured by experiments in the regime of simple shear, specifically on torsional rheometers of cone-and-plate geometry. In order to perform the indirect determination of the referred material function, one can apply the empirical correlations of [Cox and Merz \(1959\)](#) or the more general one of [Laun \(1986\)](#), which are detailed on section (4.5). Both experimental correlations provide a link between the description of the fluid's material functions obtained by oscillatory experiments and those measured on permanent shear experiments. A way to guarantee that the referred agreement is representative of the reality is to verify if the modulus of the complex viscosity $|\eta_c(\omega)|$ and the apparent viscosity $\eta(\dot{\gamma})$ are equal for correspondent values of ω and $\dot{\gamma}$. This validation has been carried out for both ferrofluids at all the applied magnetic field intensities α . However it was found to apply only for the ferrofluid EFH1, at the lowest value of magnetic field intensity, what is shown on figure (43).

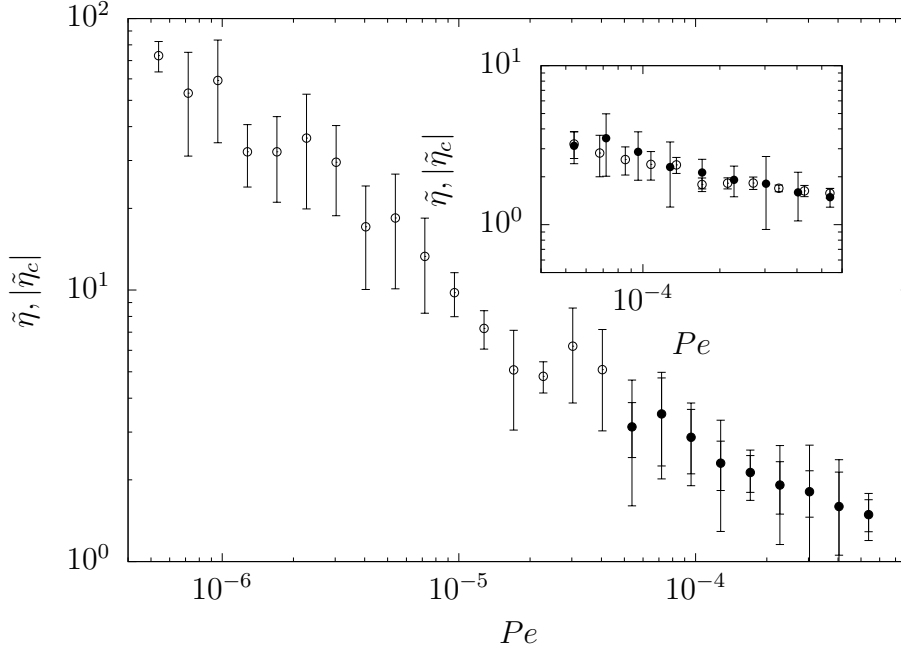


Figure 43 – EFH1: Nondimensional apparent viscosity $\tilde{\eta}$ (\bullet) and nondimensional absolute value of the complex viscosity $|\tilde{\eta}_c|$ (\circ) as functions of Pe (calculated considering $\omega = \dot{\gamma}$) at $\alpha = 4.85$. In the insert is shown a detailed view of the zone of agreement between the $\tilde{\eta}$ and $|\tilde{\eta}_c|$.

As it can be seen from figure (43), $|\eta_c(\omega)|$ and $\eta(\dot{\gamma})$ present an excellent agreement, which is better visualized in the insert of the referred figure. This validation allows the application of Laun’s rule, equation (4.41), in order to compute the first normal stress difference based on the measurements of $G'(\omega)$ and $G''(\omega)$. The resulting values, that is, N_1 as a function of $\dot{\gamma}$, were made nondimensional, being displayed as \tilde{N}_1 as a function of Pe on figure (44).

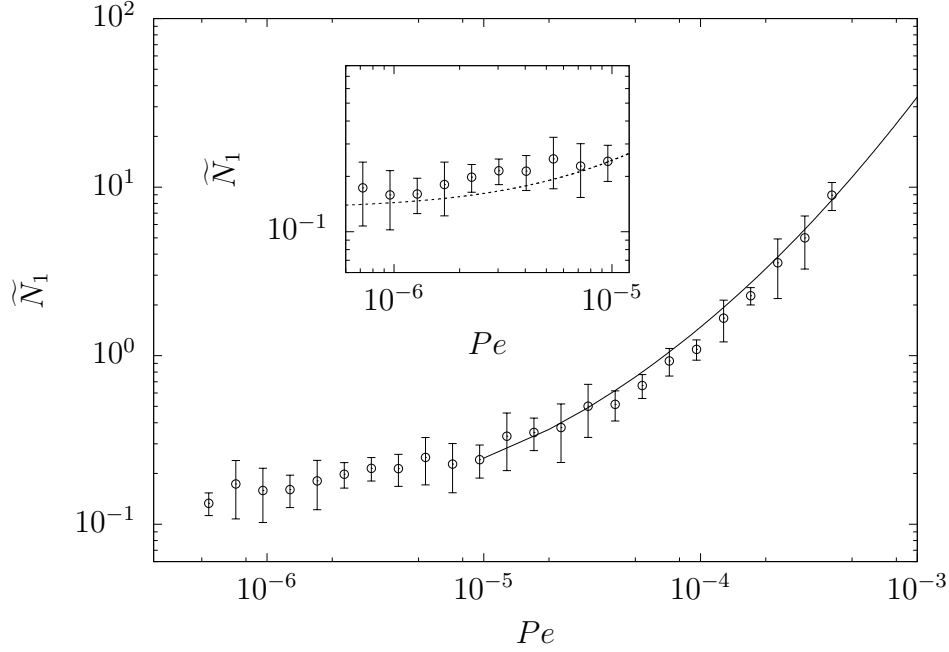


Figure 44 – Nondimensional first normal stress difference \tilde{N}_1 as a function of Pe obtained by applying Laun’s rule to the measured values of $G'(\omega)$ and $G''(\omega)$. The dashed curve, in the insert, is a fit of the experimental data for the range of small Pe to $\tilde{N}_1 = c_1 + c_2 Pe$, with $c_1 = 1.33 \times 10^{-1}$ and $c_2 = 1.11 \times 10^4$. The continuous curve is a fit of the experimental data for the complete range of Pe to $\tilde{N}_1 = c_1 Pe^2 + c_2 Pe + c_3$, with c_1 and c_2 equals to the one determined for the dashed line and $c_3 = 2.30 \times 10^7$.

Figure (44) shows a variation of several orders on \tilde{N}_1 as Pe heightens. This is a confirmation of the fact that, under an influence of an external magnetic field, the stresses in the fluid become anisotropic. This fact was first punctuated as a possibility in the theoretical work of Zubarev (1992) and has been firstly observed experimentally by Odenbach, Rylewicz and Rath (1999). In the referred figure, it is also depicted that \tilde{N}_1 has two different functional dependencies on Pe . In the range of low Pe , the first difference of normal stresses displays a linear dependence on Pe , whereas, in a regime of medium/high Pe , this dependence becomes quadratic. The linear behavior is possibly explained by collisional effects between the magnetic field induced chains and agglomerates, that leads to an initial anisotropy of the microstructure and, as a result, to the appearance of normal stresses. The quadratic dependence is generated, according to Zubarev (1992), by a collective alignment of the field induced chains and structures within the fluid with the direction of the magnetic field.

7 Final Considerations

7.1 Conclusions

The viscosity of the ferrofluids EFH1 and EFH3 increased when they were subjected to an strengthening external magnetic field. This behavior, called magnetoviscous effect, has its origin in the fact that when a magnetic particle is subjected to an external magnetic field, its moment of dipole aligns with the direction of the applied field, what implies that the particle is no longer free to rotate with the vorticity of the flow. It was observed that the increase of viscosity in both ferrofluids was much intenser than what is predicted by the classical theory. This was attributed to the fact that the magnetic colloids have high volume fractions of magnetic particles, what leads to formation of chains and aggregates of particles by the action of dipolar interactions. Moreover, this structures provoke higher hindrances of rotation when aligned to the magnetic field and also, due to its larger characteristic lengths, they increase the local drag. Both mechanisms induce energy dissipation and are the motives behind the strong magnetoviscous effect observed. It is important to remark that the magnetoviscous effect of the ferrofluid EFH3 was much more pronounced than the one observed for EFH1, what comes the fact that all the energy dissipation mechanisms are stronger on EFH3, owing to the fact that this fluid has a higher volume fraction of magnetic particles.

It has also been observed a pseudoplastic behavior for both ferrofluids when under the action of a magnetic field. This shear-tinning behavior was characterized by the observation of a strong decrease of the apparent viscosity of the ferrofluids when they were subjected to increasingly strong shear rates. This effect is associated to the fact that in concentrated ferrofluids, like the ones treated in this work, the application of a magnetic field, due to dipolar interactions, is followed by the formation of chains and aggregates of particles. For weak flow conditions, the viscosity of both fluids was observed to reach high values, what is a natural consequence of the magnetoviscous effect previously discussed, however, when the flow starts to intensify, the viscosity starts to decrease rapidly, until a constant plateau is observed. This behavior is explained by two process: the first one is related to the weak flow region, in which the flow starts to induce an alignment of the field induced microstructure with its streamlines, in a process that results on the reduction of local drag and, as a result, of the suspension's viscosity. Nontheless, the main process

responsible for the reduction of viscosity is the breakup of the field induced microstructures, leading to chains and agglomerates with ever small length scales, that generate less energy dissipation effects, leading to the strong reduction of the apparent viscosity. The plateau of constant viscosity observed for high values of shear flow has its origin on the fact that the flow is so strong that the magnetic field induced is almost vanished, and, as a result, also its effects on the viscosity. Due to the formation of a microstructure, it has also been verified the existence of yield stress for both fluids, when in the presence of a magnetic field. All the effects describe for the shear-thinning behavior were observed to be more intense the higher the intensity of the magnetic field, what is related to the fact that stronger magnetic fields produce microstructures formed by stabler and larger particle's chains and agglomerates. The behavior of the apparent viscosity as a function of the shear flow intensity was well modeled by Sisko's viscosity model and the same dependence for the shear stress was successfully described by Herschel-Bulkley's model. The last one permitted the obtainment of the yield stress, for each fluid, at each condition of magnetic field intensity investigated.

It was also observed that, in the presence of a magnetic field, the ferrofluids EFH1 and EFH3 become viscoelastic liquids. This was first verified in the experiments of step-strain, conducted with a small angular strain, for increasing values of magnetic field intensity. In all field conditions, the fluids presented a delay on its process of stress relaxation, which is a direct sign of the presence of elastic behavior. This elastic properties arise from the formation of a microstructure, due to the action of the magnetic field. The process of relaxation is generally characterized by a single time of relaxation, which traduces the action of the main mechanism of stress relaxation acting in the fluid. In this case, the shear stress relaxes to zero after the cessation of flow. Nonetheless, the relaxation process, of the ferrofluids in analysis, was found to be highly complex, characterized by more than one time of relaxation and by the relaxation of the shear stress for a non-zero value, after the cessation of the flow. The residual stress can be understood as the yield stress of the fluid, due to the fact that it represents the minimum stress to which the stress relax, or from other point of view, the minimum stress that must be applied, in order for the fluid starts to flow. This process of relaxation was found to be well modeled by an adaptation of Maxwell's viscoelastic constitutive model. The adaptation was the inclusion of a term regarding the residual stress. Using this model it was possible to determine the times of relaxation, of each fluid, at each condition of magnetic field intensity. The ferrofluid EFH1 was well described by two relaxation times and EFH3 by three, for every condition of field. The more complex stress relaxation of EFH3 rises from its bigger volume fraction of particles in relation to EFH1. The main time of relaxation of both fluid, as well as their residual stresses, were found to be exponentially related to the intensity of the magnetic field, in the experiments reported on this dissertation.

The effect of the shear flow intensity in the stress relaxation of the ferrofluid was also investigated. Step-strains with variable angular strains were performed for two

conditions of constant intensity magnetic fields, a weak and a strong one. The stress relaxation function was observed to reach ever lower plateaus as the intensity of the applied flow was heightening. The residual stress, was calculated by multiplying the value of this plateau by the angular strain applied. This analysis lead to the obtainment of the dependence of the residual stress on the shear flow intensity, which has shown two very distinct behaviors, depending on the range of the applied flow intensity. For very low flow intensities, the residual stress was found to increase linearly with the flow intensity, until it reaches a maximum and starts do decrease rapidly as the flow strengthens. The first effect has not yet been covered in the specific literature of rheology of ferrofluids. This work suggests that this behavior is associated to the fact that, for the low regime of flow intensities, the shear rate is not strong enough to produce plastic deformations or even breakups of the field-induced structures, being characterized by a regime dominated by elastic (reversible) deformations, that are not able to change permanently the overall topology of the microstructure. This behavior shifts when the yielding point is reached and the flow starts to provoke plastic deformations, even leading to the breakup of the magnetic field induced structures. For extremely high values of flow intensity, the structures are supposed to break down completely leading to a vanish of the residual stress.

Dynamic rheological characterizations have been carried out for both ferrofluid at several magnetic field conditions. It was verified, from the results obtained from the experiments of small amplitude oscillatory shear, that both ferrofluids have a storage modulus and a loss modulus different from zero in the complete range of frequencies applied, when they are in the presence of an external magnetic field. This is another strong confirmation that both fluids are viscoelastic. It is important to note that this observation comes from the fact that the formation of structures of magnetic particles by the action of the magnetic field increases the dissipation and, also, injects elasticity in the system of the fluid. This effect is intenser the higher the magnetic field intensity is, what justifies the observed exponential dependence of the storage modulus and of the viscosity modulus on the intensity of the magnetic field, considering a fixed frequency of excitation.

The storage and loss modulus have presented two behaviors dependent on the excitation frequency. For low values of frequency, the loss modulus was found to be higher than the storage modulus, which is explained by the fact that the characteristic flow time is much longer than the one of the fluid in this case. Therefore, the field-induced microstructure is not affected by the flow, staying relaxed, what implicated that in no addition of elasticity to the suspension, that behaves, predominantly, like a viscous liquid. For high values of frequency, the characteristic flow time is small compared to the time of relaxation of the fluid, what makes the flow perceive the field induced microstructure as already deformed. This indicates a dominance of the solid (elastic) character of the material, given that the field-induced structure tries to relax but is impeded by the flow. The frequency, in which the curves of the storage and loss modulus were found to intercept,

decreases as the intensity of the magnetic field increases. That is, the predominant liquid-like behavior changes to a dominant solid-like for a lower frequency value as the magnetic field becomes more intense. This can be explained by the fact that the characteristic time of the fluid increases when the magnetic field heightens, that is, its characteristic frequency decreases and, thus, the fluid changes its predominant rheological behavior for smaller frequencies of excitation.

A comparison between the complex viscosity and the apparent viscosity for compatible values of frequency and shear rate has been carried out for both ferrofluids in all conditions of magnetic field studied. However, the agreement between the two sets of data was just verified for the ferrofluid EFH1 at the lowest magnetic field intensity applied. This compatibility validated the use of Laun's rule to calculate, from the storage and the loss modulus, the first normal stresses difference. The fact that the fluid, when subjected to a magnetic field, presents a first normal stress difference is a solid indication that the fluid become anisotropic. This material function presented two kinds of functional dependencies on the shear rate. For weak flows, the first normal stresses difference displayed a linear dependence on the shear rate. This is related to collisional effects between the chains and particles of the magnetic field-induced microstructure. For medium-high flow intensities, the first normal stresses difference was observed to depend quadratically on the shear-rate, which is a straightforward consequence of the alignment of the field induced microstructure of the fluid with the magnetic field direction.

7.2 Suggestions for future works

As possible future works, it can be pointed out:

- Carry out a thorough analysis of the validity, for ferrofluids, of the linear viscoelastic flow regime based only on the choice of a small value of angular strain from a range in which the storage modulus is independent of it. What can be done by using the Kramers-Kronig and the Fourier transform of the stress relaxation function, following the methodology discussed in [Pereira \(2017\)](#).
- Directly measure the normal stresses differences using a cone-and-plate rheometer for various conditions of magnetic field intensity. Compare the values, obtained for this material function, using this methodology to the ones calculated from data obtained on oscillatory shear through empirical correlations, like the ones proposed by [Cox and Merz \(1959\)](#) and [Laun \(1986\)](#).
- Perform experimental rheological studies, in the presence of external magnetic field, with samples of ferrofluids composed by the same base fluid and surfactant additives, but varying on a wide range of volume fraction of particles. The characterization of the dependence of the material functions on the volume fraction of magnetic

particles is of high importance, due to the fact that, as shown in this dissertation, the variation of this parameter has severe influence on the overall rheological behavior of ferrofluids.

- Compare the experimental results, described on this dissertation, with numerical simulations.
- Perform the same experimental protocols define on this dissertation to analyze the influence of the application of an external magnetic field and of the volume fraction of magnetic particles on the rheology of magnetorheological suspensions. This study is important due to the fact that this type of fluid presents much intenser dependence of its material functions on the intensity of the magnetic field applied, owing to the large characteristic length of its particles, which is around $100 \mu\text{m}$.

Bibliography

ALEXIOU, C. et al. Targeted tumor therapy with "magnetic drug targeting": Therapeutic efficacy of ferrofluid bound mitoxantrone. In: *Ferrofluids*. [S.l.]: Springer, 2002. p. 233–251. Citado na página 4.

ARIS, R. *Vectors, tensors and the basic equations of fluid mechanics*. [S.l.]: Courier Corporation, 2012. Citado 7 vezes nas páginas 18, 19, 20, 21, 28, 33, and 71.

BACRI, J.-C.; CEBERS, A. O.; PERZYNSKI, R. Behavior of a magnetic fluid microdrop in a rotating magnetic field. *Physical review letters*, APS, v. 72, n. 17, p. 2705, 1994. Citado na página 10.

BAILEY, R. L. Lesser known applications of ferrofluids. *Journal of magnetism and magnetic materials*, Elsevier, v. 39, n. 1-2, p. 178–182, 1983. Citado na página 3.

BARNES, H. A.; HUTTON, J. F.; WALTERS, K. *An introduction to rheology*. [S.l.]: Elsevier, 1989. v. 3. Citado 5 vezes nas páginas 39, 40, 41, 52, and 58.

BATCHELOR, G. K. *An introduction to fluid dynamics*. [S.l.]: Cambridge university press, 2000. Citado 5 vezes nas páginas 16, 17, 19, 31, and 35.

BATCHELOR, G. K.; GREEN, J. T. The hydrodynamic interaction of two small freely-moving spheres in a linear flow field. *Journal of Fluid Mechanics*, Cambridge Univ Press, v. 56, n. 02, p. 375–400, 1972. Citado na página 33.

BERKOVSKI, B.; BASHTOVOY, V. *Magnetic fluids and applications handbook*. *Begel House, New York*, 1996. Citado na página 3.

BIRD, R. B.; ARMSTRONG, R. C.; HASSAGER, O. Dynamics of polymeric liquids. volume 1: fluid mechanics. *A Wiley-Interscience Publication, John Wiley & Sons, New York*, 1987. Citado 7 vezes nas páginas 36, 37, 40, 41, 49, 50, and 98.

BIRD, R. B. et al. Dynamics of polymer liquids vol. 2 kinetic theory. *A Wiley-Interscience Publication, John Wiley & Sons, New York*, 1987. Citado 2 vezes nas páginas 58 and 92.

BORIN, D. Y. et al. Ferrofluid with clustered iron nanoparticles: Slow relaxation of rheological properties under joint action of shear flow and magnetic field. *Journal of Magnetism and Magnetic Materials*, Elsevier, v. 323, n. 10, p. 1273–1277, 2011. Citado 2 vezes nas páginas 12 and 98.

BORIN, D. Y. et al. Stress relaxation in a ferrofluid with clustered nanoparticles. *Journal of Physics: Condensed Matter*, IOP Publishing, v. 26, n. 40, p. 406002, 2014. Citado 6 vezes nas páginas 13, 92, 98, 101, 107, and 116.

- BRUNKE, O. et al. Determination of the magnetic particle distribution in tumour tissue by means of x-ray tomography. *Journal of Physics: Condensed Matter*, IOP Publishing, v. 18, n. 38, p. S2903, 2006. Citado na página 4.
- BRUSENTOV, N. A. et al. Magnetic fluid hyperthermia of the mouse experimental tumor. *Journal of Magnetism and Magnetic Materials*, Elsevier, v. 252, p. 378–380, 2002. Citado na página 4.
- COX, W.; MERZ, E. Rheology of polymer melts - a correlation of dynamic and steady flow measurements. In: ASTM INTERNATIONAL. *International Symposium on Plastics Testing and Standardization*. [S.l.], 1959. Citado 3 vezes nas páginas 57, 118, and 124.
- CUNHA, F. R. Fundamentos da hidrodinâmica de fluidos magnéticos. *Turbulência (BS Carmo, GR Assi, JR Meneghini, JAP Aranha, and EV Volpe, eds.)*, v. 8, p. 257–339, 2012. Citado 2 vezes nas páginas 5 and 30.
- CUNHA, F. R. *Lecture notes of the course dynamics of Non-Newtonian fluids*. Tese (Doutorado) — University of Brasília, 2016. Citado na página 40.
- CUNHA, F. R. A note on the stress tensor and magnetization evolution for magnetic dilute suspensions of rigid spherical particles. *to be submitted*, 2019. Universidade de Brasília, Brasília - DF. Citado na página 31.
- CUNHA, F. R.; ROSA, A. P.; DIAS, N. J. Rheology of a very dilute magnetic suspension with micro-structures of nanoparticles. *Journal of Magnetism and Magnetic Materials*, Elsevier, v. 397, p. 266–274, 2016. Citado na página 10.
- CUNHA, F. R.; SOBRAL, Y. D. Characterization of the physical parameters in a process of magnetic separation and pressure-driven flow of a magnetic fluid. *Physica A: Statistical Mechanics and its Applications*, Elsevier, v. 343, p. 36–64, 2004. Citado na página 6.
- DIAS, N. J. S. *Caracterização reológica de fluidos complexos em cisalhamento linear e tubo capilar*. Tese (Doutorado) — Programa de pós-graduação em ciências mecânicas. Universidade de Brasília, Brasília - DF, 2015. Citado na página 4.
- DOI, M.; EDWARDS, S. F. *The theory of polymer dynamics*. [S.l.]: oxford university press, 1988. v. 73. Citado na página 13.
- EINSTEIN, A. A new determination of the molecular dimensions (vol 19, pg 289, 1906). *Annalen der physik*, v. 34, n. 3, p. 591–592, 1911. Citado na página 9.
- EINSTEIN, A. et al. On the motion of small particles suspended in liquids at rest required by the molecular-kinetic theory of heat. *Annalen der physik*, v. 17, p. 549–560, 1905. Citado 2 vezes nas páginas 1 and 74.
- FANNIN, P. C. Magnetic spectroscopy as an aide in understanding magnetic fluids. In: *Ferrofluids*. [S.l.]: Springer, 2002. p. 19–32. Citado na página 9.
- FRENKEL, Y. I. Kinetic theory of liquids. Dover, 1955. Citado na página 9.
- GLÖCKL, G. et al. The effect of field parameters, nanoparticle properties and immobilization on the specific heating power in magnetic particle hyperthermia. *Journal of Physics: Condensed Matter*, IOP Publishing, v. 18, n. 38, p. S2935, 2006. Citado na página 4.

- GONTIJO, R. G.; CUNHA, F. R. Dynamic numerical simulations of magnetically interacting suspensions in creeping flow. *Powder technology*, Elsevier, v. 279, p. 146–165, 2015. Citado na página 10.
- GRAHAM, M. D. *Microhydrodynamics, Brownian motion, and complex fluids*. [S.l.]: Cambridge University Press, 2018. v. 58. Citado na página 32.
- GRANT, I. S.; PHILLIPS, W. R. *Electromagnetism*. [S.l.]: John Wiley & Sons, 2013. Citado 2 vezes nas páginas 21 and 24.
- HALL, W. F.; BUSENBERG, S. N. Viscosity of magnetic suspensions. *The Journal of Chemical Physics*, AIP, v. 51, n. 1, p. 137–144, 1969. Citado 3 vezes nas páginas 7, 8, and 77.
- JORDAN, A. et al. Presentation of a new magnetic field therapy system for the treatment of human solid tumors with magnetic fluid hyperthermia. *Journal of magnetism and magnetic materials*, Elsevier, v. 225, n. 1-2, p. 118–126, 2001. Citado 3 vezes nas páginas vii, 4, and 5.
- JURGONS, R. et al. Drug loaded magnetic nanoparticles for cancer therapy. *Journal of Physics: Condensed Matter*, IOP Publishing, v. 18, n. 38, p. S2893, 2006. Citado na página 4.
- KIM, S.; KARRILA, S. J. *Microhydrodynamics: principles and selected applications*. [S.l.]: Courier Corporation, 2013. Citado 2 vezes nas páginas 6 and 33.
- KLINE, S. J.; MCCLINTOCK, F. A. Describing uncertainties in single-sample experiments. *Mechanical Engineering*, v. 75, p. 3–8, 1953. Citado na página 133.
- LANDAU, L. D.; LIFSHITZ, E. M. Fluid mechanics. *Fluid Mechanics. Second Edition. 1987*. Pergamon, Oxford, 1987. Citado na página 31.
- LANDFESTER, K.; RAMIREZ, L. P. Encapsulated magnetite particles for biomedical application. *Journal of Physics: Condensed Matter*, IOP Publishing, v. 15, n. 15, p. S1345, 2003. Citado na página 1.
- LAUN, H. M. Prediction of elastic strains of polymer melts in shear and elongation. *Journal of Rheology*, SOR, v. 30, n. 3, p. 459–501, 1986. Citado 3 vezes nas páginas 57, 118, and 124.
- LI, Q.; XUAN, Y.; WANG, J. Experimental investigations on transport properties of magnetic fluids. *Experimental Thermal and Fluid Science*, Elsevier, v. 30, n. 2, p. 109–116, 2005. Citado na página 1.
- LIU, X.; JIN, L. Effect of the volume of magneto-rheological fluid on shear performance. *Measurement Science Review*, Versita, v. 11, n. 2, p. 53–56, 2011. Citado na página 14.
- LÜBBE, A. S.; ALEXIOU, C.; BERGEMANN, C. Clinical applications of magnetic drug targeting. *Journal of Surgical Research*, Elsevier, v. 95, n. 2, p. 200–206, 2001. Citado na página 4.
- MALVAR, S.; GONTIJO, R. G.; CUNHA, F. R. Nonlinear motion of an oscillating bubble immersed in a magnetic fluid. *Journal of Engineering Mathematics*, Springer, v. 108, n. 1, p. 143–170, 2018. Citado na página 35.

MARTSENYUK, M. A.; RAIKHER, Y. L.; SHLIOMIS, M. I. On the kinetics of magnetization of suspension of ferromagnetic particles. *Soviet Physics-JETP*, v. 38, n. 2, p. 413–416, 1974. Citado na página 78.

MCTAGUE, J. P. Magnetoviscosity of magnetic colloids. *The Journal of Chemical Physics*, AIP, v. 51, n. 1, p. 133–136, 1969. Citado 3 vezes nas páginas 7, 77, and 80.

MORRISON, F. A. *Understanding rheology*. [S.l.]: Oxford University Press, USA, 2001. Citado 5 vezes nas páginas 36, 37, 51, 69, and 71.

MÜLLER, R. H.; JACOBS, C.; KAYSER, O. Nanosuspensions as particulate drug formulations in therapy: rationale for development and what we can expect for the future. *Advanced drug delivery reviews*, Elsevier, v. 47, n. 1, p. 3–19, 2001. Citado na página 4.

NÉEL, L. Some new results on antiferromagnetism and ferromagnetism. *Reviews of Modern Physics*, APS, v. 25, n. 1, p. 58, 1953. Citado na página 9.

NETHE, A.; SCHOLZ, T.; STAHLMANN, H.-D. Improving the efficiency of electric machines using ferrofluids. *Journal of Physics: Condensed Matter*, IOP Publishing, v. 18, n. 38, p. S2985, 2006. Citado na página 3.

ODENBACH, S. Magnetoviscous and viscoelastic effects in ferrofluids. *International Journal of Modern Physics B*, World Scientific, v. 14, n. 16, p. 1615–1631, 2000. Citado na página 11.

ODENBACH, S. Ferrofluids: magnetically controlled suspensions. *Colloids and Surfaces A: Physicochemical and Engineering Aspects*, Elsevier, v. 217, n. 1-3, p. 171–178, 2003. Citado 6 vezes nas páginas vii, 1, 2, 3, 7, and 10.

ODENBACH, S. *Colloidal magnetic fluids: basics, development and application of ferrofluids*. [S.l.]: Springer, 2009. v. 763. Citado 7 vezes nas páginas vii, viii, 3, 9, 12, 78, and 79.

ODENBACH, S.; RAJ, K. The influence of large particles and agglomerates on the magnetoviscous effect in ferrofluids. *Magnetohydrodynamics*, Institute of Physics, University of Latvia, v. 36, n. 4, p. 312–319, 2000. Citado na página 10.

ODENBACH, S.; RYLEWICZ, T.; HEYEN, M. A rheometer dedicated for the investigation of viscoelastic effects in commercial magnetic fluids. *Journal of magnetism and magnetic materials*, Elsevier, v. 201, n. 1-3, p. 155–158, 1999. Citado na página 9.

ODENBACH, S.; RYLEWICZ, T.; RATH, H. Investigation of the weissenberg effect in suspensions of magnetic nanoparticles. *Physics of Fluids*, AIP, v. 11, n. 10, p. 2901–2905, 1999. Citado 2 vezes nas páginas 11 and 120.

ODENBACH, S.; STÖRK, H. Shear dependence of field-induced contributions to the viscosity of magnetic fluids at low shear rates. *Journal of magnetism and magnetic materials*, Elsevier, v. 183, n. 1-2, p. 188–194, 1998. Citado na página 9.

ODENBACH, S.; THURM, S. Magnetoviscous effects in ferrofluids. In: *Ferrofluids*. [S.l.]: Springer, 2002. p. 185–201. Citado 5 vezes nas páginas 1, 9, 11, 78, and 80.

OLDROYD, J. Non-newtonian flow of liquids and solids. *Rheology: theory and applications*, New York: Academic, v. 1, p. 653–682, 1956. Citado 2 vezes nas páginas 25 and 40.

- PANKHURST, Q. A. et al. Applications of magnetic nanoparticles in biomedicine. *Journal of physics D: Applied physics*, IOP Publishing, v. 36, n. 13, p. R167, 2003. Citado na página 4.
- PATEL, R.; UPADHYAY, R. V.; MEHTA, R. V. Viscosity measurements of a ferrofluid: comparison with various hydrodynamic equations. *Journal of colloid and interface science*, Elsevier, v. 263, n. 2, p. 661–664, 2003. Citado na página 9.
- PEREIRA, I. D. O. Reologia de líquidos viscoelásticos e termossensíveis em cisalhamento. 2017. Citado na página 124.
- POULIQUEN, D. et al. Superparamagnetic iron oxide nanoparticles as a liver mri contrast agent: contribution of microencapsulation to improved biodistribution. *Magnetic resonance imaging*, Elsevier, v. 7, n. 6, p. 619–627, 1989. Citado na página 4.
- ROSA, A. P.; GONTIJO, R. G.; CUNHA, F. R. Laminar pipe flow with drag reduction induced by a magnetic field gradient. *Applied Mathematical Modelling*, Elsevier, v. 40, n. 5-6, p. 3907–3918, 2016. Citado na página 6.
- ROSENSWEIG, R. E. Fluid dynamics and science of magnetic liquids. In: *Advances in electronics and electron physics*. [S.l.]: Elsevier, 1979. v. 48, p. 103–199. Citado 2 vezes nas páginas 3 and 9.
- ROSENSWEIG, R. E. *Ferrohydrodynamics*. [S.l.]: Courier Corporation, 2013. Citado 4 vezes nas páginas 1, 3, 5, and 84.
- ŠAFAŘÍK, I.; ŠAFAŘÍKOVÁ, M. Use of magnetic techniques for the isolation of cells. *Journal of Chromatography B: Biomedical Sciences and Applications*, Elsevier, v. 722, n. 1-2, p. 33–53, 1999. Citado na página 5.
- SALAS, F. M. A. *Modelagem microestrutural de líquidos elásticos em escoamentos*. Dissertação (Mestrado) — Programa de pós-graduação em ciências mecânicas. Universidade de Brasília, Brasília - DF, 2006. Citado 2 vezes nas páginas 27 and 43.
- SALAS, F. M. A.; OLIVEIRA, T. F.; CUNHA, F. R. A note on the extensional viscosity of elastic liquids under strong flows. *Mechanics Research Communications*, Elsevier, v. 33, n. 3, p. 401–414, 2006. Citado na página 52.
- SCHERER, C.; NETO, A. M. F. Ferrofluids: properties and applications. *Brazilian Journal of Physics*, SciELO Brasil, v. 35, n. 3A, p. 718–727, 2005. Citado 2 vezes nas páginas 3 and 5.
- SHAHNAZIAN, H.; ODENBACH, S. Rheological investigations of ferrofluids with a shear stress controlled rheometer. *Journal of Physics: Condensed Matter*, IOP Publishing, v. 20, n. 20, p. 204137, 2008. Citado na página 13.
- SHLIOMIS, M. I. Effective viscosity of magnetic suspensions. *Zh. Eksp. Teor. Fiz*, v. 61, n. 2411, p. s1971d, 1971. Citado 3 vezes nas páginas 8, 9, and 77.
- SISKO, A. The flow of lubricating greases. *Industrial & Engineering Chemistry*, ACS Publications, v. 50, n. 12, p. 1789–1792, 1958. Citado na página 38.
- STEPHEN, P. S. *Low viscosity magnetic fluid obtained by the colloidal suspension of magnetic particles*. [S.l.]: Google Patents, 1965. US Patent 3,215,572. Citado na página 3.

TANNER, R. I. *Engineering rheology*. [S.l.]: OUP Oxford, 2000. v. 52. Citado 2 vezes nas páginas 6 and 63.

TRUESDELL, C.; NOLL, W. The non-linear field theories of mechanics. In: *The non-linear field theories of mechanics*. [S.l.]: Springer, 2004. p. 1–579. Citado 3 vezes nas páginas 26, 28, and 29.

YAMAGUCHI, H. *Engineering fluid mechanics*. [S.l.]: Springer Science & Business Media, 2008. v. 85. Citado na página 26.

YANG, Y. et al. Magnetorheological properties of aqueous ferrofluids. *Nihon Reoroji Gakkaishi*, The Society of Rheology, Japan, v. 34, n. 1, p. 25–31, 2006. Citado 2 vezes nas páginas 1 and 13.

ZUBAREV, A. Y. Theory of magnetic fluids with chain aggregates. *Magnetohydrodynamics*, Consultants Bureau, v. 28, n. 1, p. 18, 1992. Citado 2 vezes nas páginas 11 and 120.

Appendix

A Uncertainty analysis

The analysis of the experimental error associated to a measured variable follows, in this dissertation, the protocol prescribe on [Kline and McClintock \(1953\)](#). In the referred work, the experimental error of the measured variable \mathcal{V} , $E(\mathcal{V})$, is defined as:

$$E(\mathcal{V}) = \max(E_i(\mathcal{V}), E_r(\mathcal{V})), \quad (\text{A.1})$$

where, $E_i(\mathcal{V})$ is the instrumental error, linked to the intrinsic variabilities of the instruments of measurement, and $E_r(\mathcal{V})$ is the random error, which is associated to the fluctuations of the measured value of the variable \mathcal{V} over a finite number of measurement realizations.

Generally, if a variable is measured directly, the value of the instrumental error is the uncertainty of the instrument used to perform the measurement. However, if the variable is measure indirectly, the estimative of the instrumental error can be obtained by knowing the functional dependence between the indirectly measured variables and the directly measured ones. Regarding this context, consider an indirectly measured variable \mathcal{V} , which was calculated based on the directly measures of n quantities $q_1, q_2, \dots, q_{n-1}, q_n$, with instrumental uncertainties $E_i(q_1), E_i(q_2), \dots, E_i(q_{n-1}), E_i(q_n)$. Thus, according to [Kline and McClintock \(1953\)](#), the instrumental error associated with $\mathcal{V}(q_1, q_2, \dots, q_{n-1}, q_n)$ is given by

$$E_i(\mathcal{V}) = \left| \frac{\partial \mathcal{V}}{\partial q_1} \right| |E_i(q_1)| + \left| \frac{\partial \mathcal{V}}{\partial q_2} \right| |E_i(q_2)| + \dots + \left| \frac{\partial \mathcal{V}}{\partial q_{n-1}} \right| |E_i(q_{n-1})| + \left| \frac{\partial \mathcal{V}}{\partial q_n} \right| |E_i(q_n)|. \quad (\text{A.2})$$

Besides that, considering a process of measurement composed of n evaluations of \mathcal{V} , the random error associated with this quantity is defined as the standard deviation of the measurements carried out over the realizations, $\text{SD}(\mathcal{V})$, which is calculated by:

$$E_r(\mathcal{V}) = \text{SD}(\mathcal{V}) = \sqrt{\frac{\sum_{k=1}^n (\mathcal{V}_k - \bar{\mathcal{V}})^2}{n - 1}}, \quad (\text{A.3})$$

where \mathcal{V}_k is the value of the referred variable in the k -th realization and $\bar{\mathcal{V}}$ is the mean value of \mathcal{V} , defined as:

$$\bar{\mathcal{V}} = \frac{\sum_{k=1}^n \mathcal{V}_k}{n}. \quad (\text{A.4})$$

It is important to remark that, when the relationship between the quantity being indirectly measured and the ones that are actually being directly measured, is unknown, the experimental error will be defined uniquely by the random error.

In this dissertation, an experimental point, representing the measured variable \mathcal{V} is defined as: $\bar{\mathcal{V}} \pm E(\mathcal{V})$. This representation is used to display, in graphs and on tables, the experimental uncertainty of the quantities measured in the experiments.

A.1 Uncertainty associated with the viscosity measured in simple shear

The uncertainty of the viscosity $E(\eta)$, measured with the parallel disks rheometer, was considered as the maximum of its random error $E_r(\eta)$ and instrumental error $E_i(\eta)$. The instrumental error is estimated here from the expression relating the viscosity to the mechanic torque and the shear rate applied, equation (5.30). Based on this, the instrumental error is given by:

$$E_i(\eta) = \left| \frac{\partial \eta}{\partial \mathcal{T}} \right| |E_i(\mathcal{T})| + \left| \frac{\partial \eta}{\partial R} \right| |E_i(R)| + \left| \frac{\partial \eta}{\partial \dot{\gamma}} \right| |E_i(\dot{\gamma})|. \quad (\text{A.5})$$

According to the manufacturer of the rheometer, the torque uncertainty is $0.2 \mu\text{N}$, and the one of the radius of the disk used in the experiment is 1×10^{-5} . The uncertainty associated with the shear rate is $1 \times 10^{-3} \text{ s}^{-1}$.